



iJRASET

International Journal For Research in
Applied Science and Engineering Technology



INTERNATIONAL JOURNAL FOR RESEARCH

IN APPLIED SCIENCE & ENGINEERING TECHNOLOGY

Volume: 10 **Issue:** IX **Month of publication:** September 2022

DOI: <https://doi.org/10.22214/ijraset.2022.46774>

www.ijraset.com

Call: ☎ 08813907089

E-mail ID: ijraset@gmail.com

Experiments on Turbocharger Compressor Acoustics

Dr. Bishnujee Singh

Ph.D. Engineering, IIC University of Technology

Abstract: *As environmental regulations get tougher and turbocharging requirements become higher, the acoustic emission of downsized engines has become a concern. Turbochargers are now required to operate at lower mass flow rates and higher boost pressures, forcing them to work.*

In this thesis, I explore and analyze the acoustic turbocharger compressors and propose methods to characterize them. I also conducted experiments on various industrial turbochargers to see how different flow properties affect the sound they make. The literature review focuses on the experimental techniques used to understand the flow characteristics of a compressor. Different methodologies are proposed and implemented; experimental measurements are taken in an anechoic chamber and compared with numerical simulations.

We describe the noise produced by a compressor, including measurements of its spectral content. The noise spectrum contained low-frequency sounds which were linked with deep surges, higher frequency broadband noises from tip clearance interaction, and whooshing noises of particular concern for the automotive industry. These measurements were made over the whole speed range of the compressor.

Finally, more experimental and numerical research are recommended to go deeper into these difficulties and better understand how intake designs might delay and minimize the emergence of harmful acoustic events.

Key words: *Experiments, Turbocharger, Compressor, Acoustics*

SUMMARY

As stringent regulation of internal combustion engines increases, turbocharger noise becomes more pressing.

We will explore the relationship between acoustic emission (the noise emitted by machinery) and flow behavior in unstable conditions, to identify ways to characterize the acoustic emission of turbo group compressors.

To determine best practices for evaluating the performance of compressors, a literature review was carried out using eight different articles published between 2008 and 2013. Authors were identified and contacted to learn more about the methodologies they used in their experiments and to confirm or refute any findings. The comparison of their methods showed good potential with regard to accuracy; this was further confirmed by two different groups of experts. An anechoic chamber with a custom-built test bench was used to complete the acoustic characterization of the compressor's sound output, allowing for both steady-state and transient analysis to be performed on it.

During a measurement campaign, acoustic engineers identified different noise phenomena, including tonal noise due to the passage of the blade, low-frequency noise produced by deep pumping, and the high-frequency sound produced by the interaction of flow in the blade tip clearance. The last phenomenon is of interest to automotive manufacturers because of its particularly wide frequency. Low-frequency noise masked by high-frequency sound increases in level as output decreases until it is masked by deep pumping.

Once the experimental data have been compared with a numerical model, it is determined whether the model is valid, and if it is not, different post-processing techniques are proposed, which will allow for further investigation into the flow behavior under different conditions, as well as into the mechanisms that may be responsible for whoosh generation.

Experimental work that uses temperature measurements near the rotor to find data that can be used to explain reverse flow demonstrates how the findings from simulations can be verified. Observations of the flow around a rotor show large-scale movement of air parcels in an unstable manner; this phenomenon is called whoosh. A series of computational simulations are performed to predict the amount of reverse flow under such conditions, revealing a downward trend in reverse flow as rotor speed increases. These predictions are then tested experimentally by installing temperature probes near the rotor and monitoring the local temperature evolution. The results confirm those from the simulations and suggest that flow reversals are strongly linked to temperature variations.

Different experimental campaigns were carried out in which alterations to the intake geometry upstream of the compressor were tested to determine if the flow presentation had an impact on the acoustic compressor performance. Experimental campaigns were conducted to determine how the shape of the geometry immediately influenced its acoustic routine in the following years. The use of pools, nozzles, and guiding vanes helped to lower the amount of noise emitted by a jet engine. In a parametric study of a 90-degree elbow, it was discovered that the radius of the elbow has an effect on the circumferential temperature distribution and noise levels. This finding suggests that changes in geometry that promote less or more refluxes have an impact on whoosh noise because any spectral content produced by a jet engine in the compressor's diffuser is converted upstream.

Experimental and numerical studies explore this issue in more depth. Such studies help engineers design more effective compressors, which result in better compression systems. In light of the results, future studies should focus on the potential benefits of modifying compressor inlet geometry to delay or prevent the occurrence of such severe acoustic events.

DIVISION OF WORK BETWEEN RESEARCH FACILITIES

Collaboration with Research facilities of Cayley Aerospace Inc and NASA Jet Propulsion Laboratory was used to complete the study that led to this thesis. All publications on which this thesis is based include the responder a sole author. The respondent applied the provided approach to several experimental settings, took measurements, analyzed the data, and drew the given conclusions.

I. INTRODUCTION

In recent decades, turbocharging has played a significant role in the improvement of vehicle powerplants, particularly in the automotive industry. Increasing numbers of gasoline engines, as well as practically all diesel engines in automobiles, are using turbochargers to increase their performance. Turbocharging, which was previously considered of as a technique of boosting charge in the cylinders, is being utilized to minimize fuel consumption by downsizing and slowing down the engine's combustion chambers. It is thus possible to achieve considerable reductions in both fuel consumption and emissions by the use of a smaller engine that operates at a greater load at a lower speed than the larger engine. However, the only method to do this is by adding a turbocharger to enhance the boosting pressure. In response to these developments, the flow range of the turbomachinery being used is being driven to increasingly restricted specifications. In order to minimize the surge limit flow and improve the flow range in the compressor, ported shrouds and enhanced compressor entry designs have been created, which range from a lower surge limit to larger choked flows. There seems to be a highly noisy and constant working environment as a result of using this strategy. The quality of the turbocharger is more significant to luxury automotive manufacturers than the overall sound output of the unit. Noise known as "whoosh," which is particularly noticeable in regions of near-surge operation, is considered to be unwelcome. Whoosh noise has the highest frequency of 3 kHz. Whoosh noises were more likely to be heard by the driver under 2500 rpm, as well as during rapid tip-out or tip-in movements when the turbo compressor was working near the surge line. With a certain speed and a certain amount of mass flow, the pressure ratio rises as the mass flow increases. Compressor's output hose was found to be to blame for the squeaks. Two people who work for Homco and Teng say that their jobs are important (2009) conducted a study in a semi-anechoic chamber to quantify radiated noise from a powertrain dyno operating under full load circumstances. It was possible to lessen the whooshing noise by either altering the compressor trim or by employing pre-whirl devices. It was decided to use several types of resonators at different points in the intake line in order to lessen the whooshing noise even further. When Mendonça, Baris, and Capon (2012) took readings of the sound pressure level (SPL) spectrum in the intake and outflow ducts, they were able to figure out how the flow-induced acoustics of the compressor worked. The spectra showed that there was a narrow band of noise at about 70% of the rotational speed, as well as a tone noise that came from the blades passing through each other. The presence of a spiraling pattern of narrowband noise upstream of the compressor impeller has been detected. As seen by the flow-field velocity vectors and velocity contours, there was a low-momentum patch in the flow field that rotated at a slower rate than the wheel's rotation. For the first time, stalling inducers have been found to be a source of narrow-band noise that could one day be eliminated. Figurella and other researchers used a

steady-flow turbocharger test bench to look at the acoustic and performance characteristics of turbocharger compressors. They built the test bench. Because of the rotor-order frequency and its harmonics, most of the noise coming from the choke comes from that frequency and its other harmonics (including BPF). When the flow rate was cut, the compressor started making more noise in the 4–12 kHz range (thus reducing the slope of the speed lines). If the mass flow rate goes below a particular threshold, it is possible that local flow reversal is taking place, as indicated by a fast reduction in overall SPL in the 4–12 kHz frequency range. According to the literature research, whoosh noise is characterized as a wideband noise occurring in the frequency range of 1 kHz–3 kHz or 4 kHz–12 kHz.

According to Kundera, noise pollution from internal combustion engines has had a significant impact on our impression of the megalopolis and its inhabitants (1992). According to Kundera, urban residents were concerned about noise pollution long before we realized how chemical emissions affected human health and the environment. "We were concerned about noise pollution long before we realized how chemical emissions affected human health and the environment," he says. Aside from that, Kundera says that this cacophony is filled with the shouts of advancement.

A. Turbochargers

Shipping is a low-cost, dependable means of transportation that contributes significantly to national economies. As an archipelagic state, each of Indonesia's islands has its own principal commercial commodity, necessitating the use of effective and efficient transportation to establish a competitive economy in comparison to other nations.

Container ships play a vital role in a country's Supply chain management, which requires that goods be moved efficiently and effectively. As a result, ongoing research on container ship capabilities is required. A technical examination of container ships encompasses factors of design, economy, and performance. Only one of these variables may be the subject of a more extensive research aimed at improving container ship performance.

There are numerous potential areas to research in regard to ship performance, such as measuring the performance of a ship's main engine, which is a crucial technique for optimizing a ship's performance as the primary means of ocean transportation. One of the most essential considerations is the economy of fuel usage in terms of lowering operating costs and lowering emissions.

As a result, ship owners have expressed a great desire to enhance the efficiency of their ships' fuel usage.

According to Ravaglioli in 2015, "optimizing the control of the turbocharger has become a major problem in current engine management systems because there has been a rise in the need to cut pollution and fuel consumption."

Prior research has shown that a right mix of turbocharging method and engine downsizing may result in lower pollutant emissions and improved engine efficiency." Thus, an exploration on further developing motor execution is desperately expected, based on Ravaglioli, this is how (2015). "Turbocharging strategy and motor scaling back" can be strengthened, he says. This means that using a certain kind of turbocharger will make the motor more powerful by increasing the pressure it puts on the engine, which will also make air flow in and out of the engine more efficient and make it easier for it to start. Turbocharger: Motor: The energy and nuclear power of the fumes gas are used to turn the turbine of the turbocharger. which is the essential working component of the turbocharger. Turbochargers are comprised of turbines and blowers that are associated by a shaft association, which makes the blower rotate also. Later on, turbocharger examination will focus on expanding the following so that a steady volume burning chamber can make more power. The goal of a turbocharger is to pack the air so that more oxygen can get into the ignition chamber, " composes Kech (2014, p.). Therefore, more gas is utilized, and the motor's power yield ascends

It is recommended by Kech in 2014 that the quantity of turbocharging match the motor's power. As a matter of fact, turbochargers have a wide speed range and can be set up to have a lot of lift pressure. The functional condition of the fundamental motor's dynamic exhibits that the heap motor produces power utilizing an unmistakable trademark. It very well might be surmised that a turbocharger requires an ideal working region, since fumes gas created by an assortment of burden motors produces variable tension and temperature supplies for the turbocharger to deal with.

More study is required to determine which turbochargers are suited to the dynamic main engine's operating circumstances. The compressor map graphic depicts the surge line and efficiency, showing the operating region of the turbocharger. At the highest pressure point, surging occurs, whereas the flow rate capacity is met at the lowest position. The compressor map may also be used to assess the turbocharger's efficiency.

As a result, a project investigation is urgently needed to discover which turbocharger is the most suited based on load engine circumstances and primary engine power output that may be enhanced by turbocharger. The study of MV. Meatus Palembang looks at current turbocharger characteristics and various types of turbochargers to see how well each one performs under the operating circumstances of a dynamic main engine. The major purpose of this study is to optimize engine performance on the MV. Meratus Palembang.

The combustion process will be aided by more compressed air. Although turbocharging has only recently gained mainstream acceptance in the automotive industry, the concept has been around for millennia. Dr. Alfred Bauchi, a native Swiss, was the first to get a patent for a turbocharger for an engine, which was granted in 1905. Instead of ships or vehicles, the earliest turbochargers were created for use in aircrafts. When it came to turbochargers, the early models were a long cry from the complex technology available today. Among other things, a lack of appropriate metal and bearing technology hindered their development, and this is something that is still being developed today. The materials that were used in the engines were unable to withstand the extreme temperatures. The notion of turbocharging, on the other hand, dates all the way back to the late 1800s, when both Gottlieb Daimler and Rudolf Diesel conducted research into forced induction. As technology evolved, smaller engines were ultimately outfitted with superior materials to match their size.

The oil crisis of the 1970s, on the other hand, generated a resurgence of interest in the topic of fuel efficiency. Turbocharging's "downsizing" provided a tremendous opportunity for cleaner engines to be developed without compromising performance. Turbochargers play a significant role in the development of modern high-efficiency vehicle engines. A turbocharger is now found in the great majority of high-performance SI engines, as well as in practically every automobile and industrial diesel engine on the market today. As a result, the acoustics of the turbocharger have become a concern. Turbochargers comprising a turbine and a compressor, powered by exhaust gas, are used to improve the thermodynamic efficiency of internal combustion engines. As a consequence, by using the energy contained in the exhaust gas, the cylinders of the engine may be filled with an even more combustible mixture, increasing the efficiency of the engine. Modern turbochargers use variable geometry turbines (VTGs), which provide more flexibility and efficiency over a wider range of operating circumstances than previous generations. Turbocharger compressors are available in a number of configurations, with centrifugal compressors being the most prevalent. In addition to spinning at high speed, the compressor wheel directs exhaust to an intercooler, which cools the exhaust gas before returning it to the engine, resulting in a cleaner exhaust. This is the term used to describe the passive acoustic aspect of the turbocharger. Two parameters may be used to define passive characteristics in the plane wave range: the reflection and transmission coefficients, or the transmission loss, depending on the linear acoustic models that are used to determine the passive characteristics. Aerodynamic sound produced by a turbo-active engine is one of the acoustic qualities of the engine in question. The passive and active characteristics of a turbocharger have an impact on the sound environment in a duct system. To create sound in a fluid, Lighthill's conventional theory suggests that there are three primary approaches that may be used. These are as follows: Dipole and quadrupole sources are both instances of changes in surface pressure, and the volume flow is an example of a dipole source. One and only time when the spinning blades of a machine, such as those of a turbocharger, travel at or near the speed of sound can a monopole source be formed. While travelling at supersonic speeds, the blades themselves will generate spinning shock waves as they pass through the atmosphere. In a supersonic state, the monopole contribution will be harmonics of the rotation frequency $0f$ in the spectrum, as shown in the diagram. Typical buzz-saw noises produced by modern aircraft engines include rotating shock waves and rotating shock wave noises. High-speed Modern technology regularly uses turbo compressors with supersonic tip speeds as a common feature. In rotating machinery, there are many different types of dipole or fluctuating pressure sources can be found. Machinery that revolves. Disruptions in the inflow of air are the principal source of time-varying blade pressures, which may be quantified as a second-order influence on blade pressure. Non-stationary flow distortions, such as turbulence, may be divided into two types: stationary and non-stationary flow distortions. Turbulence will create periodic acoustic signals, while stationary distortions will produce broadband sounds. Turbulence will produce periodic acoustic signals. The periodic signals will be composed of harmonics of the frequency of blade passage (BPF). It is necessary to employ rotor-alone tonal noise when there are no pauses in the flow of air.

Aside from rotor-stator interactions, which include pressure variations caused by the contact of intake and exit guide vanes with the rotor, rotor-stator interactions also contribute to additional dipole noise. This periodic noise is also compensated for by the BPF harmonics. Additionally, flow separation along the leading edge of the surge and the blade tip is a critical aspect in the operation. Tip clearance noise is a term used to describe these types of noise that produce a wide spectral peak corresponding to about half of the BPF (TCN). A wide-band source of turbulence in the stream is created by the stream's turbulence; however, this source is not usually required, unless the stream produces a jet with a Mach number near to one. For their part, turbochargers don't need this quadrupole source at all; instead, they employ high-pressure valves and jet engines to generate the necessary pressure. It has been discovered that the effect of turbocharger noise on the intake side, i.e. the compressor side, is more important than the impact of turbocharger noise on the exhaust side, owing to the substantially higher dampening capabilities of present mufflers on the exhaust side. As previously discussed, the most prevalent forms of aerodynamic sound in Turbo compressor are tonal, buzz-saw, and tip clearance noise, with the latter three being the most common. In a recent article [1], Rämmäl and Bom summarized the most basic results in turbocharger acoustics]. Further research by these same authors [2] into the transmission of sound in a turbo-compressor working under real-world conditions resulted in the publication of the first comprehensive experimental study of this kind. An investigation of the consistency of real and simulated 2-port data from a 1-D wave model for vehicle Turbo compressor revealed that the data was quite similar in the low-frequency band. According to the authors, the first time an automobile turbo-compressor running at real operating points was anticipated using an acoustic two-port acoustic wave model was used was in the development of the model. A recent publication [4] summarizes the results of the whole experimental characterization of the turbocharger. The turbine and compressor sides of three independent automobile units were tested in both upstream and downstream directions under a variety of operating situations. On the basis of these data, generalizations concerning the frequency-dependent behavior of transmission loss have been drawn. It is the goal of this study to bring together current findings from KTH's research on automobile turbocharger acoustics, as well as recent advances in experimental methodology. It is our intention to look into the measurement of active data, or sound power spectra in particular, and to show you some of the results. It is also being researched if it is possible to construct quasi-stationary models for the passive portion. These models include the loss that happens in the turbocharger unit, which is a significant component of the overall model. A further discussion is included on how to estimate these losses using acoustic 2-port data, which is discussed in further detail. Heat transfer has a significant impact on the performance of an on-board turbocharger. It is, however, not generally taken into consideration in turbocharged engine simulations. In general, a one-dimensional gas dynamics engine simulation employs turbocharger performance maps that are recorded without quantifying and qualifying the heat transfer, regardless of whether they are measured on the hot-flow or cold-flow gas-stand. Because heat transfer scenarios for on-engine turbochargers differ, the maps must be adjusted and rectified in the 1-D engine simulation, which mass and efficiency multipliers typically do for both the turbine and the compressor. The multipliers alter the maps and are often different for each load point. The efficiency multiplier, in particular, varies depending on the heat transfer condition on the turbocharger. Heat transfer causes a divergence from turbocharger performance maps as well as an increase in the complexity of the turbocharged engine simulation. While mounted on engines, turbochargers work in a variety of heat transfer scenarios. The primary goals of this thesis are as follows: heat transfer modelling of a turbocharger to quantify and qualify heat transfer mechanisms, improving turbocharged engine simulation by including heat transfer in the turbocharger, evaluating the use of two different turbocharger performance maps concerning the heat transfer situation (cold-measured and hot-measured turbocharger performance maps) in the simulation of a measured turbocharged engine, and prediction of turbocharger wall temperatures. Experiments were conducted on a water-oil-cooled turbocharger mounted on a 2-liter GDI engine for various load points of the engine and varied heat transfer circumstances on the turbocharger employing insulators, an additional cooling fan, radiation shields, and water-cooling settings. In addition, many thermocouples were placed on the turbocharger's exposed surfaces to compute external heat transfers. According to the turbocharger heat transfer study, the internal heat transfer from the bearing housing to the compressor has a considerable impact on the compressor. The internal heat transfer from the turbine to the bearing housing, as well as the exterior heat transfer of the turbine housing, have the greatest impact on the turbine. The exterior heat transfers of the compressor housing and bearing housing, as well as frictional power, are unimportant in the turbocharger heat transfer study. The additional cooling fan has a substantial impact on the turbocharger's energy balance.

While the exterior heat transfer of the bearing housing and internal heat transfer from the bearing housing to the compressor are both influenced by water, the latter is more important. The energy balance of the turbocharger seems to be unaffected by the radiation barrier that separates the turbine from the compressor. The results of this research demonstrate the importance of including turbocharger heat transfer while simulating engines. As a result, the turbine efficiency multiplier and compressor efficiency multiplier may be predicted with more accuracy, and the turbine output temperature can be brought closer to the measurement. The compressor output temperature is also brought into line with the data without needing to make any adjustments to the map. The quantity of simulated heat flow to the compressor is affected by the heat transfer scenario during the testing of turbocharger performance. Turbine intake temperature, oil heat flux, and water heat flux all play a role in determining the heat transfer condition. The needed turbine efficiency multiplier is affected more by the turbine's heat transfer scenario than it is by the quantity of turbine heat flow. The heat flow from the turbine seems to be more dependent on the amount of energy being fed into the turbine. The fact that varied heat conditions on the turbocharger have no significant effect on the compressor pressure ratio is of major importance. The efficiency of the turbine and compressor are the most critical characteristics impacted by this. The turbocharger's working fluid temperature is influenced by the component temperatures. The experiment also predicts the turbocharger wall temperatures. In the future, transient engine simulations will be more accurate thanks to this forecast. Automakers are seeking to enhance the efficiency of internal combustion engines as climate change and energy conservation become more important. The exhaust process wastes a substantial quantity of fuel energy, which contributes to inefficiency.

Some of the energy is recovered by turbochargers, which raises intake pressure and so improves power density and the efficiency of internal combustion engines. Downsized, lower volume engines may now offer power outputs that are on par with bigger, non-turbocharged ones.

There are a lot of moving parts in a turbocharger, thus it's not as widely understood as some of the other more advanced components of an internal combustion engine as a whole. As a result, there are several advantages to creating a facility and model for evaluating system performance.

Diagram of a typical turbocharged engine system, as shown in Figure 1. The turbine and compressor are joined by a shaft and bearing system in the turbocharger. Exhaust gas from the turbine is heated and pressurized to generate electricity. Using the same shaft, this power is transmitted to a centrifugal compressor that raises the air pressure before it enters the engine. As a result, a smaller engine may produce the same amount of torque as the bigger one, thanks in part to a higher 2 pressure. As a result of lower bearing and cylinder wall surface areas, as well as a part of the otherwise lost energy being recovered by the turbine, the total system efficiency is improved. For example, according to Baines (2005), a non-turbocharged engine wastes 30-40% of the total energy created during the combustion process. Additionally, the smaller engine makes the car more compact. With turbocharging, diesel and spark ignition engines alike may now benefit from improved efficiency, decreased emissions and smaller package size. There are two most common techniques of forced induction, a turbocharger and a supercharger, both of which are seen in Figure 1. From mid to high engine speeds, turbocharged systems tend to have more power and efficiency, while superchargers tend to perform better at lower engine speeds. In contrast to turbocharging, supercharging uses mechanically driven screws to boost air pressure, therefore there is no efficiency gain from reusing spent combustion energy. Because of this, turbocharging is the most frequent form of forced induction in today's automobile sector. Twin or parallel turbocharging, with one turbocharger per bank of cylinders, is often used in engines with more than one cylinder bank. Additionally, sequential systems with numerous turbochargers are employed to enhance the range of operation of the forced induction system. A turbocharger and supercharger are used to take advantage of the turbocharger's high mass flow rate and the supercharger's fast reaction. Since turbochargers are so widely used, it is essential to have a thorough understanding of the various turbomachinery components and their performance characteristics.

However, although centrifugal compressors dominate turbochargers, both axial and centrifugal compressors may be used to increase pressure. When working with an axial compressor, the flow is twisted at a set radius from its hub to the blade tip.

Nonetheless, in centrifugal compressors, the flow enters and leaves the impeller at the tip, which has a bigger radius than the hub, while in reciprocating compressors the flow enters and departs at the hub. As a result of the centrifugal compressor's wider radius, it can achieve higher pressure levels than the axial compressor can (Korpela, 2009). In axial compressors, numerous stages are needed to obtain pressure ratios greater than small ones (Baines, 2005).

When it comes to high-pressure equipment such as gas turbine engines and aviation propulsion, multiple-stage axial compressors are often the preferred option. However, they are smaller than multiple-stage centrifugal compressors (Peng, 2008). Because all flow turning occurs at a fixed radius on the blade of the turbine rather than rotating from the outer radius inward, axial turbines lower pressure less than radial turbines, just as they raise pressure less than centrifugal compressors. Axial turbines are more efficient, but they have a lower working range than radial turbines. Hence they are often utilized in systems that run for long periods at a single operating point.

Most automobile turbochargers use centrifugal compressors or radial turbines since they don't need as many stages, which lowers their cost, complexity, and manufacturing requirements while also increasing their operating range.

This year marks the centennial anniversary of the development of turbocharging technology. Patents for centrifugal superchargers were gained by Gottlieb Daimler in 1885 and Louis Renault in 1902, both of whom used centrifugal superchargers to achieve their results. Although this was the case, Alfred Büchi's Imperial Patent Office of the German Reich [10] patent No204630, which was issued in 1905, was the first design for a turbocharger to be published.

Even though the Mercedes Kompressor series of racing and luxury sports vehicles made its appearance as early as 1921, the majority of mass-produced automobiles at the time were powered by small, naturally aspirated engines.

The loss of air density at high altitudes is compensated for by the use of turbochargers, which were first used in aircraft and later in vehicles to enhance horsepower while simultaneously widening the operating range of the engine. Turbochargers for the B-17 Flying Fortress were built with the help of Cliff Garrett's business as an example.

It was the Chevrolet Corvair Monza Jet fire that were the first vehicles to utilize turbocharging technology when it was initially introduced in the 1960s. Despite its early problems, this technique eventually led in the creation of more sophisticated engines, which improved overall performance. In the 1970s, there were significant shifts in the automobile market. The oil crisis, as well as improved dependability, more environmental regulations, and the introduction of turbocharged Formula One vehicles, all contributed to this advancement. Diesel engines gained popularity in the 1980s and 1990s, and they were a major player in the business during that time period.

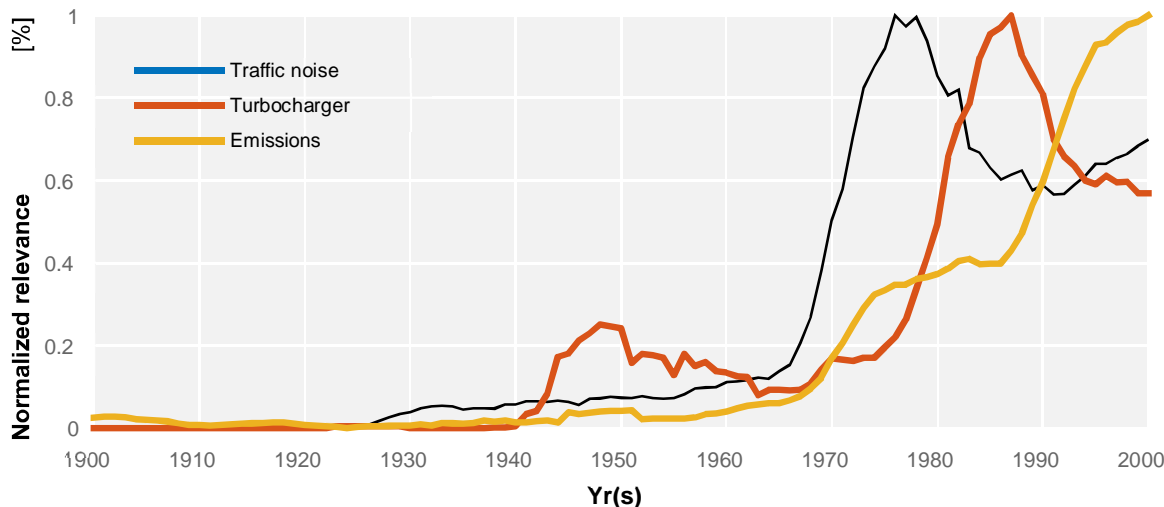


Figure 1:Google Books indexed the normalized significance of chosen English phrases in literature.

Figure 1.2 was the first time that the phrases "turbocharger" and "traffic noise" were used in English literature. A major increase in "turbocharger" allusions occurred during World War II when turbocharging aircraft became the norm. However, its popularity peaked about 1980. From 1965 through 1975, "traffic noise" becomes a major issue.

Emissions issues have risen gradually over the last decade, as seen in the graph to the right. There are new laws for automobiles, such as CO, NO_x, CO₂, PM, and others shown in this image. The reduction of displacement and cylinder count in gasoline and diesel engines is a common trend aimed at improving efficiency and lowering emissions. These trends are expected to continue as rules become stricter [11].

Because smaller displacement engines need higher power and torque, turbocharging is becoming increasingly widespread in the petroleum industry.

There are six types of turbochargers:

- 1) **Single Turbochargers:** Single turbochargers may be configured in an endless number of ways. Depending on the compressor wheel size and turbine, the torque characteristics will be drastically different. Large turbos create a lot of top-end power, while smaller turbos spool up quickly and produce greater low-end oomph. There are also single turbos with ball bearings and journal bearings. Ball bearings reduce friction in the compressor and turbine, allowing them to spool quicker (while adding cost).
- 2) **Twin-turbo:** The use of two turbochargers provides a broader range of options than the use of a single turbocharger, and the same is true for single turbochargers. Each cylinder bank may be equipped with its own turbocharger. It is possible to use both a single turbocharger for low RPM and a larger turbocharger for high RPM in tandem.
- 3) **Twin-scroll turbo:** In almost every way, twin-scroll turbochargers outperform single-scroll turbochargers. The exhaust pulses are divided using two scrolls. For instance, cylinders 1 and 4 of a four-cylinder engine (firing sequence 1-3-4-2) may be connected to one turbo scroll while cylinders 2 and 3 are connected to another. What are the advantages? As the piston reaches the bottom dead In Cylinder 1, the exhaust valve opens mid-power stroke. This ends the power stroke in Cylinder 1. A normal single-roll turbo manifold has two exhaust valves that are briefly open at the same time. It is possible to separate the scrolls in order to get around this impediment.
- 4) **Turbocharger with Variable Geometry:** VGTs are one of the most distinctive kinds of turbocharging, but owing to the expense and exotic material needs, manufacturing is restricted (though they are rather prevalent in diesel engines). The A/R ratio increases as the rpm increases, allowing for more airflow. As a consequence, turbo latency is minimized, the boost threshold is reduced, and the torque band is wide and smooth.
- 5) **Variable twin-scroll Turbocharger:** Variable twin-scroll turbos combine VGTs with twin-scroll turbos. It uses the same notion of high and low A: R ratios for greater and lower RPMs. A variable valve, on the other hand, now controls the discharge of exhaust gases.
- 6) **Electric Turbochargers:** Almost all of the problems of a turbocharger are solved by introducing a strong electric motor into the mix. Although the electric approach is unquestionably the next step in contemporary turbocharging, it is not without its drawbacks.

B. Noise Emissions

Turbocharger noise is a cause of concern for many of the company's customers. As internal combustion engines are downsized and used to higher charge pressures, It has only recently been discovered that the noise produced by turbochargers is a significant factor in vehicle performance. Feld and colleagues (1) go into great depth about how to set up an acoustic test lab for big marine turbocharger compressors, which is a very important topic. As a consequence of input distortion and vaned diffuser noise, the presence of blade passing frequency (BPF) noise was explored. To protect the engine exhaust system from turbocharger noise, Brand and colleagues (4) presented their research on acoustic decoupling. Brand and colleagues (4) Schweizer and Sievert looked into the noise created by the rotor-bearing-shaft system and found it to be rather loud (5).

Tanna et al. (6) presented their study on the use of a ported shroud to minimize BPF noise in turbocharger compressors, which was funded by the National Science Foundation. Lee and other people did research on the noise made by turbochargers (7).

Measure the noise from a turbocharger test rig with a free-field microphone that is 8 feet away from the compressor intake in a quiet place. for this study. A narrow band of noise with a frequency roughly three times the rotor rpm was found to be the dominant frequency in most settings. It was determined that the experimental setup was at fault. Sheng (8) demonstrated turbocharger noises and correctly identified many of them. For example, Cabral et al. (9), in their study of turbocharger flow instability, There were some sounds made and scatted by the compressor near the surge.

There is a lot more broadband noise near surges than at other times. At 45 percent shaft speed, they found that there was a hump in the noise. This hump was linked to a spinning stall. A study by Karimet et al.(10) looked at the 'hiss/whoosh' or broad noise made by a turbocharger compressor when it was running at no design settings. The goal was to figure out the best intake guide vanes and grooves/steps in front of the impeller arrangement.

Using acoustic cues, R. Dehner and colleagues (11) were able to determine if a turbocharger compressor was unstable in the low-flow zone.

Surges and incidence angle were determined to be related at the impeller intake and other sites, according to the researchers. The identification and treatment of surge noise were investigated by Kuang X. and colleagues (12). It was discussed in detail by Bom and Rämmal(13) in their study how to build a tiny noise suppressor for the kHz frequency range. It took Broatch et al. (14) both experiments and computer simulations to look at the wideband noise of a turbocharger compressor that was running at a peak pressure ratio of 2.24:1 and making a lot of noise. at high temperatures. Using acoustic climate chamber, Biet and Baar (15) devised a method for measuring turbocharger acoustic data in cold locations. Gupta et al. (16) investigated methods for reducing turbocharger whistling noises in the passenger compartment of automobiles. It was highlighted that the origins of noise, whether aerodynamic or mechanical in nature, should be determined. With the consideration of rotation, thermal expansion, and shaft motion, During their study, Galindo et al. (17) looked at how a small, turbocharged compressor would sound when it was running in near-surge conditions. None of the things people did changed very much.

It was thought that because the tip clearance is in an area of strong spinning flow in this operating state, there was no coherent noise source mechanism that could be used to make noise. Turbines make a lot of noise because they move air through the engine.

This requires a thorough understanding of the fluid dynamics side of noise, which is not yet in place. Most of the time, the source of the noise isn't found, or the noise is just called "instability" or "rotational stall." In a turbocharger, the compressor is the main source of the noise that comes from the turbine and compressor. turbine noise isn't a big deal now because of how flow acceleration works, how much weight and space is needed for a bigger and heavier turbine casing as well as how modern mufflers and after-treatment systems can dampen the noise a little bit. Instability is responsible for the production of noise.

This study investigates compressor noise from the perspective of aerodynamics as a consequence of this. The underlining mechanism of the noise, or how the compressor makes a variety of noises, will be the primary focus of this paper. Additionally, the techniques for decreasing these noises will be explained.

The noise made by the blades as they pass by:

Blade loading is the major source of the noise. The noise generated by blade thickness should be minimal, therefore we won't go over it here. When a blade rotates, the pressure differential (loading) between the two surfaces causes a pressure disturbance.

Noise due to flow instability

The three major components of a turbocharger compressor are a centrifugal impeller, a diffuser, and a volute housing, all of which are centrifugal in design. The impeller and diffuser slow the flow before the fluxes divide, and they are subject to precise diffusion constraints during this time. Volute housings have a dual effect on flow rates: if they are larger than those for which they were designed, they will accelerate flow in them; if they are lower than those for which they were designed, they will spread and eventually stall flow. Flow separations are unreliable, and the development of vortices is a common occurrence. When the surge control on a compressor is turned off, it is common to hear strong tonal and wideband noises. In this case, the blower is being utilized as a stream dispersion gadget to its most extreme possible limit. Stream precariousness inside blowers brings about various clamor producing processes, which are examined in additional detail further down this page. Just open cover impellers with cover freedom, as well as vaneless diffusers, are accessible for this application.

Scandalousness is the norm a vehicle or a "cruiser." Many individuals observe the shortfall of this omnipresent metropolitan foundation sound upsetting since it is so recognizable to them. Traffic, then again, is the main source of contamination in metropolitan regions.

It's not difficult to see what autos mean for the commotion climate in metropolitan spots; stopped up streets show up as more significant level wellsprings of clamor contamination that stretch out to more uncommon areas because of gridlock. This theory was finished on the grounds of Cayley Aerospace Inc, which has a traffic limitation in the lower left of the image.

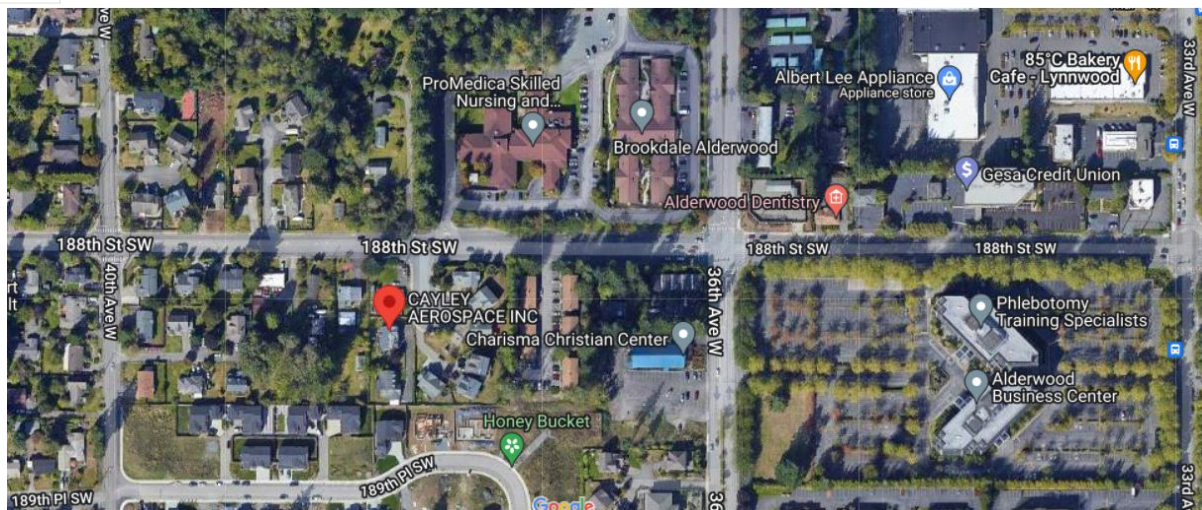


Figure 1.1: An outline of the human body. The worldwide commotion levels around the Cayley Aerospace Inc's outline the meaning of street traffic as a reason for metropolitan clamor contamination, as shown by the information (Lynnwood, Washington). Commotion levels are portrayed on a scale going from calmer (1) to noisier (5) in view of standardized estimations (5).

Then again, commotion contamination from cars is the consequence of a long and tangled series of occasions. It is the ignition commotion that makes the main commitment to the general clamor created by a vehicle. This commotion is created by numerous concurrent blasts in the ignition offices of every chamber, with innumerable blasts happening each second of activity. At the point when a vehicle is moving, its engine vehicle commotion is comprised of a blend of streamlined clamor made via air streaming around structures and through admission and fumes pipes and mechanical commotion brought about by tire contact with the black-top of the street. Turbochargers are delivering a developing amount of mechanical commotion, which is an issue for drivers.

It is one more significant reason for worry for controllers and clients the same, as we examined before in this section concerning NVH (Noise Vibration and Harshness) discharges. A turbocharger in a more modest motor might assist with reducing uproarious fumes throbs while additionally supporting thumping opposition [13], but it has been shown [15] that a contracted motor delivers more commotion than a comparable motor with a bigger removal under specific working circumstances. Turbocharging requests that are expanded additionally scrutinized the blower's limitations. One such limitation is as far as possible [16], which happens when the blower's wind stream inverts, permitting air to leave upstream as opposed to downstream. Auriel Stodola [17] offered the accompanying expression in 1927: " "asking," which is the sudden arrival of packed air from a radial blower into the air once in a while [...], is a troublesome issue that has overwhelmed outward blower fashioners [...]. The event of the flood is brought about by the powerful balance of the rising part of the trademark bend becoming temperamental."

Pressure proportion bothers are related with expanded clamor result and stream insecurities during stream speed increase, as we will show in the following segment. To examine these hazards in additional detail, guides and spectrograms will be utilized. It is additionally important to inspect the nature of the commotion and the general sound power while examining acoustic discharges. Analyzing the models in [18] and Nor et alwork[19] shows this point.

C. Current State

Turbocharging efficiency, as well as noise and pollution problems, have been major study topics. Several potential solutions to these problems are being researched. Several researchers conduct investigations on the compressor's interior flow patterns. Others are more interested in the aural field that is broadcast from outside.

CFD simulations demonstrate how air travels within and around the compressor.

The total efficiency of a turbocharger has a large impact on performance. Less turbine power is required to drive the compressor to achieve the desired boost pressure. Using a larger turbine casting A/R reduces the average pressure in the exhaust manifold.

The parasitic loss of the engine is decreased, and the engine fuel consumption is improved since the pistons operate against this lower pressure on their upstroke while pushing residual exhaust gas out of the engine cylinders. As a result, when matching a turbocharger to an engine, it is preferable to aim for the maximum feasible turbocharger overall efficiency.

The performance map of the compressor may be used to determine the compressor's efficiency. Turbocharger manufacturers create these maps by putting the turbocharger on a performance test stand and monitoring its performance over the whole airflow and speed range.

Additionally, numerical characterization of experimental and acoustic difficulties is performed. The recommended choices include changing the intake or casing geometries, as well as adding various silencers and resonators to the compressor pipes.

The goal of this study is to identify acoustic phenomena that vary with wind speed. While some, such as tonal noise produced by blade passes (such as Blade Passing Frequency (BPF)), are easy to understand, others, such as the periodic noise produced by turbulent wind waves, have proven more difficult. The producing techniques of wideband noise—whoosh—produced by airfoils, for example, have been studied.

Low-speed (2500rpm) and partial load operation might result in annoyance or possibly a malfunction if the sounds are not addressed. Although a minor whistling may be regarded by the driver as pleasant

The whistling is an acoustic feedback from the engine's power output while it is running at high speed and full load.

As a result, a development tool must precisely model the turbocharger's multiple gas and rotor dynamic excitation sources across the whole speed range.

Further thought should be given to the basically instigated clamor spread across the different motor parts.

It is proposed in this exploration that a two-stage method be utilized to build an apparatus that can appraise the commotion level of a super charger: Initial estimations were done on turbochargers (TC) from a traveler vehicle and a substantial motor while performing broad boundary varieties to describe the different clamor peculiarities brought about by the various applications and to evaluate the individual overwhelming elements of the acoustics of the turbochargers. Furthermore, utilizing stream, multi-body, and dynamic limited component reproduction, a half breed figuring approach in light of these three strategies has been formulated.

A stuff driven siphon used to drive air into a gas powered motor was first evolved in 1885 by Gottlieb Daimler, a German architect who was working in the late nineteenth hundred years. Since all constrained enlistment gadgets are arranged as superchargers, turbochargers were previously alluded to as turbosuperchargers. Notwithstanding the way that turbochargers are actually delegated superchargers, "supercharger" is by and large held for precisely fueled constrained acceptance frameworks nowadays. While both turbochargers and conventional superchargers are truly determined by the motor, the fundamental distinction between them is that a supercharger is controlled by a turbine that is driven by fumes gas from the motor, and that a turbocharger doesn't have this limit. The responsiveness of turbochargers is many times lower when contrasted with the responsiveness of a precisely determined supercharger "Twin charger" alludes to a motor that has both a supercharger and a turbocharger introduced in it. While controlling a supercharger, a mechanical burden is put on the motor, which is achieved utilizing belts, chains, shafts, and cog wheels. A supercharger is installed on the Rolls Royce Merlin motor, for example, and it consumes approximately 150 percent of the motor's output to operate (110 kW). However, there are certain disadvantages. The motor requires 150 hp (110 kW) to operate the supercharger, but it also requires 400 horsepower (300 kW), which adds 250 lb-ft of torque to the automobile (190 kW). The primary problem of a supercharger is now apparent: the motor should be able to choose between its combined power and the power required to operate the supercharger.

The more unfortunate adiabatic productivity of specific superchargers, when contrasted with turbochargers, is another downside (particularly Roots-type superchargers). It is the capacity of a blower to pack air without adding over the top hotness to that air that is estimated in adiabatic productivity (AEC) units. Regardless, considerably under ideal conditions, the pressure interaction brings about a higher result temperature; notwithstanding, more proficient blowers produce less additional hotness. Superchargers, instead of turbochargers, create considerably more hotness in the air. As an outcome, for a given volume and tension of air, the turbocharged air is colder and denser, holding more oxygen atoms and, thus, having more likely power than the supercharged air. It is normal for turbochargers to give 15% to 30 percent more power than traditional motors in useful applications.

This is expected simply to varieties in adiabatic effectiveness, with turbochargers conveying 15% to 30 percent more noteworthy power by and large (in any case, because of hotness move from the hot exhaust, extensive warming happens). In any case, this is principally a qualification in blower type instead of blower drive system: a diffusive sort supercharger blower is almost indistinguishable from a turbocharger blower, with almost indistinguishable outlet air temperatures, however with a similar detriment of low lift at low motor paces, just like a turbocharger blower.

A turbocharger, then again, doesn't force a direct mechanical weight on the motor, but turbochargers can increment fumes back tension on motors, which increments siphoning misfortune.

Because of the greater back pressure applied on the cylinder fumes stroke, this is more effective since the majority of the energy driving the turbine is provided by the as yet growing fumes gas, which would somehow be scattered as hotness through the tailpipe. For turbocharging, the greatest downside is alluded to as "slack" or "spool time," which is something contrary to what is seen with supercharging. In the car business, this is characterized as the timeframe between the interest for higher power (the kickoff of the choke) and the turbocharger(s) delivering expanded admission pressure, and consequently, expanded power.

Because of the way that turbochargers rely upon the gathering of fumes gas strain to work the turbine, choke slack creates during activity. In factor yield frameworks, for example, car motors, the fumes gas tension out of gear, low motor velocities, or low choke is frequently deficient to work the turbine, requiring the turbine to be turned down. In the wake of arriving at a specific speed (rpm), the turbine area starts to spool up, or turn at a sufficiently high rate to create consumption pressure that is more noteworthy than pneumatic force.

A blend of a fumes driven turbocharger and a motor driven supercharger might assist with beating the inadequacies of every framework independently and together.

Twin charging is the name given to this innovation.

Because of the way that the motor utilizes mechanical assistance to charge air just at lower motor velocities and at beginning, the precisely helped turbocharger on Electro-Motive Diesel's two-phase motors isn't exactly a twin charger. Genuine turbocharging is utilized after you arrive at the fifth score on the motor's rpm scale. Dissimilar to a turbocharger, which utilizes the blower part of the super blower just during beginning, and in light of the fact that two-cycle motors can't normally suction, and as indicated by SAE definitions, a two-phase motor with a precisely helped blower it is thought of as normally suctioned to during inactive and low choke

More up to date superchargers are electrically worked, which simplifies it to use them right at low velocities when super slack is an issue, instead of at higher paces. Commercialization is additionally progressing for turbochargers that coordinate an electric engine for use at low velocities

Turbochargers have been around beginning around 1905, when Alfred Büchi, a Swiss specialist working at Sulzer, got a patent. This is in many cases viewed as the start of turbocharging innovation.

In this creation, a fumes driven pivotal stream turbine and blower were put on an equivalent shaft, and the motor was portrayed as a compound outspread motor.

Whenever the principal model was finished in 1915, it was expected to beat the power misfortune brought about via airplane motors because of the decreased thickness of air at high elevations.

The model, then again, ended up being untrustworthy, and it was never created. Auguste Rateau, a French steam turbine designer, sought a patent for turbochargers in 1916, with the express purpose of incorporating them into the Renault engines used in French fighter aircraft. This patent was granted quickly for turbochargers. The National Advisory Committee for Aeronautics (NACA) and Sanford Alexander Moss demonstrated in 1917 that a turbocharger might enable an engine to operate at altitudes of up to 4,250 metres (13,944 ft) above ocean level without encountering any power misfortune (contrasted and the influence delivered adrift level). In the United States, the testing was done at Pikes Peak using a Liberty L-12 aero plane motor.

After effectively introducing turbochargers on ten-chamber diesel motors in 1925, Alfred Büchi proceeded to build the power yield from 1,300 kW to 1,860 kW. This was the world's most memorable business organization of a turbocharger (1,750 to 2,500 hp).

Notwithstanding two major traveler sends, the "Preussen" and "Hansestadt Danzig," this motor was utilized by the German Ministry of Transport. It was authorized to various makers, and turbochargers began to be utilized in an assortment of utilizations like shipboard drive, railroad vehicles, and enormous fixed motors.

During the Second World War, turbochargers were used on a variety of aeroplane motors. The first was the Boeing B-17 Flying Fortress, which used General Electric turbochargers in 1938.

Consolidated B-24 Liberator, the Lockheed P-38 Lightning, the Republic P-47 Thunderbolt, and the Republic P-51 Mustang aren't the only planes that flew in World War II: and trial models of the Focke-Wulf Few 190 were all early turbocharged airplane.

During the 1930s, the Swiss truck fabricating firm Saurer fostered a pragmatic use for trucks that demonstrated effective. Turbocharging was accessible as a choice on the BXD and BZD motors turning over in 1931. As shown by Sulzer, Saurer, and Brown, Boveri and Cie, the Swiss business was a trailblazer in the advancement of turbocharging motors.

Auto producers turned over researching turbocharged motors during the 1950s, yet the challenges of "super slack" and the massive size of the turbocharger couldn't be settled at that point. Turbocharging in vehicles turned out to be progressively common because of the 1973 oil emergency and the 1977 Clean Air Act changes, and diminishing fuel utilization and exhaust pollutants is presently utilized. In normally suctioned cylinder motors, consumption gases are drawn or "pushed" into the motor by air pressure making up for the volumetric shortcoming made by the descending stroke of the cylinder (which makes a low-pressure region), in a way undifferentiated from bringing fluid through a needle into the motor. This term alludes to the distinction between the amount of air that is really acquired and the sum that would be attracted assuming the motor had the option to keep up with barometrical strain. With a turbocharger, you might expand the volumetric proficiency of a motor by raising the strain of the admission gas.

D. Objectives

This thesis address three main objectives: acoustic analysis, methodology, and application. These dissimilar but connected objectives are enumerated as follows:

We explore how acoustical measurement techniques can be used to characterize the sound field inside a jet engine and to validate computer simulations of this sound field. This can give us new insights into noise generated by the compressor, especially under unstable flow conditions. And we can study the effect of different inlet geometries (such as twin-annular-fan or rectangular) on jet noise.

- 1) We present a comprehensive method for characterizing the acoustic emissions from an operating engine, from the instruments used to capture the data to analyze and process that data.
- 2) We expand the corpus on the experimental results on the acoustics of turbocharger compressors across their various operating conditions: as research has been limited, this work will help us understand known phenomena and help identify areas for further study.

E. Mission Statement

Analyzing the acoustic properties, methodology, and applications of turbochargers. How can acoustical measurement techniques be used to characterize the sound field inside a jet engine and to validate computer simulations of this sound field?

F. Thesis Outline

In Chapter 2, which will serve as the introduction, we will conduct a full literature analysis of turbocharger compressor noise, which will be followed by a discussion of the results in Chapter 1. Developments in experimental compressor testing as well as literature on numerical modelling are discussed in this research. Both of these are significant in improving our knowledge of the sources of the flow field in acoustic emission.

In Chapter 3, we describe the many approaches that were used in the experimental campaign that was done throughout this thesis, as well as the facilities and equipment that were used. Some of these techniques will include processes for measuring exterior sound radiation, while others will be mainly concerned with characterizing the inside sound field. We also look at the theoretical basis, limitations, and best practices for implementing the approaches that have been offered. The results of the experiment will be shown in Chapter 4 using the method described above. Pressure spectra will be used to find important sounds. and the development of these phenomena will be examined using noise maps and spectrograms acquired at different compressor operating settings.

In Chapter 5, the engine test cell will be utilized to put the ideas taught in Chapter 3 to the test and see how well they work. Also examined is a comparison between the performance of the pressure-pressure intensity probe as well as the use of two microphones. A non-anechoic environment, like the engine test cell, makes external measurements difficult, but an example of an acoustical particle velocity approach will be discussed in order to get around this.

In Chapter 6, we'll look at how the outcomes of the trials may be used to initialize and validate numerical models, as well as how they can be used to improve the accuracy of the models. These simulations, when subjected to a variety of post-processing operations, may give insight into the flow field's peculiarities and provide further experimental results that may be useful in understanding the mechanisms involved in noise generation.

To better understand how blocked flow cells reverse and reintegrate back into the main flow phenomena when sonic emission is created, a comprehensive investigation of the flow field and its thermodynamic properties in the inducer and final section of the compressor's input duct is necessary. A detailed discussion of this issue will be provided later on in Chapter 7.

Chapter 8 will cover the experimental investigation of various geometrical configurations and their influence on compressor behavior, with a particular emphasis on noise emission. Also shown will be the relationship between compressor wheel shape and noise emissions as well as compressor performance in the upstream compressor.

Finally, Chapter 9 presents a conclusion reached as a result of the tests, and the result analysis will provide recommendations for future research that will be utilized to gather further information on the subject.

II. LITERATURE REVIEW

To give a better framework for the creation of this study, a literature survey was done, with an emphasis on research of automobile turbocharger acoustics. When appropriate, techniques from related areas of fluid mechanics and turbomachinery were used. As a consequence, this study is worthy of a section. Examining how the input shape upstream of the compressor wheel impacts the system's performance along with the noise emissions is another facet of these flow topologies that deserves investigation. This impact not only provides insight into the mechanisms that create certain auditory problems, but it also allows for mitigation.

Mixed Flow Turbines

In the early 1950s, the idea of a mixed turbine was looked into for aero planes. As early as the early 1970s, the idea of using a mixed-flow turbine to make up for the limitations of a radial turbine was put forward. People who work in science have spent the last 30 years proving that the mixed flow turbine is better because it has a lower speed ratio. Because it has some drawbacks, such as a heavier weight and more difficult design for stress reduction, the mixed flow turbine is still a good choice. is likely the best alternative for replacing a radial turbine in order to keep up with ever-increasing engine requirements.

Turbocharging using Variable Geometry:

Albeit the idea of VGT is not altogether new (the principal models were distributed in the mid-1960s), it has acquired consideration as of late. Until the mid-1980s, VGTs were utilized distinctly in gas turbine plants and trial turbochargers. VGT has various detriments, including unwavering quality (when presented to high temperatures and destructive exhaust gases for extensive timeframes), intricacy (because of the VGT activation component and control framework), and significant expense. Then again, ongoing examination has would in general find satisfactory answers for the vast majority of these difficulties, and VGTs fundamentally affect the plan of little diesel motors. Various VGT techniques have been researched throughout the long term, including the moving volute tongue, turning spout vanes, mobile sidewall, and sliding spout. While examining the exhibition of different VGT types, it was laid out that turning vanes and sliding spouts give the best blend of execution and unwavering quality and are henceforth the favored plans for current turbochargers. The tremendous greater part of VGT research keeps on being led utilizing consistent state information. Exemptions have developed experimental boundaries for contrasting steady and unsound information utilizing arrived at the midpoint of beating information and VGT. Then again, the cutting-edge trial office empowers both consistent and beat stream testing of the VGT, which is outfitted with a blended stream turbine interestingly. VGT consistent state

testing is utilized to produce ACT working timetables. Nonetheless, earlier examination has shown that turbin execution under throbbing stream significantly goes amiss from the semi consistent suspicion. Since an outcome, precarious state VGT testing is important to plan other, maybe more ideal ACT working timetables and to give an establishment for contrasting and ACT information, as unsound tests are more agent of certifiable motor execution.

A. Observational Research

While axial compressor acoustic emission has been the topic of substantial research for more than fifty years centrifugal turbocharger investigations are fairly sparse [20, 21]. Many efforts in the previous literature on centrifugal turbomachinery were focused on huge fans or centrifugal pumps, with compact turbochargers becoming more significant.

The first is the significant study done at Pennsylvania State University where centrifugal pump has been mounted in an anechoic flow bench to evaluate its acoustic performance at least since the 1990s [22].

This configuration allowed various researchers to study not only in-duct noise (as and radiating noise [22, 24].

An analogous experimental program was carried out starting around the turn of the millennium. Inside an anechoic room, Wolfram and Carolus [26] uses a centrifugal pump.

In this example, measurements were taken using anemometers pointed at the blades that could turn at will to investigate "azimuthal rotating modes". A single microphone is used to measure radiated noise [27, 28].

The Siegen and Penn State operations reveal exciting characteristics, such as detecting Blade Passing Frequency peaks on the acoustic spectrum which is perfect indications of a relationship between stall and noise. Also mentioned are dimensionless numbers like the Strouhal and Helmholtz numbers [22, 23]. However, there are significant distinctions between these massive centrifugal pumps and compact turbocharger compressors in automotive applications. They are also impacted by the reciprocating engine's pulsing flow, which is reflected in the auditory signature. This last point will be discussed in Chapter 5. Selected studies will be studied in the following subsections to address discrepancies and focus the literature study on the unique difficulties presented by "turbocharger compressors", focusing on measuring methodology and acoustic data produced.

1) Turbocharger Noise Measurement Techniques

There have been a few acoustic research studies published in the literature on tiny centrifugal turbocharger compressors, but they are few and far between. Numerous models are manufactured by vehicle or compressor manufacturers concerned with compressor noise emissions. There are several other ways for detecting the acoustic emission of vehicle turbochargers.

There are two types of studies that seek to measure internal flow noise. Research in the first group may be classified into two groups. Sound data acquired from the outside—not from within the compressor housing or inlet and outlet ducts—is used in these research. Evans and Ward [30, 31] evaluated sound radiation using a simple four-mic system. Four microphones were focused towards a turbocharged engine from the same plane. They were strewn about one meter distant from the engine at a 90° angle. The sound pressure level (SPL) was determined using the pressure readings of these four microphones, which were then averaged across them, to create a single signal that could be used to generate spectrograms and sound spectra.

Teng and Homco [16] utilized a comparable arrangement to test an assortment of whoosh sound decrease countermeasures, including motor adjustment, blower channel/outlet resonators, blower trim change, and a twirl age gadget (see Fig. 1). Portray the turbocharger gathering's far-field emanated sound by averaging four topographically positioned amplifiers in the anechoic chamber during the trial; further points of interest are in subsection 3.4.2 of part 3. Aside from far-field radiation, another acoustic issue is opening commotion, which is brought about by the admission of air into the turbocharger input pipe's entrance.

As found in Figure 8, Lee et al. [34] utilize a Brüel and Kjr free field mouthpiece coordinated at the blower delta. The amplifier was set 0.8 meters far off from the entry to keep away from "stream impacts." Guillou et al. [35] measured ingestion commotion utilizing a comparable strategy. A solitary mouthpiece was set 0.4 m from the blower input chime mouth with the turbocharger's hub adjusted.

Figurella recommended an elective method. For this situation, a Brüel and Kjaer Type 2235 Sound Level Meter was introduced at a 45° point to the admission hub and 0.25 m from the information channel opening.

Figurella et al. led their examination utilizing a 14-inch mouthpiece situated at the ideal area, 0.25 m from the opening and 45° from the hub [37]. The two instruments are displayed in Fig. 1 from the previously mentioned research [37]. During the analysis that brought about the arrangement of this postulation, two free-field receivers were set a ways off of 10 and 20 cm from the information pipe hole. Part 3's Section 3.4.1 plunges more into this contention.

Pressure sensors are utilized to screen the sound field inside the info and result conduits in a third methodology for assessing how much clamor a blower produces. Since most creation offices need anechoic chambers, this disposes of the need for anechoic circumstances in the test cell. Another significant advantage is that by zeroing in on the stream field, the impact of the channel material and calculation's radiative properties might be disregarded, which helps upgrade testing consistency.

Since these advantages make this last method especially engaging for study into the starting points of air acoustically delivered commotion, an emphasis on looking at current writing on inward stream clamor has been set. Torchon [29] zeroed in on the acoustic portrayal of turbocharger clamor during motor activity by observing in-pipe airborne commotion close to the blower outlet (see Fig. 1).

Gaudé et al. [38] of Honeywell Turbo Technologies drove a concentrated assessment concerning different vibroacoustic beginning stages of turbocharger uproar. It was outlined how accelerometers and strain sensors mounted to the lines were used to perceive unquestionable vibroacoustic occasions. Despite the shortfall of a formal, alluded to vital explanation in this work, the acoustic upheaval force was evaluated using wave decay with three sensors, showing the extent of plane wave frequencies for the presented channels.

Raptor and Neise [39] used a grouping of methodologies to choose the presence of acoustic modes in the line. The first was a 12" beneficiary with an unsettling influence defend arranged in an alternating piece of the smokestack stack. ISO 5136 can evaluate the circumferentially found the center worth of sound strain level subsequently (SPL). This rotatable piece may be outfitted with four consecutive rings, each with four flush-mounted condenser mouthpieces, to focus on acoustic modes.

Guillou et al. [35] used an equivalent strategy, XCS-190-5D low-pressure sensors were installed at a 90-degree angle to the blower confirmation connector, with four sensors each. Using this method was always successful. The output pipe of this project likewise utilized a single Kulite type XTEL-160-50G. A single in-pipe fast strain sensor [36, 37] was also utilized by Figurella et al. to measure pipe strains. A Kistler-made transducer (type 4045A2) was used in both the blower's input channel and the exhaust pipe (model 4045A2 or 4045A5).

Pai et al. [40, 41] used a single sensor to screen sound strain levels inside the blower inlet course (in this model, an intensifier). There was moreover an encompassing collector present, but the data from it was barred from their assessment. Tiijoka et al. [42] used another system, sorting out the usage of a trio of strain transducers in both the blower's input and leave pipes. A cross-ghost averaging method was used to survey the strength of the inciting centers.

| Reference | Measurement | Type | Location |
|---------------|--|------|------------------------|
| Trochon [29] | 1 in-duct sensor at the outlet | SPL | Out |
| Evans [30] | 4-microphone averaging around engine | SPL | External |
| Gaudé [38] | 2by3-sensor arrays (wave decomp.) | SIL | In and Out in and |
| Raitor [39] | 1 mic or 4by4 mic sections and up to 5-outlet sensors | SPL | Out |
| Teng [16] | 4-microphone averaging around engine | SPL | External |
| Guillou[35] | 1-Kulite (outlet), 4-Kulite(inlet)and 1 mic at 0.4m | SPL | In and Out and Orifice |
| Lee[34] | 1 microphone at 0.8m from orifice | SPL | Orifice |
| Tiikojä[42] | 2*3 sensor microphone (inlet) and 1 microphone | SPL | In and Out |
| Figurella[36] | (ambientpiezores. transducers and 1 mic at 0.25 m | SPL | In and Out and |
| Figurella[37] | and 453-piezores. transducers and SLM at 0.25 m and 45Sensor | SPL | Orifice |
| Pai[41] | arrays (cross spectra average)) [∞] | | In and Out and Orifice |
| | | | In and External |

Table 2.1: Synthesis of several acoustical characterizations approaches for turbocharger compressors reported in the literature, covering location and measurement type.

A summary of the information gathered in this subsection is shown in table 2.1. Only one reference [38] employed sound intensity, which is more robust by definition. On the other hand, the sound pressure level can be altered by the geometric configuration and measuring site. It is clear that, while data have been published for intake, outflow, orifice, and external noise, no research has been done for all four possibilities simultaneously.

2) Inside the Turbocharger

A turbocharger, which is an engine component, is responsible for increasing the air pressure inside the cylinders. It is the hot gases exiting the cylinders that are used to power a turbocharger, which is connected to the engine's exhaust system. An intake compressor is placed between the air filter and the intake manifold, and it is powered by the gas that passes past the turbine during the combustion process. Air pressure in the piston chamber is increased by means of the compressor, which is located between the pistons. allowing for more fuel to be burned and therefore increasing horsepower.

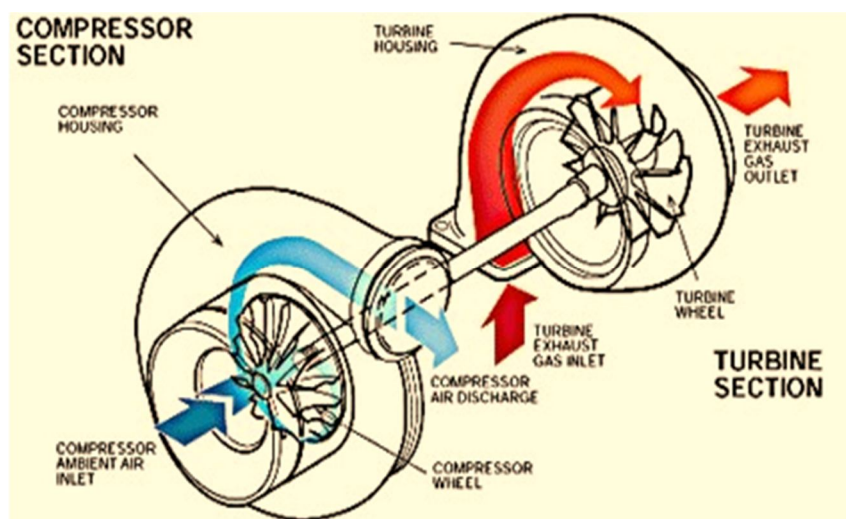


Figure 2: turbocharger inner view

When exhaust from an engine's cylinders travels into a turbine, the turbine begins to spin (similar to the rotary movement of a fan). The quicker the blades spin, the more exhaust passes through them. Another form of pump called a compressor compresses air and puts it into the engine's cylinders at the other end of the shaft to which the turbine.

Turbine shafts spin at rates of up to 150,000 rpm, thus they need to be supported carefully. In those circumstances, most bearings would burst, hence most turbochargers employ a fluid bearing. A thin coating of oil is continually injected around the shaft of the bearings to cool and lubricate the turbocharger elements. The shaft may spin smoothly and without friction thanks to the fluid bearing.

3) Relevant Outcome

In this post, after reviewing all of the methods individuals have discovered to reduce turbocharger noise in the literature, we will look at a few of the most important acoustic data that has come out of these papers. Some of the research was targeted at determining where noise originated, but others had other objectives and merely looked at noise as a number, rather than investigating its characteristics or how it was created, for example.

The work of Gaudé et al. [38], who have produced a comprehensive list of noise-producing mechanisms in turbochargers, serves as an excellent introduction. Table 2.2 depicts the categorization of the data. Tone can be caused by a number of factors, including an out of balance rotor and faults in the compressor wheel. The sound of turbine and compressor blades moving in and out of the air is a second cause of sound pollution. especially the primary ones in the latter's case.

Broadband noise, which includes the various tones and their harmonics, is referred to as "hiss," and the source mechanism is associated with compressor stage turbulence. The frequency range suggested for this turbulence-related phenomenon is 0–20 kHz, but no more information is provided.

Trochon [29] foresaw a similar separation when he classified compressor noise from turbochargers into "pulsation noise" (tonal noise caused by blade movement) and "blow noise," a wideband noise. According to the author, aerodynamic turbulence with a big mass flow and a low shaft speed occurs "inside the compressor." In Fig. 1, we can see that wideband noise occurs between 1.5 and 2.5 kHz.

When it comes to a "whoosh" noise, Evans and Ward [30] get right to the point. "Generic wideband noise" is the name given to this type of noise. 750 Hz to more than 10 kHz are reported by the scientists to be the range of this noise. There is a noticeable concentration of energy between 1.5 and 3 kHz, however. This has a "hiss" noise to it, similar to the prior example. Authors, on the other hand, say whoosh may be related with activity that is just beginning to rise. During this situation, blade stall, reverse flow, and the recirculation of intake air all contribute to higher turbulence.

Raitor and Neise [39] assert that tip clearance noise (TCN) occurs at frequencies lower than the blade passing frequency (BPF). According to Kameier and Neise [43], TCN may produce rotational instability and stall cell propagation in axial turbo compressors; as seen in Fig. 8, this TCN is present in the input duct between 3–5.5 kHz.

The graphic also depicts BPF and its harmonics. At greater rates, a strong "buzz-saw" multi-tonal noise may be heard at the entry, but not in the outflow (see Fig. 10). TCN is also present in the outflow channel. Additionally, the Mach number shows whether TCN or BPF dominates the impeller tip. There is extra broadband material between 1.2 and 2 kHz, and a minor amount between 2 and 2.8 kHz, both of which are equivalent to the whoosh above the noise.

Fig. 3 shows an idealized representation of the sample SIL spectrum, highlighting fundamental acoustic phenomena that have been studied in the literature. Tone noise peaks are BPF and harmonics, while TCN is broad. In contrast, BPF and its harmonics are tone noise peaks. Wideband effects include whoosh (lower frequency), TCN (higher frequency), and BPF (tonal noise peak).

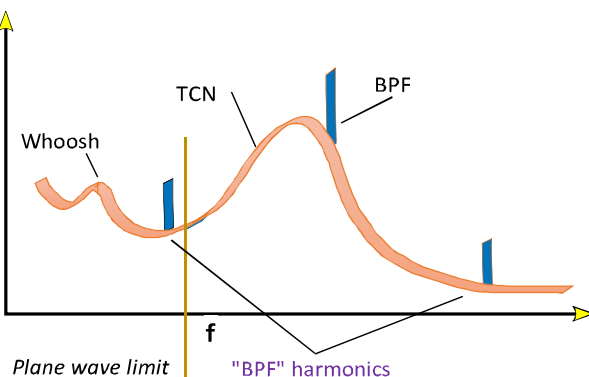


Figure 3: The most acoustic events in a turbocharger compressor outlet are depicted in this idealized picture of a typical SIL spectrum in a turbocharger.

Teng and Homco [16] used Evans and Ward's work to gain further information about the particular position of the whooshing sounds. In Figure 5, the reference authors identify whoosh noise as mostly occurring in the 4.5–7 kHz range. Because it is restricted to a maximum frequency of 10 kHz, the figure does not exhibit a BPF tone. This band's amplitude and frequency, as well as its abrupt lower frequency cut-off, might imply that it's more intimately linked to the TCN. The authors' spectrogram (Fig. 2) reveals a distinct broadband component between 1–2 kHz in all full-load test settings, which is more compatible with earlier whoosh results. A type K thermocouple was positioned extremely near to the compressor intake to establish the link between wideband noise and surge initiation. The reference's Fig. 7 depicts a possible relationship between temperature rise and the content of 5–7 kHz sound pressure. The authors believe the wideband noise they found is linked to hot backflow generated by blade stall.

Guillou et al. [35] make no mention of noise spectra. Nonetheless, for various flow regimes, the authors show the pressure FFT in the exit duct. Figure 7 demonstrates how, especially in the lower right plot, obvious broadband arises between 2–3.5 kHz (stable regime). Although the powerful low-frequency signals typical of surge states hide this occurrence, it happens in both stall and surge states.

Lee et al. [34] concentrate their research on "pulsation noise," which they claim is generated by shaft and blade imbalance, as well as BPF noise, which is caused by the blades' cyclic motion. Its harmonics are discussed (see Figs. 9&10). He finds a distinct "hump" in the precise statistics. Nonetheless, suggest that it may be rejected due to the experimental setting because the turbocharger maker did not disclose it. This wideband noise, which might be connected to whoosh, emerged between 3-4.5kHz in this example. Also, it present when the compressor was not connected to the intake and output ducts (see Fig. 11), indicating an internal source.

Tiikojä et al. [42] investigate temporal differences between two important components. Stationary distortions cause periodic tones to be identified. When there are no inflow interruptions, these tones are referred to as rotor-alone tonal noise. At BPF harmonics, fluctuating pressure fields created by the intake and exit guide vanes in conjunction with the rotor are regarded as a further source of tonal noise.

Non-stationary disturbances (turbulence) are referred to as "wide band noise," however their importance in turbochargers is questioned. Due to spinning shock waves linked to blade tips that reach supersonic speeds, the tonal phenomena is nicknamed "buzz-saw noise." With frequencies ranging from 5 to 10 kHz in the outlet and 4 to 7.5 kHz in the inlet, TCN is also classified and labeled as such.

There is a significant increase in the availability of smaller broadband currently. This bandwidth is between 0.6 and 2.5 kHz, which correlates to the above-mentioned whoosh noise difficulties at lower frequencies. Figurella et al. [36] describe a remarkable phenomenon in which discrete sound peaks (tones) are focused on synchronous (rotor) speed and blade pass frequencies (rotor speed times number of main blades). A "whoosh or blow noise" is a term that refers to a "broadband flow noise." The frequency varies between 4 and 12 kHz, and the results are shown. On the other hand, the reference's intake sound pressure level spectra (Figs. 4&5) demonstrate a more gradual rise, occurring exclusively between 5-7kHz.

In the study by Figurella et al. [37], broadband noise appeared in a frequency range that is higher than previous whoosh studies, and smaller broadband sounds were observed. The researchers did not record individual spectra, but the sound maps of the compressor showed a significant increase in noise in this band as the gradient of iso speed lines approaches zero, indicating a relationship with the re-emergence of recirculating backflows.

The broadband sounds from this compressor are more consistent with previous observations of whoosh, a sound often associated with TCN. In fact, the researchers recorded two different broadband spectra in their experiments, one in the 0.8–2 kHz range and another in the 4–12 kHz range. The sound maps of the compressor show that noise levels increase significantly in the 4–12 kHz band as the gradient of iso speed lines approaches zero, indicating a relationship with the re-emergence of recirculating backflows.

Pai et al. [41] refer to whoosh noise as "broadband noise," however they don't specify a frequency band. Additionally, it is associated with running near surge in petrol engines, such as in transient circumstances such as throttle tip-in or tip-in tip-out, as well as with certain steady-state settings. In the 3–4 kHz range, the possibility of acoustic radial mode resonance serving as a pressure disturbance amplifier is considered. According to the spectrogram in Fig. 6, if isolated noise broadband content was detected in the required frequency range, it was most likely between 2.5 and 3.5 kHz, with additional broadband content between 4 and 5 kHz.

When it comes to turbocharger compressors, the literature consistently defines two categories of occurrences: tone noises and spinning pressure gradients. Tone noises are linked with the spinning of the wheel, which results in rotational pressure differences. In transonic or supersonic situations, where shock waves attach to the blades and cause extra spinning pressure gradients, harmonics may occur.

However, there is adequate evidence of repeating wideband noise at frequencies below the BPF, which have been reported to range between 0.6 and 12 kHz in the literature. While TCN and whoosh noise appear to have different frequency ranges and occurrences, some sources confuse the two. The authors report whoosh at high frequencies, which is more typical of TCN, as well as some of the clearest lower frequency wideband noise seen in our literature review in Fig. 2. Finally, turbocharger compressors display two distinct phenomena: a lower frequency whoosh between 1–4 kHz and a higher frequency phenomenon known as TCN. There is no obvious method for making these broadband sounds, unlike BPF tonal noise. As seen by the examples above, some writers attribute these occurrences to "turbulence." Others, on the other hand, attribute them to things like delayed backflow interaction (like modal resonance), tip clearance effects, and other things. As a result, further research is required to fully appreciate the issue.

B. Simulations

A correlation between wideband noise and three-dimensional flow effects surrounding the impeller of a compressor has been suggested, as well as the difficulties associated with performing an adequate experimental characterization, numerical modelling of the problem using Computational Fluid Dynamics is a viable option (CFD).

Mendonça et al. [45] established that turbocharger compressor noise spectra are reasonable. The latter seems to vary in frequency between the entrance and exit ducts.

Lee et al. [34] investigation comprised a computational fluid dynamics (CFD) compressor simulation that matched empirically proven operating conditions. However, when a single-revolution simulation was run, no consistency between predicted and observed noise spectra was seen (Figs. 17&18). Karim et al. [44] demonstrated that lowering the leading-edge step successfully confirmed a CFD projection of whoosh noise reduction. The entire number of observations is shown, not the noise spectrum.

Percentage of rotation order (RO2): The perceived bandwidth (whoosh noise) is expressed as 0.5 to 0.9 RO2 per cent of the rotation order (50-90 percent of a shaft rotating frequency). The BPF peaks are only visible in the exit ducts, as shown in Fig. 2. Earlier research has demonstrated that CFD models can reliably simulate laboratory noise effects. A red flag is if the frequency content predicted by the CFD model does not match the frequency content seen in the field (efficiency, compression ratio, mass flow) or even aggregated noise levels. [34] Lee.

It was found that the projected and measured flow configurations agreed qualitatively in Hellstrom's [46] CFD simulations coupled to Guillou's [47] experimental Visualization work. While it may be difficult to discern this spiral-like backflow structure from experimental data, data such as the iso surface of negative axial velocity in Figure 10 is critical for assessing CFD findings. It's possible to evaluate non-acoustic research initiatives that yield empirically validated information regarding the flow field near compressor intakes, particularly when simulated operating conditions are applied to analyze stall or surge events. It's possible to predict an upsurge in the population by using the analytical methods presented by Margot et al. The phenomena were numerically studied by Lang et al. [49]. Instead of increasing output pressure by decreasing input pressure, he utilized a flow-reversal compressor. In Lang's experiment, the compressor's simulated behavior was compared to what actually happened. Additional geometries including straight ducts, elbows, and reservoirs were modelled as well. The duct taper may be seen in the straight inlet arrangement. Reversed flow extends up to 2.5 in this scenario. inducer diameters beyond the leading edge of the wheel. Each shape has its own specific reversed flow pattern. The impact of surge margins is shown theoretically and empirically.

Galindo et al. [50] used computational modelling to investigate the effect of tip clearance on the higher frequency broadband phenomena known as TCN. They found that varied tip clearance ratios had no discernible effect on the acoustic signature. As a consequence, the exact flow mechanism behind this event is unclear.

C. Field of Local Inlet Flow

The latter technique is utilized for CFD validation since it enables measurement of whole field areas rather than a single point, as the LDA and HWA procedures do. Clear windows are inserted into the diffuser casing of each of the three cases so that flow and impeller contact can be kept track of in each case. The majority of study on the effect of intake air on turbochargers has been on diffusers. Guillou, Gancedo, and colleagues [35, 66–68] used a test setup with a turbocharged compressor and an open bell mouth intake, which allowed for direct photography of the flow without any barriers as the seeded ambient air was eaten. Hellström et al. [46] used this method to compare numerical CFD simulations that used this strategy. In studies examining the transverse velocity field, the flow was illuminated with a laser sheet perpendicular to the compressor axis and near the bell opening. As an extension of this design, a short polycarbonate ported shroud was put between the bell mouth and the compressor. The laser sheet may pass through the transparent shroud of multiple aero planes. Axial velocity fields were obtained in [35, 67] by aligning the laser sheet with the compressor axis and photographing at an angle rather than perpendicular to it due to the absence of the bell mouth. By combining two cameras, a stereoscopic approach may produce the required axial velocity field as if the camera were perpendicular to the lit plane. Rather of being visible in this configuration, the compressor intake is attached to a long conduit that contains the filter and flow meter in real-world vehicle applications. These ducts contain the reversed flow, forcing it to reintegrate with the main flow. Given that the shape of the input near the compressor has been shown to have a substantial effect on the onset and frequency of deep surge instabilities [69], a characterization with limited reversed flow in the duct should be explored.

D. The Effect of Inlet Geometry

In the literature, all three of these people: Galindo et al. [70], Serrano et al.... Wang et al. [72] have proven the imp On the efficiency and surge margin, the process of changing the shape of the input right before the compressor wheel (and therefore the air presentation).

Increases in surge margin and efficiency in a turbocharger system are only marginally useful. While a study has been conducted on this subject, data on the effect of air presentation on turbocharger compressor noise are few, since the majority of research has concentrated only on deep surge dynamics [73, 74]. As a consequence, one of the objectives of this research is to investigate this auditory impact experimentally and to characterize the flow field characteristics associated with it.

Li et al. [76] examine the acoustic effects of the elbow overpressure spectral content at different sites. It is critical to do empirically validated research on BPF amplitude variation. A lot more research needs to be done to figure out how elbow-induced flow irregularities and the volute tongue work together to make acoustic noise, at least in terms of tonal BPF noise.

Taper ratios can be used to increase the surge margin of a compressor. Researchers have studied tapered conduits and reservoirs to increase surge margins. Lang [49] has researched taper ratios and determined that by increasing the conduit or reservoir's diameter as it approaches the compressor inlet, the compression percentage can be increased by up to 15%. Galindo et al. [77] also conducted research related to tapered ducts, where they determined that for surge margins of 8%, the duct should flare at a ratio of 0.3 or less, while for a margin of 10%, the flared duct should not exceed a ratio of 0.5. Desantis et al. [78] looked at a convergent-divergent nozzles that were designed in order to increase surge margins; however, noise output was not considered. Swirl producing devices positioned upstream of compressors have also been researched. Researchers have claimed that these swirl producing devices help improve base loading and thereby increasing the pressure ratio and improving the overall performance of a compressor [79, 80].

Despite this, the auditory output was ignored. Additionally, a ported shroud has been suggested to boost surge margin [35, 81]. In this construction, flow bleed holes are added to the impeller wall that connects to the compressor intake.

Some businesses have constructed openings on splitter blades that lead to low-pressure slots to reduce the impacts of noise generated by flow reversal. This design helps to prevent choke by increasing the turbine blade's lower flow-regime capacity. This novel method, however, has resulted in a new issue: auditory interference. In a 2007 publication published in the Journal of Sound and Vibration, Chen and Yin identified this phenomena. Complete-bladed compressors with a ported shroud had lower BPF (tonal) and total noise than compressors with a splitter and entire blades, according to their research.

Smaller engines and increased demand for low-end torque have made centrifugal compressor performance at low mass flow rates problematic. The main issue in this working zone is the surge induced by the compressor inlet shape. This research will examine how varied input geometries effect compressor efficiency, noise, and surge margin. Each setup is tested on a centrifugal compressor engine test bench. Both steady and transient (tip-out) tests are possible. The findings demonstrate that the compressor parameters are very sensitive to changes in the geometry upstream of the compressor intake.

E. Turbo-unit Acoustic Characterization

In addition to the plane-wave data released in [4,] the present work describes the measurement of certain passive scattering matrix data. These conclusions were obtained by extrapolation from plane-wave data. A review of the theory is provided, with a focus on previously unknown characteristics like sound power determination beyond the plane wave range. [4] describes how to collect passive plane-wave data (i.e., scattering matrix).

Apart from mufflers, additional components in a contemporary car's exhaust and intake system such as air filters, coolers, catalytic converters, and particulate filters all affect the pressure pulses or sound field produced by the system. Sound scattering (reflection and transmission) and sound generation from turbochargers are studied. Sound reflection from an open-ended pipe, such as an internal combustion engine's exhaust tailpipe, is also studied.

By measuring the acoustic two-port, it was possible to develop accurate and affordable procedures for completely characterizing turbochargers. A number of modifications are suggested to enhance the quality of the results in comparison to earlier investigations. Additionally, three separate vehicle turbochargers are studied, with data for both compressor and turbine sound scattering included. The results for sound transmission, which is critical for a turbocharger's ability to reduce engine noise, are plotted against a dimensionless frequency scale for each of the conditions analyzed (Helmholtz-number). As a result, generalizations about the behavior of any turbocharger may be made based on the data.

Additionally, the sound generation was examined, and three methods for assessing sound power were presented. The approaches were used to investigate the sound produced by a turbocharged compressor at different operation points and to identify the source processes.

The obtained data is critical for correct exhaust system modelling since it provides the acoustical characteristics at the exhaust tail-pipe. The reflection coefficient testing results were compared to Munt's notion about flow duct apertures. To explore the effect of temperature on the reflection properties, measurements were performed at air jet speeds up to Mach 0.4 and flow temperatures up to 100°C. The experimental data corroborated the Munt hypothesis.

1) Determine the Passive 2-port Data

In order to determine the sound transmission of an automotive turbocharger, researchers treat the turbocharger as an acoustic 2-port. This means that for frequencies in the domain under consideration, the following relationship holds [139]. Sound waves, when they meet a reflection or transmission boundary between two media (such as air and water), experience an impedance mismatch. The sound wave propagates outwards or into the two-port depending on the impedance of the media it is reflecting or being transmitted.

$$\begin{bmatrix} P_a^+ \\ P_b^+ \end{bmatrix} = \begin{bmatrix} S_{11} & S_{12} \\ S_{21} & S_{22} \end{bmatrix} \cdot \begin{bmatrix} P_a^+ \\ P_b^+ \end{bmatrix} + \begin{bmatrix} P_a^{s+} \\ P_b^{s+} \end{bmatrix} \quad \dots\dots\dots (2.5.1)$$

Furthermore, the superscript s denotes the source delivered sound, whereas a and b (or 1 and 2) refer to opposite sides of the two-port (downstream side).

It is possible to calculate the dissipating grid by putting down move capabilities between detected signals and external sources e. Both acoustic test states required for the dispersion lattice can be obtained by applying acoustic excitation on opposite sides of the test object. Thus, Eq. 1 could be written as:

$$\begin{bmatrix} H_{ea+}^I & H_{ea+}^{II} \\ H_{eb+}^I & H_{eb+}^{II} \end{bmatrix} = \begin{bmatrix} S_{11} & S_{12} \\ S_{21} & S_{22} \end{bmatrix} \begin{bmatrix} H_{ea-}^I & H_{ea-}^{II} \\ H_{eb-}^I & H_{eb-}^{II} \end{bmatrix}$$

Where the superscript shows the different tests. During the two-receiver method, hex is the name for the work done by the voltage e that drives the drivers. With the parts of the S-network, we can figure out how the two-port device's inactive acoustic effects will be measured. The transmission misfortune (TL) can be dealt with in this way:

$$TL_u = 10 \cdot \log \left(\frac{W_{e+}}{W_{e-}} \right) = 10 \cdot \log \left(\frac{(1+M_e)^2 A_e \cdot \rho_e \cdot c_e}{(1+M_e)^2 A_e \cdot \rho_e \cdot c_e |S_{11}|^2} \right),$$

$$TL_d = 10 \cdot \log \left(\frac{W_{e+}}{W_{e-}} \right) = 10 \cdot \log \left(\frac{(1+M_e)^2 A_e \cdot \rho_e \cdot c_e}{(1+M_e)^2 A_e \cdot \rho_e \cdot c_e |S_{21}|^2} \right),$$

In this case, TLu and TLd represent the transmission misfortunes experienced upstream and downstream, respectively. Additionally, W+ and W-represent the episode acoustic powers experienced upstream and downstream, respectively. Finally, M represents the Mach number. and c is the sound speed.

F. Conclusions

We arrived to the following broad findings after reviewing several research on various aspects of turbocharger compressor noise emission:

Axial compressors have been the topic of aero-acoustic study since the 1950s, however noise creation in small centrifugal compressors is uncommon. There are various distinct techniques to the experimental acoustical characterization of turbochargers in the literature. Instrumentation, measured variables, sensor location, and other variables are examples of variables.

Tonal sounds associated to a blade passing frequency (BPF) and its harmonics, as well as broadband noise at frequencies lower than BPF, are commonly identified in studies. Although no obvious mechanism has been found, the latter is frequently associated to halted blades and backflows. Pressure and temperature indicators were used to evaluate the unstable flow phenomena in the compressor inducer and intake. PIV measurements of the velocity field are frequently done at compressors having an open bell-mouth, rather than confining the reversed flow in a straight pipe.

The interplay of gas stream turbulence with compressor wall clearance flow causes tip-clearance flow noise. Choking whoosh is a frequent term for it. Separated flow in the compressor intake, on the other hand, is the most common cause of suction side stall noise. This might be due to a combination of poor intake duct tip clearances and irregular suction forces. Computational Fluid Dynamics (CFD) simulations have been demonstrated to be effective in studying unsteady flow and identifying suitable noise-reduction methods for both whoosh and stalling forms of broadband noise.

III. METHODOLOGY FOR MEASURING NOISE EMISSION

Aside from the overall experiment, the step-by-step signal processing necessary to get final, combined data will be discussed, with examples of each stage's outcomes. To guarantee that the findings are relevant and robust, the multiple theoretical and practical bounds and constraints of measurements and processing procedures will be carefully considered.

The examined turbocharger noise phenomena may be split into four acoustic phenomena induced by distinct physical factors. These four occurrences may be interpreted as tonal noises:

1) *Unbalancing Whistle*

Large unbalancing forces may develop in turbocharger systems due to high rotor speeds. These rotational forces are proportional to the turbocharger's speed frequency, resulting in a tonal noise known as an unbalancing whistle

2) *Pulsation Noise*

The pulsating noise is caused by the turbocharger rotor rotating at a high frequency. Rotor asymmetries, which create alternate forces as the irregularities rotate relative to the stationary housing, are the physical origins of this phenomena. The air ducts, which are agitated by pressure changes, are the principal source of this noise.

3) *Rotating Noise*

The pressure differential between the pressure and suction sides of the specific rotor blades, as well as the blades passing through the housing tongue, causes the spinning noise. The product of the TC-speed and the number of blades on the turbine or compressor wheel determines the frequency of excitation [3]. The rotational noise of the passenger vehicle TC is mostly above the hearing range due to the high turbocharger rpm. As a result, this phenomena only plays a minor part in our inquiry. In contrast, because to its lower rotation speed, the truck engine's critical bigger TC emits rotational noise in the frequency range up to 13 kHz. Under full load, the whirling noise may be plainly heard.

4) *Constant-tone Noise*

Because the frequency of the constant-tone is not proportional to the turbocharger speed, it differs from the other three noise occurrences. The phenomenon is connected with a constant frequency vs rotor speed after a little rising slope at low TC-speed. The lateral bending vibration of the TC-shaft in the hydrodynamical oil film of the journal-bearings of the rotor defines this frequency. The usual TC values for a passenger automobile are approximately 1 kHz, and for a truck, around 500Hz.

5) *Influencing Factors*

Several parameters were modified throughout the experimental studies in order to find the main influential aspects for the distinct noise phenomena. Figures -1 and -2 depict the relationship between the constant tone and the unbalancing whistle and the unbalancing of the moving components, as well as the temperature of the oil. At 200,000 rpm, the indicated acceleration level was measured on the compressor side of the TC. Grub screws on the compressor side added imbalance to the previously existing unbalance created by manufacturing tolerance ranges. Two turbochargers, each with an extra mass of 20 and 40 milligrams, were put to the test. Figure -1, as predicted, demonstrates a clear relationship between the unbalancing whistle level and the applied mass. In this case, the first-order level rises in a linear pattern in response to the imbalance. In contrast, with an imbalance mass greater than 20mg, the continuous tone's acceleration level drops dramatically.

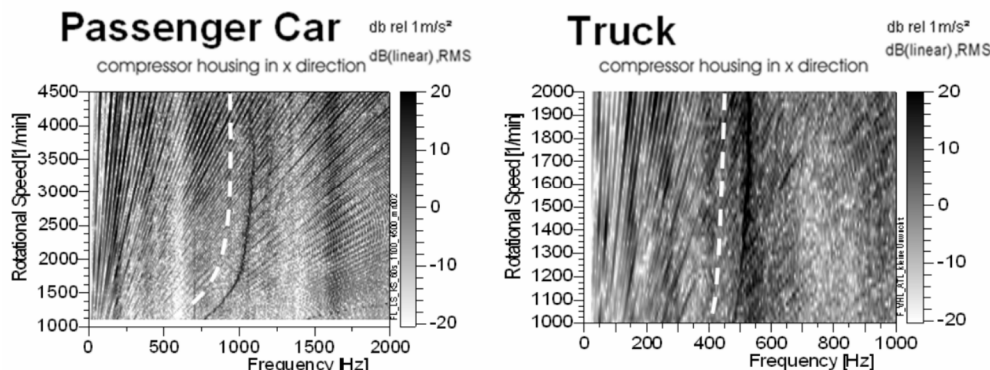


Figure 4 Unbalanced whistle Noise and Pulsation Noise due to added mass

Oil temperature, and therefore oil viscosity, were altered between 30 and 90 degrees Celsius to investigate the influence of oil temperature, oil viscosity, turbocharger noise, and so forth (Figure -2). It appears that as oil temperature rises, the initial turbocharger order and the constant-tone level will decrease. Increasing oil temperature has just a small effect on the continuous tone's shift to lower frequencies, aside from the effects on the first order level. The hydrodynamic bearing's dampening effect on the TC may be affected by the change in oil viscosity.-inherent rotor's vibration behavior.

A. Infrastructure

Even though turbochargers increase the amount of power available to a vehicle, that additional power is not derived directly from the waste fumes gas, which can be confusing to some individuals. When we use a turbocharger, we can harness a part of the energy contained in the fumes to power the blower, allowing the engine to consume more gasoline each second. The more gasoline used by the vehicle is responsible for the vehicle's increased power. Its only function is to regulate the turbocharger, and since the turbocharger is not connected to the vehicle's driving rod or wheels, it does not directly contribute to the vehicle's driving force in any way. The effect is the same: it allows a comparable engine to burn gasoline at a faster pace, which makes it all the more spectacular.

Whenever a turbocharger increases the output power of a motor, a larger, better turbocharger will result in a significant increase in output power. In theory, you may continue to improve your turbocharger in order to make your engine more powerful, but you will eventually reach a breaking point. The chambers are very massive, and there is simply an inordinate amount of fuel that they can burn. The amount of air you can force into them via a channel of specified size, and the amount of fumes gas you can remove, are both limited, which limits the amount of energy you can utilize to run your turbocharger. Ultimately, there are additional stumbling blocks that become a vital aspect that you must take into consideration as well; you cannot just turbocharge your way to endlessness! The bulk of the research in this thesis was conducted in a university laboratory setting. There are two major installations on this location.

This flow bench might be used to calibrate turbochargers or to provide air to other facilities. Section 3.1.1 will go into further depth about this arrangement. A massive anechoic chamber next to the flow bench may be used to accept external air from the flow bench or to house a separate engine. The compressor's acoustic emission was determined by altering the commercial engine's intake manifold. Section 3.1.3 has a description of this configuration. This project encompasses both a piezoelectric sensor calibration impulse test bench and a manufacturing facility for specialized measurement and instrumentation components.

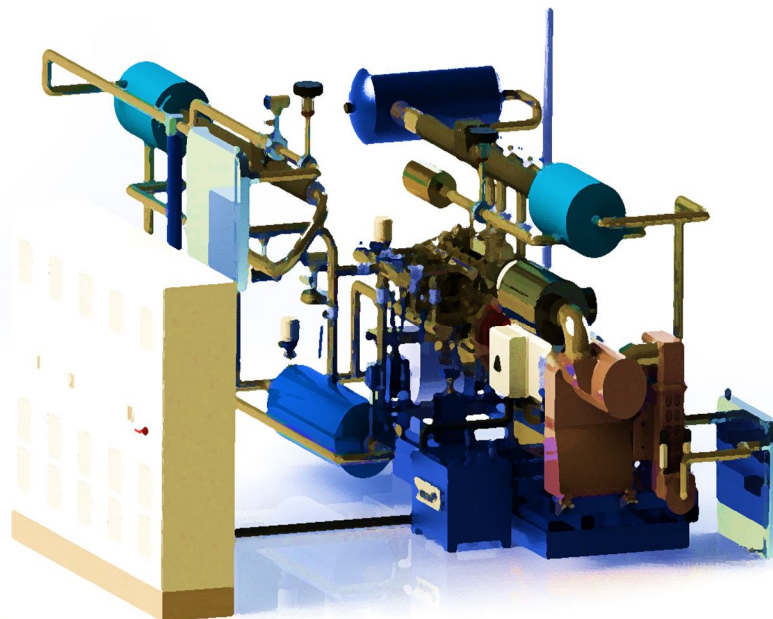
1) Flow-testing Apparatus

The turbocharger was positioned inside the flow setup cell, on a supporting frame within the anechoic chamber, and the flow test rig was used as a flow provider to power the turbocharger turbine.

[83] presents a high-level overview of the amenities in addition to a detailed explanation. This new supercharger system corrects the previous turbocharger group and provides extra engine cycle management. This control can provide sufficient compressed air at the appropriate moment to either generate a turbocharger in one chamber or increase the performance of an existing turbocharger in another.

This prototype engine is designed to replace the turbocharger with a bigger, more efficient one. The previous turbocharger was removed to enable the engine's exhaust gas to pass straight from the cylinders to the new turbocharger. This link more precisely simulates real-world operating circumstances and may be tweaked to include just individual cylinders in the exhaust flow in order to compare their pulsing content. Additionally, if a smooth yet non-pulsating flow of exhaust gas is needed, it may be channeled via a settling tank, where it will be smoothed down and result in the continuous flow.

The pulsating flow characteristics investigated in this thesis complicated the development of aeroacoustics technologies. Continuous-flow jet noise was used in the test rig and anechoic chamber. However, Chapter 5 validates the suggested approaches and obtains adequate findings using real-world engine conditions.



Engine core, asynchronous dynamometer, screw compressor, and air distribution system with control valves and reservoirs are shown in this flow rig diagram shown in Figure 5.

The compressed air can be distributed between the engine's intake and the exterior circuit using a second reservoir with a discharge valve. This can be directed to another chamber or silenced and vented to the outer environment. A water intercooler decreases the temperature of compressed air, allowing for greater control of flow qualities at low temperatures. This temperature, as well as the compressed air's other flow parameters, are recorded by a control system. The engine and dynamometer are controlled by separate instruments, and the turbocharger variables are recorded in real time and saved on a In this case, we are talking about the Yokogawa DL716 DAQ.

2) An echo-free Room

The anechoic chamber at Laboratory 5K is a great thing. spanning 9.5 9 7.2 meters in length and insulated from outside vibrations. The chamber was designed by architect Jorge Selaron, and its inside walls are made up of 0.8-meter-long fiberglass wedges with a 0.2-square-meter base. The internal area created by these wedges is roughly 7.5 meters long, 6.5 meters wide, and 6 meters tall.

The acoustic environment in this chamber is certified to have no reflections from the walls below 100 Hz. Low-frequency waves are likely to start reflecting at this point. Optimally sound and vibration-isolated, the grated floor is beveled to the floor wedges and provides a smooth, comfortable working surface. The four large steel pillars keep engines (and other heavy equipment) from damaging the floor while supporting a substantial load.

While the turbocharger was being tested, the load-bearing pillars were left unobstructed to avoid any interference with measurements. Figure 4 clearly shows how this lightweight turbocharger was installed in the testing frame.

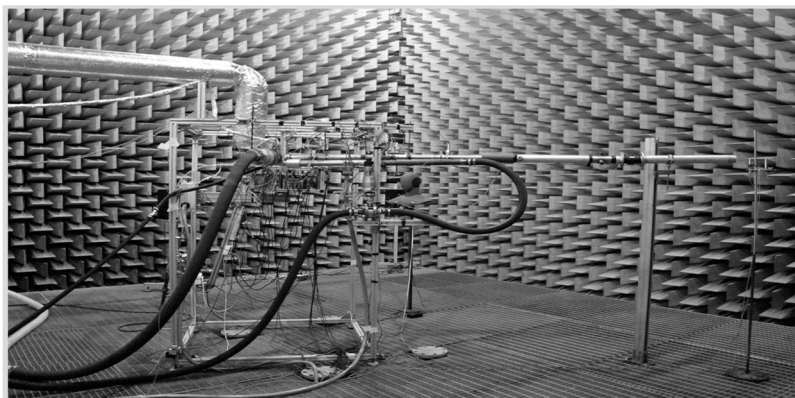


Figure 6: The interior of the anechoic chamber reveals the turbocharger setup and pipes required to operate it.

The pneumatic turbine is used to allow the turbocharger to operate. Compressed air is fed into the turbine from a flow rig that was talked about in a previous section. It then goes through a reservoir with a nozzle, which slows down the airflow and reduces the noise it makes. It takes the air from the chamber and sends it through a pipe to the extra room. Closed-loop oil reservoirs are located under the pipes, which supply the cooling jackets for required sensors. Cooling water is also provided to those circuits.

The control system monitors and gathers data, such as pipe pressures, temperatures, mass flow, compressor speeds, and system conditions. The oil temperature is regulated, the compressor operation settings are changed for various applications, and a Yokogawa DL716 DAQ system is used to record the dynamic pressure.

3) In this case, the Eddy Current Dynamometer is used to measure how much electricity is

Dynamometers are used to measure power, which may be used to determine the efficiency of turbocharger turbines. Small turbomachines, such as turbocharger turbines, need a dynamometer to run at very high rates, often 100,000 to 200,000 rpm. The dynamometer's rotating portion must be light in weight and have a low polar inertia; otherwise, the turbocharger's bearing system would fail. The power range needed of the dynamometer is enormous due to the diverse working circumstances of the turbocharger turbines. When using quasi-steady techniques to simulate the pulsing flow conditions in the engine manifold and turbocharger, a turbine map with a broad range of operating circumstances is necessary. A conceivable approach for obtaining such a map is to load the turbine using the turbocharger's compressor; however, due to the compressor's surge and choke margins, the range of data obtained would be inadequate. As a loading device, an eddy current dynamometer provides a far greater range of tests without the aerodynamic restrictions of the compressor it currently replaces. The immediate performance of a turbocharger turbine does not follow the steady characteristic curve (7) because of the pulsing inflow situation; instead, a hysteresis loop that encircles the steady result is formed. It is necessary to know the polar inertia of the rotating assembly of the dynamometer in order to determine the instantaneous torque or power of the turbines; hence, an eddy-current based dynamometer is preferable than a hydraulic dynamometer. Furthermore, due to the lightness of the dynamometer utilized, the turbine's immediate performance may be monitored without significant dampening effects. Because of the large demagnetization field created by eddy currents, permanent magnet technology could not match the criteria of turbocharger dynamometers in the past. Rare-earth magnets, such as Neodymium-iron-boron magnets, have become viable in dynamometers due to their great resistance to demagnetization. Eddy-currents are created inside a conducting disk when it is subjected to a changing magnetic field caused by the relative motion of a permanent magnet translating over its surface. These eddy-currents produce their own magnetic field that opposes the source field, causing reactive pressures on the magnet. Both a repulsion and a retardation force, both forces are present. The dynamometer takes use of this latter force; the retardation force multiplied by the relative velocity equals the power received by the dynamometer. This power is also the amount of heat that must be evacuated from the stators in order for the system to remain stable. The dynamometer idea is shown in Figure 2 as a simplified form. The dynamometer uses eddy-current braking to create a low inertia axial flux rotor by integrating Neodymium-Iron-Boron magnets in a spider. The rotor is made up of 14 ground Neodymium-Iron-Boron magnets with a depth of 10mm.

To make a 14-pole axial flux rotor, they were arranged in an aluminum spider with alternating polarity. This rotor rotates in the same direction as the stators, which are stationary water-cooled conducting plates on each side of the rotor (Fig. 3). Externally, a carbon-fiber ring with an overall diameter of 80mm was utilized to support the magnets, while a central steel spigot was employed to establish the requisite interference fit in order to lock the magnets in place. On each side of the rotor, water-cooled stators were installed. This enables for more power to be dissipated while also addressing the issue of axial thrust caused by eddy-currents. A stepper motor system was used to regulate the movement of the stators from a distance. The power that the dynamometer absorbs may be changed by changing the space between the stators and the rotor. This setup involves extremely few parts and results in a mechanically simple, inexpensive, and compact design. The stators were cooled with untreated water flowing radially across their rear surface at a rate of around 35 liters per minute. The coolant enters and leaves the rig axially to avoid interfering with the torque measurement and so does not contribute to the observed torque. By putting the whole system freely on a pair of gimble bearings, the torque was measured immediately. The torque generated by the turbine is determined by a lever arm attached to the free-floating components reacting against a load transducer (minus the resistance torque of the gimble bearings).

4) Active Control Turbocharger

For VGT testing, a spout less Holset H3B turbocharger turbine was changed in accordance with take a spout. An uncommonly unstable (1.5mm thickness) portion, adjusted shape, sliding spout was created due to the limited area gave. Two minimal bearing pads, which fit between the spout and the actuator arm and help with deciphering the transforming advancement of the weight into an immediate development by the spout, are used to mount the spout on to its affecting arm (trouble) through two embedded association centers towards the back end (away from the volute).

An internal assistant, which goes probably as a direction surface for the spout as well as the exducer a piece of the turbine, coordinates the spout towards the throat. The total get together is housed in an external aide, which is molded into a section at its base end, to which the burden is connected and may uninhibitedly turn. Six long M5 bolts keep the entire get together intact and interface it to the turbine's face. The turbine's throat width is 26mm, and the spout might block around 22mm of that stream width prior to arriving at the stops.

Aside from the spout, the entire framework was fabricated of 6082-T6 aluminum compound, which was lightweight and sufficiently able to endure weariness (on account of the burden), which was a significant concern during activity. The burden accomplished a security element of ten as far as the greatest twisting power applied to it at its corners during the most extreme activity by the bearing cushions. The spout was built of CFRP, which offered sufficient protection from the high tension wind stream utilized during testing while at the same time keeping a very light weight, which is basic for the ACT's general power execution. In ACT mode, the spout was driven by a V406 electrodynamic shaker. The shaker was utilized to give the power expected to accomplish the ideal frequencies and amplitudes during testing (60Hz and 20mm, individually).

Since the spout was driven from the turbine's exhaust side, an immediate association between the shaker and spout was unrealistic, requiring the shaker being counterbalanced to the side of the exducer. The most straightforward way for driving the spout from this position was to utilize a solitary piece, turning fork-type actuator arm.

This works on the plan, makes it more smaller, and above all, further develops exhaustion perseverance fundamentally, with the additional advantage of critical vibration damping because of the rocker-arm type activity of the burden used to drive the spout, which to a great extent hoses out what might somehow or another be serious turbocharger vibrations. The complete mass of every moving part (Parts 2, 3, 4, 8, and 9) is just 0.241kg, which was important to accomplish the power execution expected for testing, even to the detriment of vibration, since it is presently difficult to adjust the two sides of the burden because of the top part's (spout) fundamentally lighter load than the base part, which likewise contains around 0.2kg of the shaker's moving part.

5) Test Rig for Engines

An engine test cell was utilized to conduct further tests under genuine engine circumstances to evaluate the measuring methodology's dependability. An asynchronous electromagnetic dynamometer is included in the test cell described in detail in [69], which enables for continuous and transient automated testing. Fuel consumption, engine speed, and exhaust readings are all integrated into the dyno's four control systems. A new turbocharger and intercooler were also added to the EA113 engine. A pneumatic system downstream of the turbocharger can feed compressed air into the inlet manifold, delivering an additional boost during acceleration from a standstill.

By push the air into the intake manifold through a solenoid valve, the compressor's air inlet pressure is decreased. This allows the engine to have a high turbocharger boost while lowering harmful intake air temperatures. The device was utilized to simulate compressor surge circumstances throughout the investigation. Two DAQ systems were used to collect test cell acoustic data, one from Yokogawa and the other from Brüel and Kjaer. A pressure-noise intensity probe of type 4197 was employed. The results of the acoustic measurements were backed up by sensors and other equipment placed to the test cell.

B. Tested Turbochargers

The features of the facility and project mandated the usage of a range of turbochargers for this inquiry. However, in terms of size and intended use, they're all the same. The Garrett GT17 Series, which is utilized in chapters 3, 4, 6, and 8.1, is the most significant model. To acquire precise geometry, a turbocharger with six main blades and six splitter blades with a vaneless diffuser was digitized. Figure 3.5 depicts the most important dimensions. Engine testing in Chapter 5 and Section 8.2 and Chapter 7 and Section 8.3 employed two comparable turbochargers. All three were altered to accommodate various intake geometry.

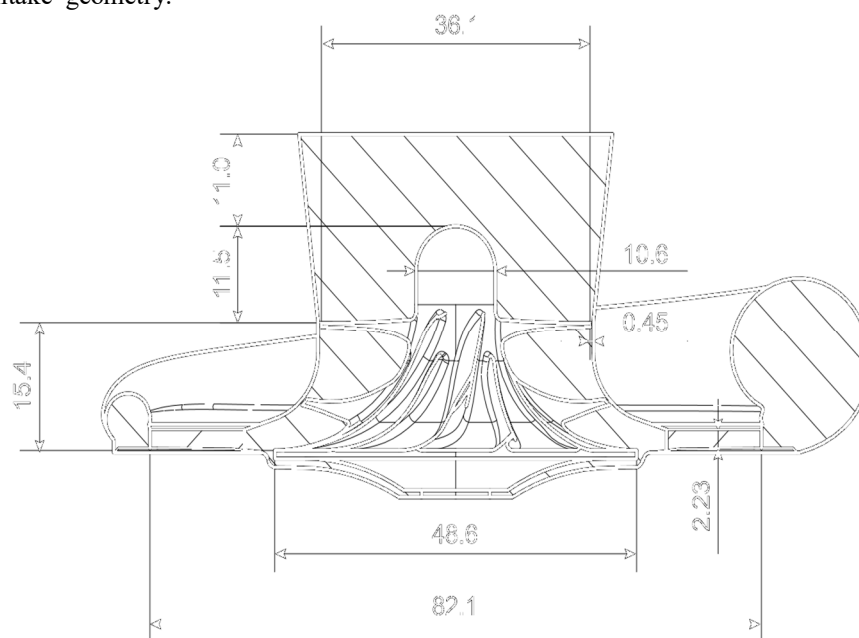


Figure 7: A dimensional design was employed for the majority of the experiment's development and some key dimensions.

C. Noise Measuring in the Ducts

This chapter discusses the shortcomings of existing literature on the thesis. We then propose an experimental methodology that addresses these shortcomings. We propose a methodology that enables you to evaluate the overall noise emissions of a turbocharger system. Although compressor manufacturers occasionally provide noise maps, they seldom provide a step-by-step process for replicating those maps. The literature on turbo-compressor noise consists of various techniques, from in-duct approaches [23] to noise measurements with commercial sound meters [36]. A limited number of resources focus on the implications of using specific measurement techniques (e.g., flow incidence angle) to investigate their phenomena of interest (e.g., source characterization).

1) The theoretical framework

The first step is to evaluate the theoretical basis for measuring acoustic output in ducts with mean flow and to choose experimental data collection techniques for implementation. The TMM is a well-known technique for digesting acoustic waves in ducts. As mentioned earlier, this breakdown occurs within the plane wave frequency band.

Beamforming is a well-known signal processing technique that is often used to locate audio sources. Indeed, beamforming can be utilized as an emission technique rather than a reception technique, which is why the term "beam generation" was coined. Emitters should be separated by a predetermined distance. Energy can be "steered" through the array by sending the same signal with a phase mismatch. Weighting is applied to sensor signals in order to prioritize energy received from a certain direction. As a result, beamforming can be thought of as a type of spatial filtering. Pinero et al. used it to determine the fluctuations in exhaust velocity. Torregrosa et al. utilized it in the ductwork of turbochargers.

a) Flow ducts' volume of sound

Detecting the scalar sound pressure level (SPL) with a single sensor provides an approximation of the sound intensity level in a duct. (SIL) is required to quantify the total amount of sound energy moving through the duct [36].

Consider the effect of a point's shape, as well as nodes and reflections inside a duct, on the sound pressure level at that location. The intensity of sound is often described as a vectorial magnitude that accounts for the fact that the source of sound will vary somewhat, causing interference, but will never reach zero. Noise pollution intensity is a more reliable measure than pressure level.

The differential pressure between two points on a duct is often used to estimate the intensity level.

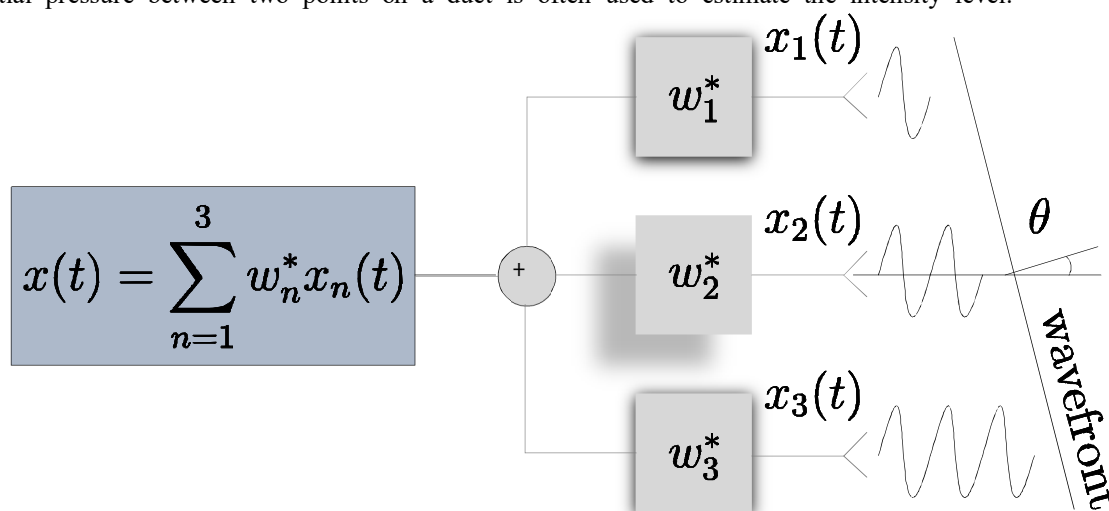


Figure 8: Three elements tuned to a specific angle (θ) can be combined to form a narrowband beamformer.

The Fourier transform is often used to obtain information about signals acquired at discrete time steps. Specifically, superscript k denotes the Fourier transform of a signal acquired at step k . The narrowband procedure is then followed for each frequency component to obtain the desired signal through the inverse transform finally:

Here, $X(f_k)$ is the $k \times n$ matrix of transformed signals, and $w^H(f_k)$ is the weights matrix for each frequency. Several schemes can be used to compute the optimal weights for the desired DOAs ($\theta = -90^\circ$ for downstream and $\theta = 90^\circ$ for upstream waves, assuming a typical flow DOA of $\theta = 90^\circ$).
 $x(t) = F^{-1}\{w^H(f_k)X(f_k)\}$ 3.3.4

We used a Linearly Constrained Minimum Variance (LCMV) beamformer in this study, a well-established procedure that minimized the overall output power (variance) while maintaining unitary gain in the precisely targeted direction. The beamforming approach described in annex 3, A can be used to compute $w^H(f_k)$ and thus X^+ and X^- . The result of this decomposition is shown in Figure 7. Piñero et al. [84] applied this method to compare the various schemes against simulated and experimental data.

2) Procedure for the Experiment

The turbocharger used in the experiment is mounted on a 1.1-litre petrol engine with 16 valves. Engine testing was conducted in two phases. Stabilized points and ramps capable of carrying a full weight should be ascended. The ramps from 1000 to 6000 rpm were 100 seconds long. Data from all four branches of the turbocharger's mass flow and temperature sensors was gathered in order to trace the whole load ramp. The sensors were separated by a distance of 35 millimeters. The distance between the source and the decomposition zone should be several diameters in order to ensure the propagation of plane waves (between 4 and 10 diameters). This was not the case with this work, though. A working engine necessitated the use of small measurement tubes, therefore this was crucial. The turbocharger gas stand tests were conducted in two stages for the engine testing. The first step was to create a detailed compressor map, together with the acoustic power in each operational location. In order to replicate a turbocharger functioning at full capacity, the gas stand was used. Consequently, during engine ramps, it was vital to determine where the turbocharger was actually working. To do this, the total-to-total compression ratio and the changed mass flow have to be calculated. It is crucial to remember that mass flow, but not rotating speed, must be adjusted for temperature changes. Due to the fact that rotational speed is directly related to auditory phenomena, the recorded rotational speed is used to calculate the corresponding frequencies. After identifying an effective technique for detecting in-duct noise, engineers must determine how to best execute the methodology for their experimental setups, gather measurements, and analyses the resulting data.

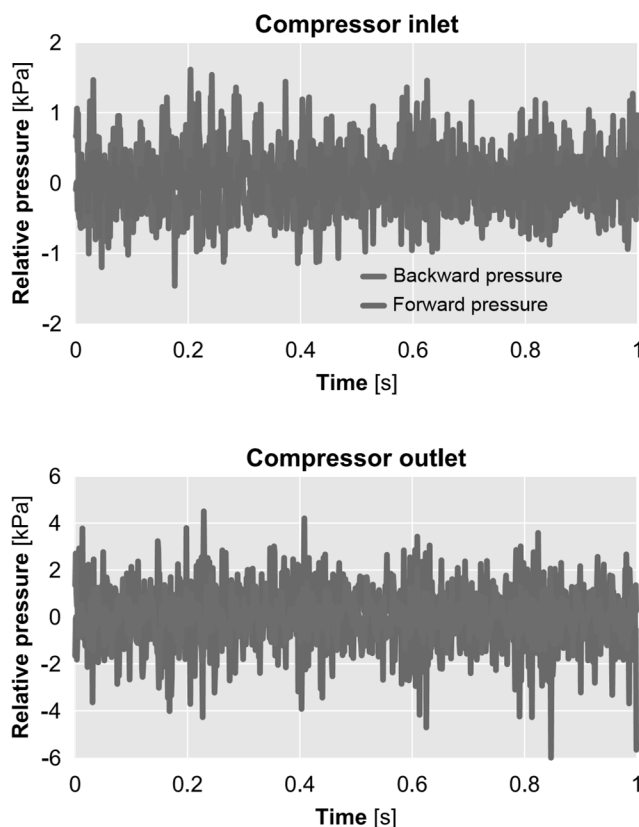


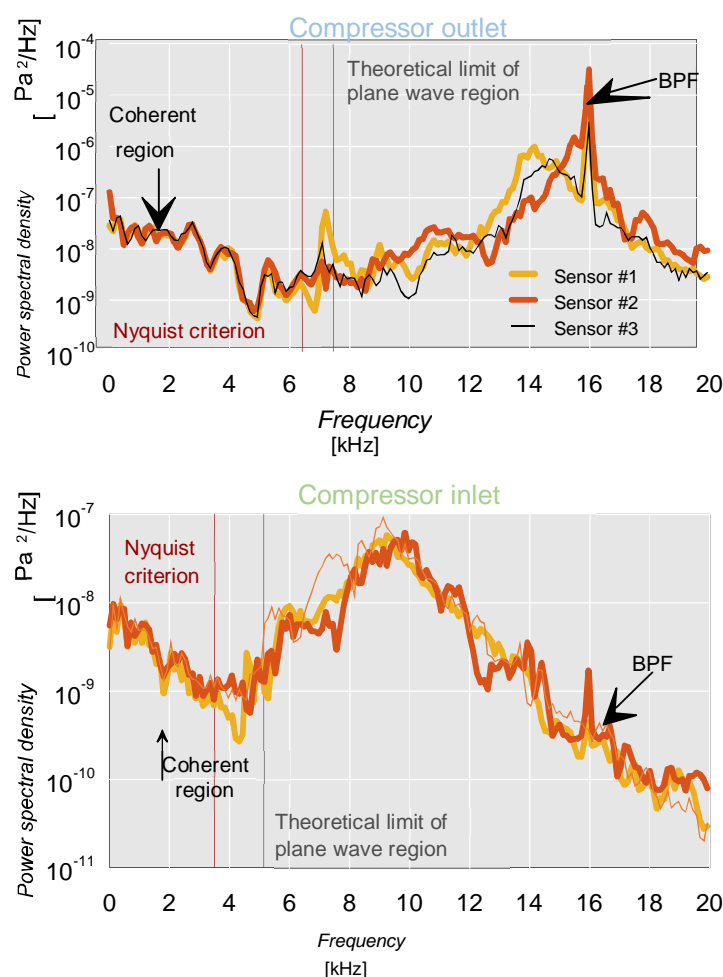
Figure 9: Pressure wave amplitudes travelling forward (towards the compressor) from the inlet are smaller than those flowing backwards (towards the inlet). At the output, the pressure waves are reversed.

Due to logistical issues, the engine results only show the TMM results, as previously stated. The Power Spectral Density in dB as a function of frequency is shown in Figure 9. The dotted vertical lines correspond to the frequency limitations for TMM use as indicated by criteria (500 Hz and 4000 Hz). The biggest peaks around 3 kHz correlate to the turbocharger's rotating speed. Cut off frequencies are different even if both curves are at the same stable point. This is due to the fact that the air temperature at the outflow is greater than the air temperature at the input.

The corresponding sound velocity and Mach numbers vary, and both are crucial factors in calculating the cut-off frequency as illustrated in equation. Because of compression, the outflow level is greater than the input level, which is typical. Another noteworthy finding is that at low frequencies, peaks show slightly below 500 Hz for engine results but not for gas station findings. In principle, TMM and beamforming are both effective approaches for plane wave decomposition. Simulations in an ideal environment confirmed this. When comparing test results, the beamforming, on the other hand, has a greater connection to our reference intensity. On the other hand, when frequency is a multiple of half the wavelength, the beamforming solution seems to escape TMM's over estimating difficulties. Tests on the engine bench and on the gas stand were completed satisfactorily. On engine stable points, the curves of Intensity Spectral Density were calculated. On the gas stand, the true turbocharger behavior during a full load ramp was effectively replicated, with sound intensity values that were realistic. The findings of the global acoustic intensity compressor maps are satisfactory. On the engine bench, the beamforming technology still has to be tested. The use of plane wave decomposition for calculating transfer or scattering matrices of turbochargers, as well as acoustic devices under mass flow and temperature characteristic of an engine, is another research field.

a) Instrumentation for Turbochargers

The quick pressure sensor arrays' design and installation are crucial for achieving reliable experimental findings. To prevent complicated structures induced by singularities, the pressure sensors should be installed in straight pipes with diameters selected to maintain the cross-sectional area of the nearby duct. Figure 8 shows an example of the predicted pressure spectra findings.



Exit pressure power spectral densities are shown in Figure 10, with the frequency restrictions indicated in Equation 3.3.6 and Equation 3.3.7. The frequency of the blade passage can also be determined using spectra.

Figure 9 shows the straight-line clearance left in front of and behind a transducer array [89], to ensure that the flow through the measurement section at the center of the array is essentially plane wave. Straight clearance should be at least 6 diameters upstream of the array and 4 diameters downstream, according to Torregrosa et al., [90].

To avoid errors in the low-frequency and high-frequency bands, transducer positions should be chosen such that nodes of the standing wave do not fall on one-fifth or one-third of a wavelength away from them [91]. Transducer positions should also be spaced far apart enough to account for the wavelength at low frequencies [92], but close enough to account for the wavelength at high frequencies [93].

In particular, it should be noted that any signal with a frequency greater than the Nyquist frequency imposed by the distance between the sensors will not be sampled correctly. For example, consider an underwater wave with a DOA θ and speed passing two (2) consecutive sensors spaced by a distance d_s :

$$T_d = \frac{d_s \sin \theta}{a} \dots\dots\dots 3.3.5$$

To prevent high-frequency spatial aliasing, the product of Ωd should be half the frequency $f_d = 1/T_d$ associated with T_d .

$$f_n \leq \frac{f_d}{2} = \frac{1}{2T_d} = \frac{a}{2d_s \sin \theta} = \frac{a}{2d_s} \dots\dots\dots 3.3.6$$

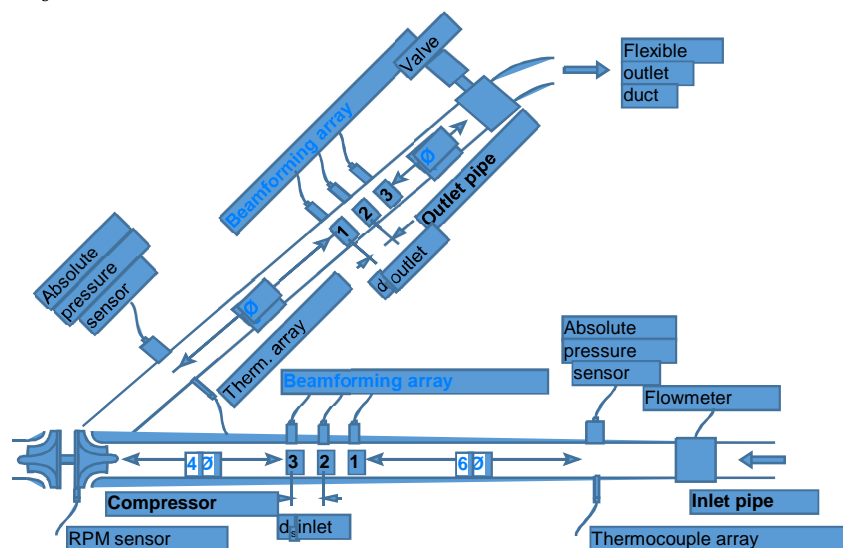


Figure 11: This figure illustrates the proposed turbocharger instrumentation setup. Color indicates the location of each three-sensor beamforming array. This figure also shows clearance requirements for beamforming arrays using a cylindrical waveguide.

According to Eriksson [94], pressure waves in a duct propagate in a planar manner at low frequencies (i.e., the pressure is the same at every point along the cross-section of the duct). This cutoff frequency may be approximated using equations 8–12.

$$f_a = 1.84 a/D \sqrt{1-M^2} \dots\dots\dots 3.3.7$$

To begin, the variables are as follows: a represents the sound speed, D represents the duct diameter, and M represents the mean Mach number. As frequency grows, the first asymmetric propagation mode increases as well, until a cut-off frequency of X is reached; beyond this point, the first circular mode propagates.

$$f_a = 3.83 a/D \sqrt{1-M^2} \dots\dots\dots 3.3.8$$

Special attention should be given while calculating limiting frequencies, since they fluctuate with temperature and mass flow. Both limitations are shown in Figure 8 for a particular operating point. The Nyquist criteria is shown in this graphic to determine the precise moment at which discrepancies between sensors begin to rise. For multi-sensor decomposition, this criteria is more restricted than the acoustic mode onset.

Additionally, picture 8 illustrates other occurrences, such as Blade Passing Frequency (BPF) tonal noise, which was covered in Chapter 2. As seen in Table 2, the primary BPF may be determined by taking the shaft speed and the number of primary blades into account.

160 krpm/60 s min 6 main blades 16 kHz BPF 3.3.9

The closer the sensors are positioned to improve the frequency resolution, the lower the spatial resolution of low-frequency waves will be. With very long wavelengths and diminishing disparities between subsequent sensors, the discrepancies between consecutive sensors may be as small as the noise threshold.

Regardless of how your linear array's sensors are mounted, it is vital that the signals from each of them be coherent. Before installing the sensors in their final configuration, test each sensor in the same section of duct by mounting them radially and calibrating them individually to ensure that any differences between sensors are due to wave propagation through the duct and not to individual transducer-to-transducer differences.

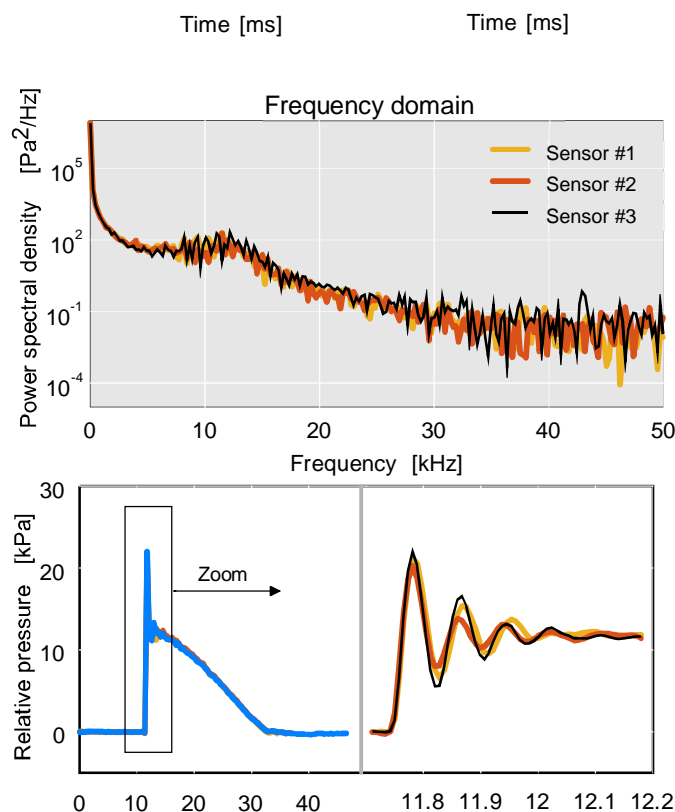


Figure 12 shows that the outlet sensors in an impulse test rig had an outstanding pressure-speed match across the entire range of their calibration.

The offset and gain of pressure transducers are calibrated in an impulse test setup, as described by Payri et al. [95]. This is accomplished by having each sensor watch a waveform, measuring the time and frequency responses, and adjusting the amplifier offset and gain to achieve the optimum match. The compressor's operating conditions map displays how the compressor will function under various scenarios by utilizing a total-to-total pressure ratio (TT) and a corrected mass flow (m) axis.

b) Measurements of the Steady State

It is common practice to use the back-pressure valve (as depicted in Figure 9) to limit airflow until the appropriate mass flow is achieved while testing the operating points of a compressor map. It is necessary to modify the turbine power at the same time in order to maintain the prescribed corrected compressor speed (N) and to maintain stable operating conditions. The valve will be opened when the compressor blades stall, disrupting the compression process, and the compressor will enter another constant corrected regime line until it reaches the required area of the compressor map.

The vertical wind shear adjustment should be implemented in line with the reference circumstances, which are specified as one day at 15oC and 1 atmosphere at mean sea level.

$$M^* = M \sqrt{\frac{101325}{P_T} \sqrt{\frac{T_T}{288.15}}}, N^* = N \sqrt{\frac{288.15}{T_T}} \dots\dots\dots 3.3.9$$

In this example, R denotes the ideal gas constant for air, ρ and T are the density and absolute temperature of the air, p is the atmospheric pressure, U is the duct velocity, A is the cross-sectional area of the duct, and cp is the specific heat of air. To calculate compressor performance using this map, one must convert pressure ratios to total-to-total pressure ratios by subtracting ambient pressure from both sides of the balance. Once this is done, standard day correction should be applied to each total-to-total pressure ratio. Figure 3 (bottom) shows recorded data points after applying normal day correction.

$$\rho = \frac{p}{RT}, U = \frac{M}{\rho A}, T_T = T + \frac{U^2}{2c_p}, P_T = P \left(\frac{T_T}{T}\right)^{\frac{\gamma}{\gamma-1}} \dots\dots\dots 3.3.10$$

3) The Experimental Facility

The Research Competence Center for Investigations on Internal Combustion Engines has created a laboratory for turbocharger characterization. The facility's objective is to precisely monitor scattering data—the factors that govern how much air will flow through a turbocharger at a given pressure—under actual operating settings chosen from compressor and turbine performance charts. Additionally, the facility may be utilized to determine the turbocharger's sound output (the active property).

An experimental rig was constructed to investigate the transmission of sound through and the generation of sound from a functioning automobile turbocharger compressor and turbine. The rig is divided into two sections: a compressor section and a turbine section, either of which may be examined using any operating parameters selected from the manufacturer's operating charts.

A turbocharger is coupled to an air compressor for equipment testing. While the turbocharger's design allows for a broad variety of applications, the compressor's particular working circumstances (high flow rate with minimal variations) make it ideal for acoustics testing. Because the system is remotely controlled, all maintenance and care may be performed without disrupting test employees or active research. A system of air compressors, air warmers, and ball valves has been fitted to boost the turbocharger's output. This permits higher boost pressures and more effective lubrication of the turbocharger bearings.

The air mass flow that powers the turbocharger turbine originates from two distant industrial compressors. For high-mass-flow testing, an 18 kW electric heater is used to raise the air temperature. The compressor output pipeline's boost pressure is adjusted electronically through valves in the operators control module (SOMAS A13-DA). An autonomous portable lubrication system is used to provide pressurized oil to the turbochargers being tested at the acoustics facility.

Turbocharger component acoustic models must adhere to real-world operating parameters.

This section contains performance maps for all turbocharger components utilized in the research, as well as the operating points examined. The table below summarizes the features of the operating points for compressors and turbines that were evaluated. Divide the compressor's absolute total output (discharge) pressure by the compressor's absolute total intake pressure to get the compressor pressure ratio. Corrected mass or volume flow rates through the compressor and turbine were estimated using centrally mounted Pitot tubes and a mass flow meter (ABB FMT500-IG).

To emulate the working circumstances of a turbocharger, the compressor and turbine mappings must be followed. The compressor and turbine maps demonstrate that the dynamic parameters of the operating points (OPs) are located on the compressor map and consist of at least two of the following three characteristics: pressure ratio (PR), mass flow rate, or volume flow rate. Using Pitot tubes, a mass flow meter (ABB FMT500-IG), and an absolute total intake pressure sensor, the dynamic characteristics are utilized to determine an operating point on the compressor map.

The thermocouple devices were used to determine the flow rate, pressure, and temperature in the pipes. The mass flow through the ducts was used to calculate the density of the air. The speed of sound in air at normal pressure and temperature was calculated using a National Instruments 9211 module—a purpose-built instrument for this purpose. Transmission loss values were determined using data collected during test sessions. To monitor the rotation of the turbocharger shaft, an eddy-current speed sensor capable of recording signals from revolving blades was utilized.

The test was conducted using pressure transducers located at the inlet and outflow cross-sections. Temperature measurements were taken using the thermocouple input module and K-type thermocouples installed in the middle of the ducts. During the test sessions, a speed sensor of the eddy-current type was focused onto the compressor wheel blades to determine the turbocharger shaft rotational speed (Micro-epsilon turbo speed DZ135). To evaluate the transmission loss of a turbocharger, speed data were collected in two pipes using eddy-current sensors fifteen inches apart. Transmission loss data were derived using the density and sound speed measurements obtained during those observations.

D. External Noise Measures

The transmission of engine noise to the cabin can be reduced by improving the accuracy of the internal sound fields. To that end, a series of experiments captured data at various locations in and around the turbocharger. This section discusses how the measurements were made, and explains results and discussions of the sections on orifice and in-duct noise in Chapter 4. Chapter 5 also includes a short discussion of an acoustic particle velocity measurement technique that was used throughout this investigation (in which a sample of findings are shown). The turbine and compressor's gas-flow dynamics are calculated using the software 'Star-CD,' which is based on a three-dimensional gas dynamic simulation (CFD). The objective is to determine how a variation in the turbine and compressor wheels impacts the gas flow's pressure excitation and the accompanying gas forces on the wheels. Additionally, the gas forces are used as an input to a multibody simulation in order to determine the structural excitation caused by the gas flow. The two forms of wheel deviation are a precisely parallel offset in the bearing clearance caused by imbalance and an angular deviation caused by rotor bending. Both deviations spin in lockstep with the rotor.

1) The orifice produces a lot of noise. The orifice produces a lot of noise.

The sound that comes from the compressor's input duct is essential because it serves as a link between the compressor's internal and external sounds. and it may have to battle with other sources of noise regardless of whether the compressor is operating. When evaluating external noise, it's important to keep in mind that reflections and other ambient factors might skew results. The turbocharger was selected to be installed within an anechoic chamber to overcome this problem. The turbocharger acts as a silencer, allowing for precise noise levels to be measured outside.

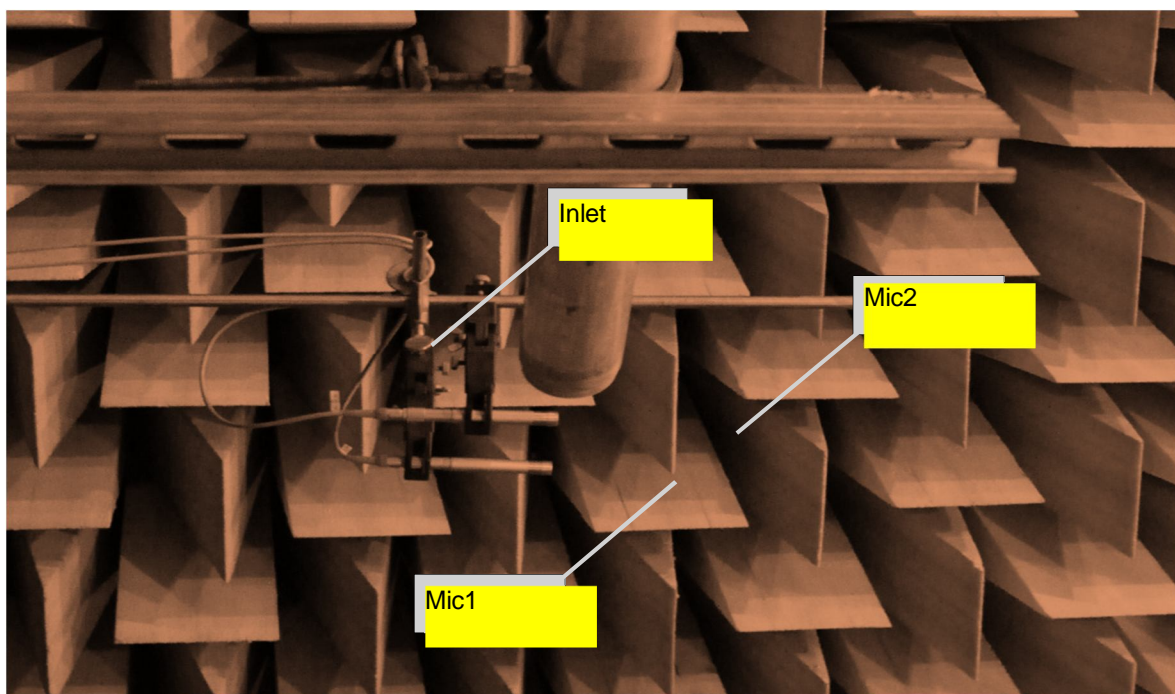


Figure 13 shows the drop in acoustic pressure when the compressor is activated by placing two free-field microphones, Mic 1 and Mic 2, 10 mm and 20 mm from the inlet duct's orifice, respectively.

Using two 1/2" Brüel & Kjaer type 4190 free-field microphones equipped with type 2669C preamplifiers and positioned next to the compressor input orifice, a spacing of ten centimeters was established between mic 1 and twenty centimeters between mic 2. Prior to the studies, a Brüel & Kjr type 4228 pistonphone was utilized to calibrate these microphones. Calibration and data collection were performed using a Brüel & Kjr PULSE system. Due to the fact that the circumstances within the anechoic chamber are identical to those in an acoustic free field, we estimate the sound intensity at each microphone as follows: $|I| = (P^2_{rms} / \rho c)$

This graphic depicts the root mean squared pressure as measured by microphone 1, which was positioned at a temperature of 22°C. Ambient pressure and sound velocity were determined using sensors mounted on the microphone stand.

$$|I_i| = \frac{P^2_{rms} S_i}{\rho c}$$

2) Far-field

Turbocharger group measurements were conducted in an anechoic enclosure to remove the reflections from the chamber walls. Additional microphones were mounted at various locations around the equipment for free-field measurements. The results were then compared with Teng and Homco for a whole engine [16]. Four microphones of the same type 4190 were placed at the center of the installation, equidistant from each other, at 1 m from it. To measure the noise generated by the turbocharger, four microphones were placed at various distances from it. The output of each microphone was recorded on a Brüel & Kjaer PULSETM DAQ system, composed of hardware and software supplied by Brüel & Kjaer. The overall noise level of the turbocharger was then calculated based on an average of the four measurements.

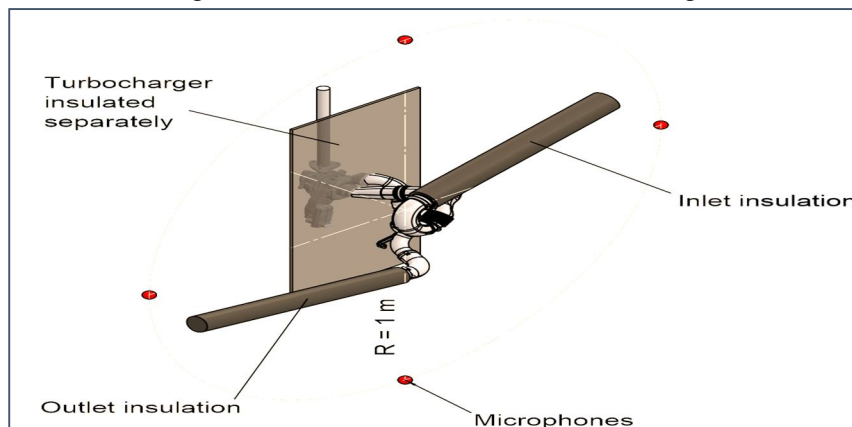


Figure 14: A radiated noise microphone is utilized in this experiment. Commercially available compressor input and outlet pipes are being fitted around the turbocharger, which will be sequentially insulated so that each part can be evaluated.

3) In close proximity

Even though free-field microphones can be used to measure the far-field noise information coming from an engine's turbocharger, successful measurements depend on having suitable acoustical conditions for the test ambient. Standard engine test cells and test rigs are not acoustically conditioned, which means that often times interferences and reflections from room furnishings are problematic. Such issues become more problematic when near-field measurements are desired, as ambient noise and reactive sound fields [98,99].

A technique for addressing these issues is directly measuring acoustic particle velocity level (PVL) with a MEMS sensor. MEMS sensor probes are now commercially available from Microflown, which has produced a probe featuring a MEMS sensor.

In chapter 5, the probe described in [101] will measure engine noise inside a standard engine cell. The measurements will be compared with those obtained from a pressure probe to assess the usefulness of the acoustic intensity probe [102]. Applications include acoustic holography for near-field situations [103] and panel-based noise evaluation in automotive cabins [104].

E. Component Selection and Product Subsystems

1) Turbocharge Selection

A turbocharger for a system is perhaps the essential decision in the entire procedure. When shopping for a turbocharger, choose one with nice features that simplifies your engine's system design and plumbing. Furthermore, make sure to avoid turbochargers that increase the engine's power while giving challenges over system design and plumbing. When choosing a turbocharger, the size of the unit must be taken into consideration. However, several other factors, including the noise level, durability, and efficiency of the turbocharger, should be considered carefully. After a lengthy process of compromises and trade-offs, the team ended up with a turbocharger that fit their specific needs.

The main idea behind turbocharger matching is to optimize the compressor and turbine combinations in order to achieve the desired boosting characteristics for a given range of engine operating circumstances. The compressor efficiency should ideally be at its highest in the engine's primary working range at full load. In addition, the distance from the surge line should be as great as feasible. The turbocharger and engine model are built to achieve this goal. If an analytical approach for estimating engine performance with several turbochargers is available, real engine testing may begin with various turbochargers that are near to the optimal fit. The development time and, as a result, the cost is decreased. To establish the working conditions of the engine, various characteristics are assumed at the beginning. As a result, in a large number of iterations, the most parameters will be determined from the created program using the FORTRAN language. At each integration step, the manifold pressure and instantaneous turbocharger speed will be anticipated, and the mass flow rates, and efficiencies of the compressor (or turbine) will be calculated using the turbomachinery performance maps. Because many estimations of key parameters are necessary, the computations will be iterative. The following is a common technique for turbocharger matching on a heavy-duty diesel engine:

- a) Calculate the compressor's pressure ratio (P_2/P_1).
- b) After assuming a realistic value of compressor efficiency, the ideal gas law is utilized to compute the input manifold temperature T_2 and air density.

Three distinct turbochargers are looked at: the HX80, the HB3, and the HX40. The wind stream needs length a more extensive area of the blower map since substantial diesel motors run over a wide speed and burden range. Figure 3 shows a regular motor wind current superimposition on a blower map, with lines of consistent motor speed (1000, 1200, 1400, 1600, 1800, 2000, and 2200 rpm) for different sorts. The three guides plainly show that the HX80 type is a suitable choice, since the working locale is found away from the flood line and in a high-effectiveness zone. At the point when the heap is changed at consistent speed, be that as it may, practically identical way of behaving is seen, with a lower pressure proportion up to 2.7 and diminished turbocharger proficiency; with working conditions having a protected edge from the flood line and close to the chock line, especially at low part load up to 25%. The HX80 type is leaned toward in light of the fact that the functional area is liberated from flood and chock lines, and most of motor speed lines are situated in the high-proficiency zone, with a reach working tension proportion of 2:4.5 and a normal worth of 3. The blower's motivation is to expand the strain before the motor's feedback complex, not to upgrade the temperature of the air. Subsequently, the effect of having an intercooler will be explored to see whether it very well may be disregarded to limit motor size. The air mass stream rate increased by 1.7 percent because of the intercooler, which is irrelevant and might be overlooked, empowering the motor size and parts to be diminished. This additionally diminishes turbocharger upkeep and makes the motor more proper for more modest motors.

2) Turbocharge Dimensions

Vehicle makers first looked into the possibility of turbocharged engines in the 1950s, but the problems of "turbo lag" and turbocharger size weren't yet resolved. The first turbocharged vehicles were the Chevrolet Corvair Monza and the Oldsmobile Jet Fire, both of which were debuted in 1962. After the 1973 oil crisis and the 1977 Clean Air Act amendments, turbocharging became increasingly common in automobiles as a means of reducing fuel consumption and exhaust pollution. The turbocharger's compressor and turbine components must be properly designed so that the compressor can supply enough airflow and the turbine can meet the engine's power requirements. Engine displacement, airflow, horsepower requirements, and turbocharger design objectives must all be considered throughout the selection process. Turbochargers begin to produce boost when the exhaust gases have enough kinetic energy. If there is not enough exhaust gas flow to turn the turbine blades, the turbocharger will not be able to compress the air entering the engine. There are a number of factors that affect the boost threshold.

At the "boost threshold rpm," there is enough exhaust gas velocity to compress the air entering the engine at that operating speed (rpm). Throttle responsiveness may be improved by lowering the "boost threshold rpm."

Finally, all outlets and inlets should have their connections checked. The compressor intake and output will very indeed be built to accept a hose clamp. If that is the case, they have a lip to help clamp them down. Their diameters are standardized to allow for the purchasing of standard-sized hoses. The bearings portion will almost certainly have an oil inlet and outlet, although it might also have one. These inlets and outputs should be evaluated to see how simple it will be to get and connect the appropriate oil and water hoses. The oil intake and outflow should never be on the same side of the pipe. They should be on opposing sides of the room. The water entry and output should be the same way. If the intake and exit are on the same face, the turbocharger's compact size might make it challenging to fit all essential connections into that small space.

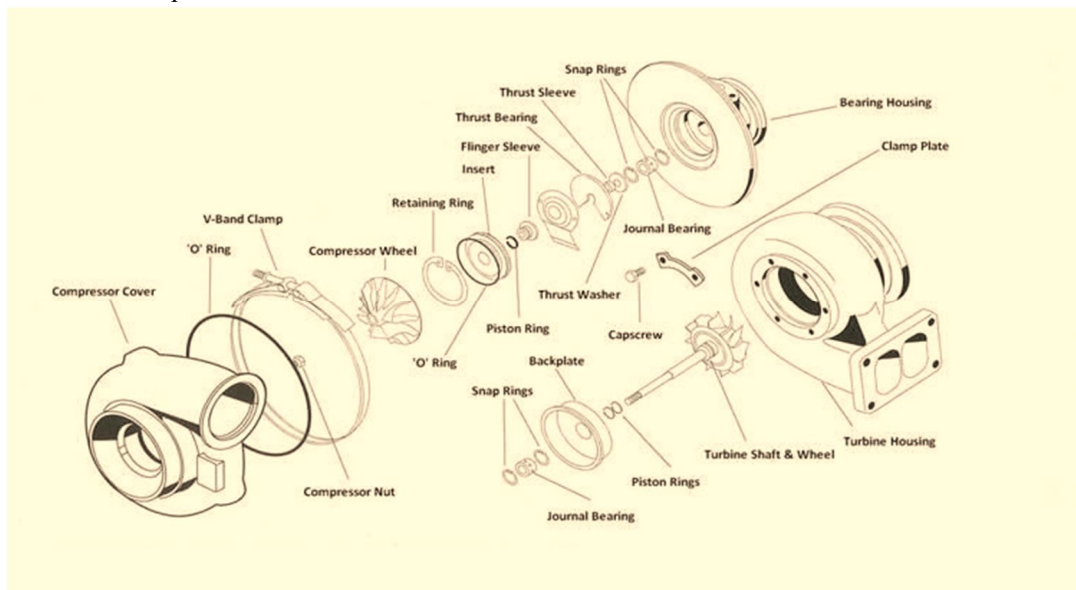


Figure 15: Turbocharger internal components

The turbine intake and outflow will almost certainly be bolt-on connections that need flanges. The turbocharger manufacturer should ideally produce flanges and gaskets for the Turbine, saving the effort to design and create special ones. Flanges and flange connectors that are thicker seal better and are less prone to break under stress. However, this data conflicted with itself—the source was never cited—and did not seem reliable. Therefore, we planned to make an intake manifold for the naturally aspirated engine, restrict its airflow, and then use a sensor to acquire data for mapping a proper compressor. Moreover, the engine is never running, and the data acquisition system has not been completed means that an ideal compressor map was never constructed. Without enough data, the process of using a compressor map to locate the most compatible turbocharger thus to proceed without being able to make the decision.

Moreover, with the restrictor in place, the turbocharger, which would be about half the size of a standard 600cc unit, could end up pushing too much air into the engine and cause it to over-speed. The team decided to find the smallest available turbo to combat this scenario while still ensuring that the restrictor would not harm engine performance.

As a consequence, the search for very small turbochargers started. However, any found turbochargers required a compressor map, which was required. Although the system could not be displayed adequately on the map, comparing the compressor maps of two turbochargers reveals which is better suited to the lower airflow rates observed in smaller engines. Will devote much work on locating alternate turbochargers. They conducted online searches, paid visits to junkyards, and spoke with motorbike technicians. Additionally, an old turbocharger located scattered about the workspace was inspected, revealing badly damaged bearings. However, after all of that, there were no practical options. The IHI RHF3 was the closest alternative to becoming a feasible option. According to the IHI website, this turbocharger is compatible with engines as small as and has a maximum airflow of 222.5 CFM. Although no entire compressor map for the RHF3 has been uncovered, Fig. 4.8 compares the RHF3's compressor map to that of other IHI RH series members.

F. Implementation Assembly and Manufacturing

1) Turbocharger

The turbocharger connects to the throttle valve using a flange. In addition, we tried to make sure the design was accurate, and the dimensions were correct so that the pressurized air would not lose its force or be leaked out. Also, because the oil turbocharger will give excellent output and long life, it reduces friction for bearings.

2) Wastegate

Fuel-powered engines benefit from a turbocharger since it aids the introduction of pneumatic stress through an association of a blower haggie gases and a gas turbine wheel via a very powerful shaft. In order to reduce rubbing and control the blower, the gas turbine receives energy from the exhaust fumes. A spiral stream is produced by the blower and the turbine wheel in nearly all automobiles. In certain applications, such as medium- and low-speed diesel engines, an outspread stream turbine wheel may be replaced by a hub stream turbine wheel. The wastegate is a small valve that controls how much boost the turbo produces. When airflow departs the manifold, it opens, and when the boost reaches the desired level, the wastegate discharges the leftover air. Furthermore, since the car would be used on a regular basis, the boost was adjusted at 8 PSI. Furthermore, in our project, the Wastegate will be external.

3) Valve Spring

The original valve lifter will be destroyed due to the high pressure generated by the turbocharger. We also had to replace the valve spring and acquire a high-strength spring. To guarantee that the chamber's head continues to flow smoothly.

4) Intercooler

A radiator designed to cool the hot "boosted" air flowing out of the turbocharger is known as an intercooler. As compressing air increases, the temperature of the air. Always, intercooling and turbocharging go hand in together. Rather than fabricating into the car's body or chassis, we build the inlet elbow to assure and maintain the automobile original. In addition, the plumbing was made of aluminum.

5) Blow of Valve

The air is bypassed via a tiny valve situated before the throttle when close. So, we will examine the blow-off valve, and an aluminum pipe will link it.

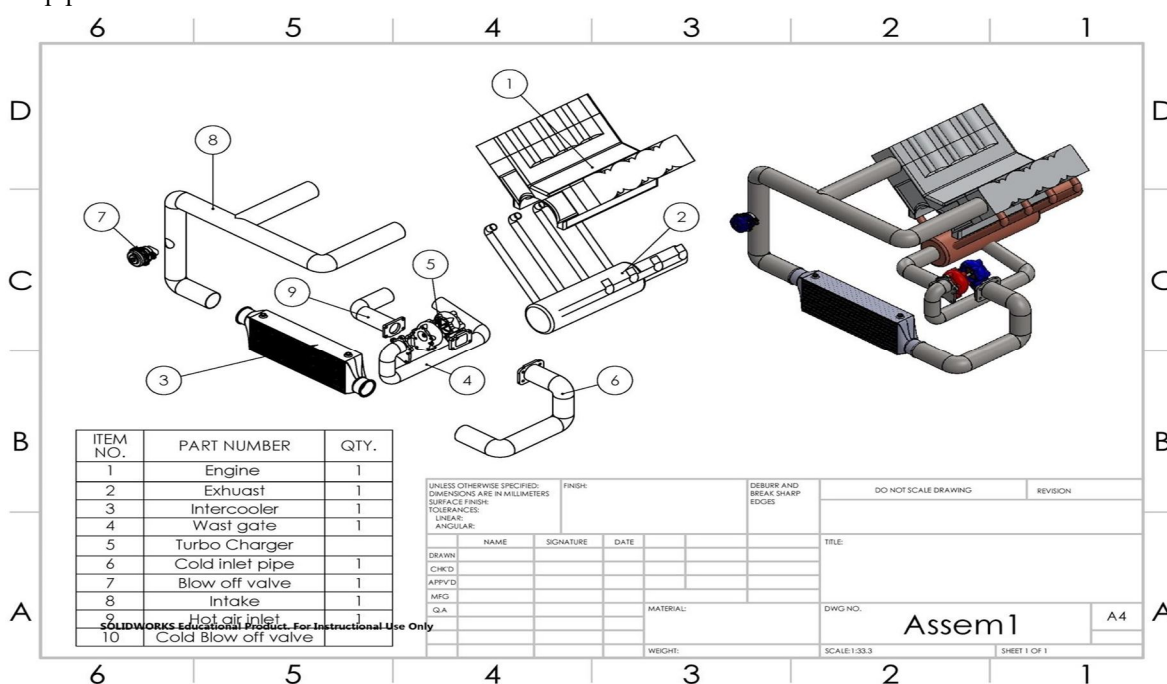


Figure 3:13: Assembly of Engine (SOLIDWORKS).

G. Conclusions

A technique for measuring turbocharger noise in flow benches or engine test cells is presented in this chapter. The studies in this chapter were carried out in test cells using various turbochargers. In-duct acoustical beamforming divides the pressure signal into upstream and downstream components.

Another benefit of a wave decomposition approach that can also resolve intensity is that it isolates the pressure data from the compressor, enhancing the spectral content of interest in cases where anechoic settings are not possible. Anechoic boundary conditions (no pressure disturbances reflecting from the borders) are employed in validation work of computational fluid dynamics models since these barriers are difficult to describe. [1] described a technique for calculating this anechoic condition. In Chapter 6 of this dissertation, this strategy is described in depth.

The proposed signal processing provides accessible visual representations in the form of noise maps of specified frequency bands of interest and approximated spectrograms of working routes when utilized to examine the acoustic intensity of the noise produced by the compressor. This might be a good place to start considering methods to reduce or eliminate certain types of noise emissions. The examples above show how this approach may be used to map the distribution and significance of known centrifugal compressor acoustical phenomena, such as medium frequency whoosh noise and low-frequency surge onset, across different turbocharger operating settings. This chapter also leads the reader through a few processes for computing sensor data while accounting for constraints such as sensor location and frequency aliasing effects.

The tests were carried out in an anechoic room, which allowed for the recording of turbocharger noise emitted both from the surface of the orifice used to regulate air flow into the engines and from all over the turbocharger's surface. The noise produced by a turbocharger while operating under in-engine circumstances was measured using an acoustic particle velocity sensor. The tests were taken at various speeds to see how noise levels change with speed.

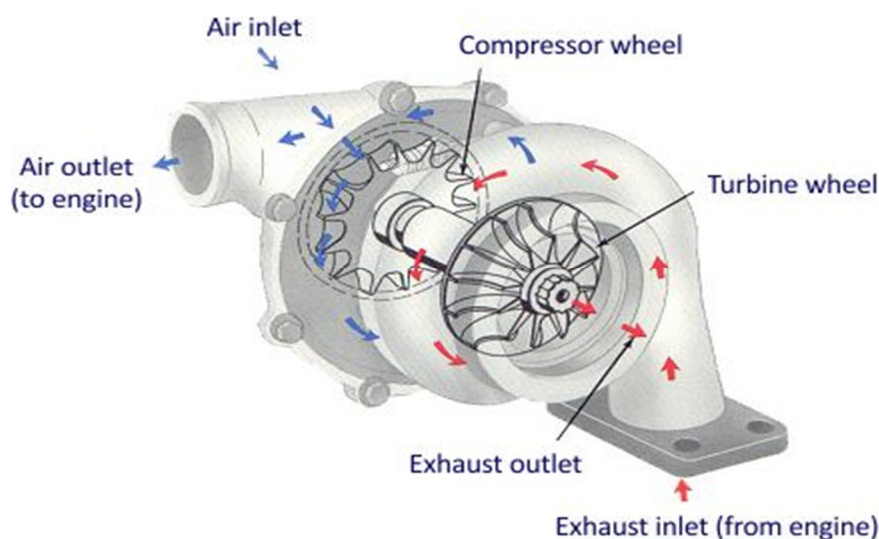


Figure 17 Turbocharger assembly

The common shaft of the turbine and compressor is supported between the compressor and the turbine thanks to a central housing bearing system (Figure 17). The rotating unit, which includes the compressor and turbine wheels, is referred to as the "shaft wheel assembly" in this context. In contrast to the rotating assemblies installed in the compressor and turbine housings, the rotating assembly in the Centre housing is installed by SWA in the Centre housing (CHRA). The majority of the time, grey cast iron is utilized for the central housing, however aluminum can also be used in some instances. Seals prevent oil from entering the compressor and turbine. Turbochargers with central housing cooling tubes are particularly well suited for high-temperature exhaust gas applications, such as spark ignition engine uses. Despite the fact that the

turbocharger bearing system appears to be straightforward, it is critical for a variety of purposes. It is to guarantee that the system is as efficient as possible, it is necessary to manage both the shaft and wheel motions, as well as the bearing friction losses. Bearing systems have received a great deal of attention as a result of their influence on turbocharger friction and the resulting impact on engine fuel efficiency.

Bearings that support the shaft are normally located between the wheels in an overhung position, with the exception of extremely large turbochargers for low-speed engines that are located between the wheels in an underhung position. Because of the flexible rotor design of the turbocharger, it may operate at speeds greater than its first and perhaps second critical speeds, placing it at risk for rotor dynamic scenarios such as spin and synchronized vibration.

Sealed bearing housings are located on either end of the bearing housing. In order to maintain friction losses to a bare minimum, the relatively large shaft movements induced by bearing clearance must be kept to a bare minimum, and the presence of unfavorable pressure gradients in some scenarios, these seals provide a challenging design problem.

These seals keep air and gas from getting into the central housing. A turbocharger usually has a Centre housing that holds a lot of pressure, but the pressure in the intake and exhaust systems can be a lot higher than the crankcase pressure of the engine. So, they would be used mostly to seal the intermediate housing when there is less pressure inside than in the intake and exhaust systems. These seals are not meant to be the main way to stop oil from getting into the exhaust and air systems from the Centre housing. People use things like oil deflectors and rotating flingers to keep the oil from getting into these seals, so they don't leak.

Turbocharger seals are different from soft lip seals, which are used on rotating equipment that moves at lower speeds and at lower temperatures. The piston ring seal is one of the most common types of seals out there today. It is made of a metal ring that looks like a piston ring. The seal doesn't move while the shaft moves. It's also possible to use a labyrinth seal. If the pressure difference changes so that the pressure in the central housing is higher than the pressure in the intake or exhaust systems, turbocharger shaft seals will not keep oil from leaking.

IV. SOUND MEASUREMENTS

This chapter discusses the results from our acoustic measurements of the turbocharger compressor. First, we study the spectrum of the turbocharger sound output in an anechoic chamber. Next, we examine the sound output of the turbocharger at a single frequency using the Fourier transform technique. Finally, we analyze only the plane wave component of the sound output.

The turbocharger's external noise, There will also be a look at things like noise from the input orifice and acoustic radiation around the system. Internal and orifice noise levels will be linked, which could make it easier to figure out how noisy the outside world is without having to test the system in a large, anechoic space.

A. Internal noise field is a term used to describe a field of noise that exists within a system.

In the first part of the experimental campaign, we gathered data from several compressor operating conditions to understand how the acoustic signature changed with different operating conditions. In this experiment, we used the previously described piezoelectric sensor arrays to record noise in turbochargers' inlet and outlet ducts across a range of operating conditions. We then processed the data to create pressure maps of the noise, sound intensity, pressure spectra, and noise maps for the inlet and outlet ducts. We also created spectrograms of the noise from different points along the inlet and outlet ducts.

The engine was tested on a bench that simulates real-life conditions in these tests. The operating points were selected in consideration of the whole compressor map provided by the manufacturer and the capabilities of the compressor test bench. The study studies at a screw compressor's performance from the point where it started to run inefficiently to a capacity just over the manufacturer's cautious deep surge limit. The two limitations are part of a measuring subset of the compressor map (Fig. 4.1), which includes the working line up to 170 krpm shaft speed. Furthermore, the deep surge limit was tested in a separate gas stand to pinpoint its exact location. The effects of gas-standpipe diameter on surge margin were measured utilizing a tapered duct in the compressor input line. These tests verified that the surge margin advised by the manufacturer is close to the actual amount observed using the approach outlined in Chapter 3.

The data points on the majority of lines in the log-log plot of shaft speed vs. air mass flow are between the manufacturer's cautious limit and the empirically quantifiable limit. The authors were able to investigate both ends of the compressor surge spectrum by comparing optimum compressor operating points at maximum thermodynamic efficiency and the most critical circumstances near deep surge.

A. Range of Plane Waves

The compressors used in automotive turbochargers can reach peak efficiencies, depending on the diameter of the pipe, the temperature of the gas, and the speed of the gas, at frequencies between 5 and 7 kHz. [38] This is important because these frequencies encompass several acoustic phenomena relevant to everyday life.

Acoustic engineers have long been interested in the middle and high frequencies of wind whistling through organ pipes since this frequency range makes analytical and numerical modeling easier. Working with wave decomposition procedures isolates the contributions of the inlet and outlet pipes. This information can be used to compute the acoustic intensity of the duct.

Equation 3.3.7 gives the frequency at which the plane wave assumption can no longer be deemed acceptable. The first asymmetric mode begins to propagate at higher frequencies.

Due to changes in flow conditions and pipe diameter, examination of this expression resulted in cut-off frequencies of around 4.7 kHz for the input duct and 7.4 kHz for the exit duct for the pipes investigated in this work. It should also be noted that this limit fluctuated significantly due to variations in velocity and temperature under various operating circumstances.

For the decomposition array of sensors specified by equation 3.3.6, the Nyquist frequency cutoff criteria was more stringent than the first asymmetric mode limit, resulting in maximum cut-off frequencies for plane wave propagation of 3.4 kHz for intake and 6.4 kHz for exit. A dashed line represents these values.

The pressure measurements acquired by individual piezoelectric sensors in both inlet and output ducts are represented as power spectral densities. Spectra are shown for both ducts along the working line at various shaft speeds. These figures show that spectrum peaks at higher-speed shaft points tend to appear at lower frequencies. Duct noise between 1 and 2.5 kHz is unique; in the literature, this phenomena is referred to as whoosh noise.

An approach identical to that indicated for the 160 krpm shaft speed line shown in dashed lines was used to examine the development of spectral content when air mass flow was lowered through moderate surge circumstances. The graph demonstrates a distinct tendency for lower frequencies to seem more "jagged" than higher frequencies, where the whoosh phenomena is more clearly seen between 1 kHz and 3 kHz. When looking at the spectra at 60 g/s and 55 g/s, it is clear that overall broadband noise levels do not drop when flow conditions decrease, but rather mirror the surrounding frequency content.

B. Pressure waves Decomposed

Using a new algorithm based on LCMV beamforming applied to pressure above data recorded by three-sensor arrays while following the working line and 160 krpm line operating conditions, a method for isolating the compressor's spectral content from the reflections and interferences of upstream and downstream ducting and components.

The spectral content of the decomposed pressure wave differs from the total pressure wave for different operating speeds. The spectral range of the decomposed pressure wave at a lower speed matches that of the higher flow speed, but the decomposed pressure wave at a higher rate is closer to that of the lower flow speed.

The buzz-saw noise characteristic of the unprocessed pressure data substantially improves following the decomposed total pressure spectrum to the decomposed signal coming from the compressor (backward wave in the inlet, forward wave in the outlet).

The opposite-traveling wave carries less energy and is less potent than the forward-traveling wave, with amplitude reductions of approximately 10 dB between 2 and 3 kHz at high speed and low flow.

Fig. 13 shows an example of the spectral decomposition of a decomposed pressure signal acquired in the inlet duct and outlet duct.

The backward wave is shown on the top plot, and the forward wave is shown on the bottom plot. The spatial Nyquist limit was reached in each case, which is reflected by peaks above the Nyquist frequency in each graph. The decomposition algorithm depicted in Fig. 13—used to decompose the inlet spectra—allows a more precise representation of the spectra, since it is not affected by the buzz-saw effect at lower frequencies.

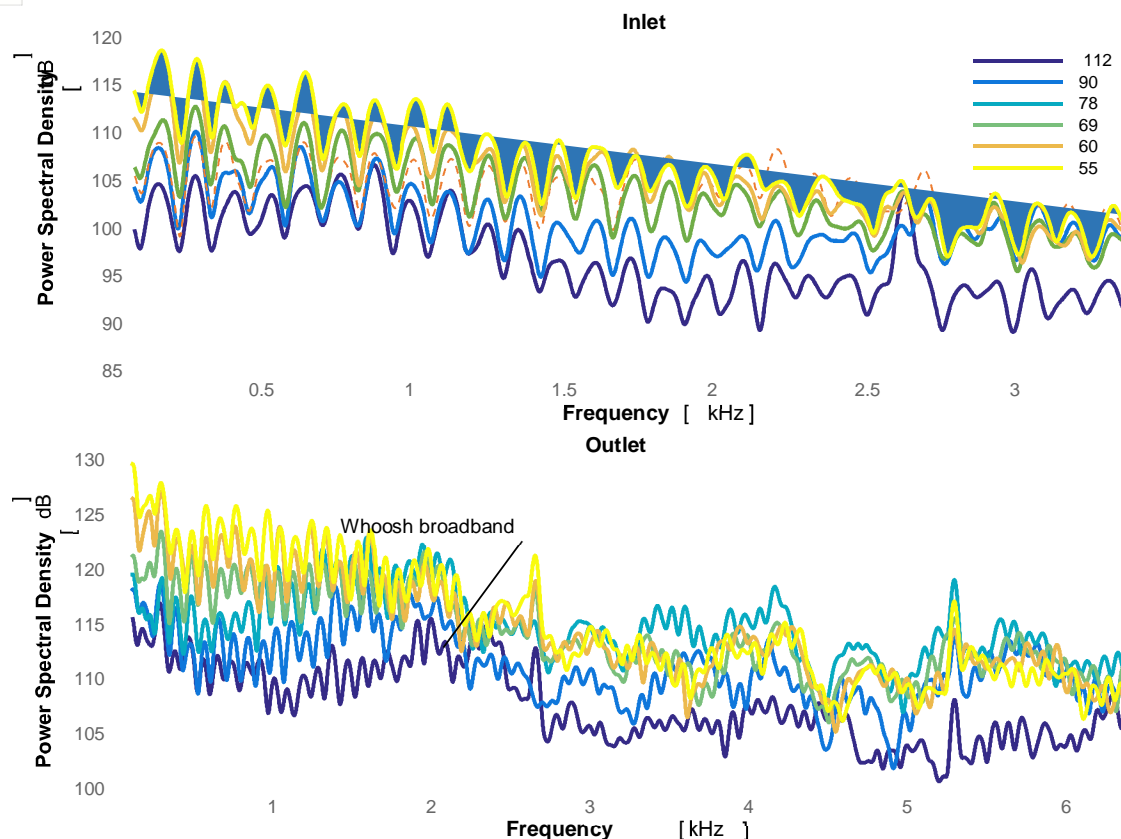


Figure 18: The spectra of total pressure (solid line) and decomposed pressure (dotted line) are plotted for both 80 krpm and the highest mass flow and 160 krpm and the lower mass flow.

C. Increase frequency

In addition to the cut-off frequencies previously indicated, acoustic waves change in such a way that they no longer follow classical wave theory. In simpler terms, this means that the decibel levels of pressure waves drastically lessen. However, it is still beneficial to analyze the raw decibel levels because they still contain useful acoustic data. The intake pressure spectrum depicts the PSD of pressure data collected by a single array sensor. The amplitude of the signal grows as the shaft speed increases, and a broadband elevation begins at 12 kHz and ends at 5 kHz. This might be connected to the TCN discussed in Chapter 2's material. BPF peaks are also apparent in the inlet spectrum, although they are more distinct at higher shaft speeds, such as 160 or 170 krpm.

The spectral content of the outlet exhibits the previously described rise in plane wave frequencies, followed by broadband at higher frequencies, which might be connected to the so-called TCN. Even for situations that are not observable in the intake spectrum, BPF peaks are visible in the output spectrum. A careful inspection of the raw pressure signal's spectral content at 160 krpm indicates that it has a wide spectrum comparable to that of the outlet spectra. This anomaly is explained by the similarity of the shaft speed lines observed at 160 and 400 krpm.

D. Sound Generation

The sound waves are generated when the air is forced through the narrow gap between the edge of a rapidly spinning object and a second surface. The sound produced is most noticeable as a high-pitched ring when the RPMs are at maximum, or when there is very little friction between the objects. When the engine runs at lower RPMs, or for an object with more friction, the sound becomes much lower in tone. The emphasis is on aerodynamically produced sound, which always reigns supreme at high RPMs. The sound generation may be derived by incorporating the source strength at low RPM levels, when the contribution from unbalances is insignificant.

When the plane wave range is reached, established methods for estimating propagating sound power (i.e. ISO) or reflection-free terminations can be used. The KTH rig is outfitted with damped terminations and dissipative silencers. As wind turbines become larger, the noise emissions from these large structures extend farther out into the surrounding environment. If a company is looking to build a wind farm, it is essential that they understand how far the sounds emitted from their turbines will travel. Previous research has found that the sound level is dependent on the frequency of the emitted sound, but this research suggests that low-frequency sounds may be more harmful than previously believed. Present studies show that it is necessary to consider spatial averaging when looking at sound propagation through turbine parts. The investigation used three transducers on each side of an axis, with some averaging between them to estimate the strength of sound emitted by various modes. Using this technique, we were able to find that different frequencies have different amounts of dispersion; that is, they travel at different speeds. In addition, different modes traveled at different speeds depending on what was in between them and the transducer. Even though this method had some assumptions, it showed that certain part configurations could result in significant differences in terms of sound propagation speed.

E. External Sound

The experimental campaign also featured a noise measurement component, which took use of the chamber's anechoic settings to measure metrics that couldn't be measured in the turbocharger test rig. We detail the equipment and technique used in these studies in Section 3.4, pointing out that external noise measurements are frequent in the scientific literature and are also a standard metric used by manufacturers. As a result, it's critical to correlate the in-duct results with exterior data. Comparisons of in-duct and external noise measurements were made possible by using two microphones placed at the same points within the duct and perpendicular to the axis line of the turbine. Previous descriptions of these measurements indicated that data was captured with two omnidirectional microphones placed at a distance of 10 and 20 mm from the inlet orifice. Also, unlike the previous orifice measurements, where acoustic data was collected simultaneously with the characterizing compressor map and thus covered the whole area explored by the compressor map, only two characteristic lines were considered in this line of investigation: engine working line (where flow noise is dominant) and 160 krpm speed line (where blade passing frequency noise is dominant). Moreover, applying acoustic insulation blankets to the inlet duct, outlet duct, and nothing at all resulted in distinct damping characteristics for each part.

1) Surface Radiation

Sound radiation data was collected at four distinct points surrounding the turbocharger assembly, in addition to utilizing the anechoic chamber to quantify orifice noise. Unlike earlier measurements, which gathered all of the compressor maps at the same time and so covered the whole sampling region, this time measurements were limited to two lines of interest: the engine functioning line and the 160 krpm speed line.

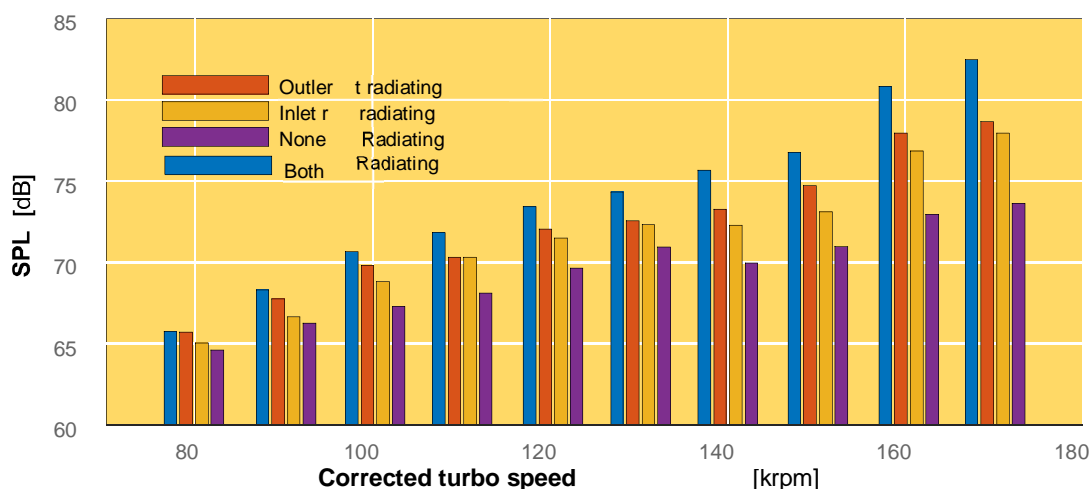


Figure 19: Averaged RMS Sound Pressure Level measured for various air mass flow rates during sequential damping experiments on the 160 krpm speed line.

Furthermore, testing was repeated with a sequential damping of the inlet duct, None of the rest. In the picture above, full-spectrum SPL is presented surrounding the four microphones, taking into account the line's operational conditions. What we hoped for: Shaft speed increased noise from exit duct. The entrance duct was quieter at any shaft speed.

2) Orifice Noise

To establish a reliable comparison between the exterior and in-duct measurements, which were obtained with free-field omnidirectional microphones set 10 and 20 mm from the entrance duct orifice, simultaneous measurements were conducted at the same data points. The 10 mm distance was chosen to match the manufacturer's internal comparative measuring procedure (the manufacturer using dimensions for 10 mm rather than 20 mm).

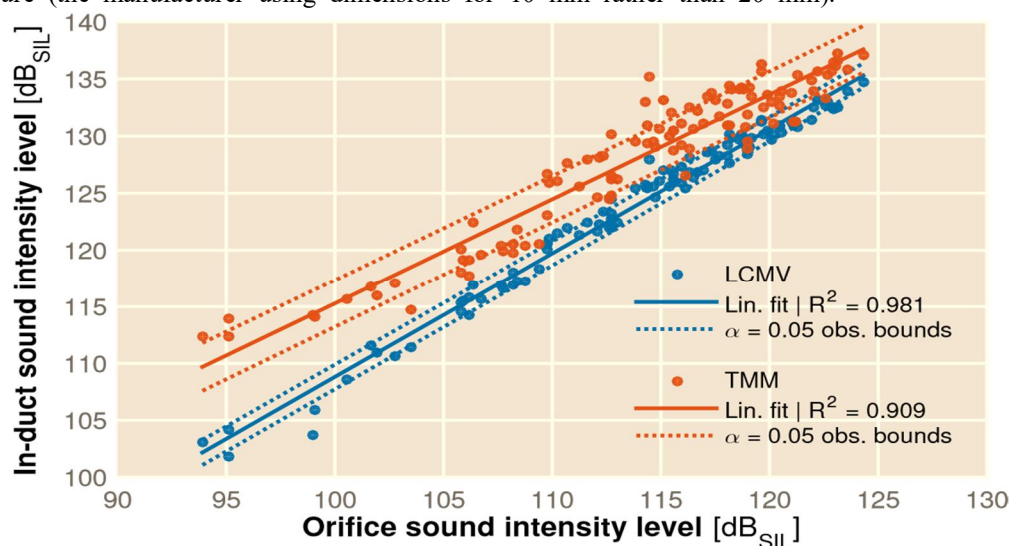


Figure 20: Correlation of the sound intensity in the inlet duct and sound intensity in the orifice, using both LCMV beamforming and the Two Microphone Method.

When free-field circumstances are used to compute intensity, the correlation illustrated in Figure 20 above reveals that in-duct sound intensity levels observed in the inlet may be reliably anticipated by measurements collected by a single microphone 10 mm from the orifice, as discussed in Chapter 3. The LCMV beamforming approach and the standard two-microphone method provide similar correlations with free-field orifice data, as indicated by R2 values of 0.83 and 0.86, respectively. The results from the second microphone were comparable [93].

F. Conclusions

The results of the experimental measuring effort are examined in this chapter. It focuses on data collected from in-duct measurements made at the compressor's air intake and air outputs in particular. The working line (representing a range of airflow rates and shaft speeds) and a speed line were utilized to conduct spectral analysis on the engine compressor's pressure data (where shaft speed was maintained at 160 krpm while airflow rate was reduced to near deep-surge conditions).

Pressure wave decomposition has been shown to be an effective method for improving the spectrum information coming from the compressor by eliminating standing waves and reflections. As a result, authors may identify critical aspects such as the blade passing frequency and its harmonics, as well as a broadband hump between 1 and 3 kHz consistent with whoosh noise. More effort is needed to discover the sources of this sound due to its poor impression in car applications. In 1982, a hump in the acoustic signature of exhaust ducts was discovered. The complex noise phenomena was more easily recognized in the outlet duct's acoustic signature, and it was more noticeable at higher shaft speeds. Variations in lower and higher frequencies concealed the presence of this hump when flow rate decreased. The hump associated with whoosh was shown to be sensitive to the mean flow velocity rather than the shaft speed or sound speed, indicating that the hump is generated by flow rather than transmission variables.

Furthermore, the recurrence of the same behavior in the future shows an abrupt collapse at plane wave transmission frequencies in all circumstances, implying that the source mechanism cannot propagate under such settings. The absence of TCN-like events in the plane wave range confirms that this type of noise is distinct from broadband whoosh, which does occur in this range.

Noise maps were created using the interpolation of in-duct acoustic intensity across the several operating conditions investigated to study forced convection noise and low-frequency phenomena. The commencement of low-frequency phenomena is mapped to surge limits, whereas the whoosh phenomenon is mapped to the characteristic line's null slope point, indicating that the two phenomena are not necessarily connected.

Due to the unanticipated propagation of high-order acoustic modes, higher-frequency analysis was complicated in this experiment. Because the plane wave assumption required at higher frequencies is erroneous, the pressure wave decomposition approach could not be employed. Even with the tiny distance between each sensor, we detected variances in noise levels, including some erroneous signals, when we looked at maps of the pressure spectrum in the three separate instruments of our array.

Because the flow is strongly whirling, a single laser PSD probe in the exit duct of an axial fan produces unsatisfactory results. In such instances, acoustic intensity measurements based on wave decomposition are preferred. Spectrograms were created using interpolated data of maps for the two flow conditions to check how content in the whoosh band—the band with the most noise—changes with shaft speed and mass flow rate.

Because sound measurements obtained at the inlet mouth could be connected with sound levels computed using a beamforming approach and microphone technologies, the turbocharger's anechoic chamber proved useful for analyzing orifice noise. The measurement error introduced by the first way was lower than that introduced by the second, indicating that employing a beamforming process to estimate orifice noise is superior than using microphones.

Finally, surface radiation was measured in a series of tests that dampened the various components. Except at high mass flow rates, these studies revealed that the exit duct contributed more to radiated noise than the entrance. Even though sound is created within the turbocharger, the vibroacoustic properties of the specific ducts can serve as major generators of sound to the environment.

V. VALIDATION ON REAL ENGINE CONDITIONS

Results from a laboratory-based experimental campaign were acquired in the preceding chapter. Turbochargers in automobiles are used in conjunction with a reciprocating combustion engine. Tonal noise might emerge on the turbine output signal as a result of pulsating engines. The turbine's speed is increased as a result of the uneven flow. The inertia of the wheel, on the other hand, minimizes this impact. As a result, these pulsations may have an impact on the compressor, affecting stall flow and other factors like as vortex shedding.

The most important thing for the industry to figure out is how to keep the highest levels of efficiency, reliability, and cost per mile when it comes to the sophisticated design of a modern heavy duty diesel engine. Making a diagnosis while you're doing something wrong is hard. In addition, it costs a lot to test engine control units (ECUs) in real engine labs. In the engine lab, some operations and environmental constraints can't be fully addressed. Diesel engine modelling simulations, on the other hand, can help. These simulations not only give estimates for some hard-to-measure engine characteristics, but they also save time and money. A mode called the verification and validation (V-cycle) mode, which is based on computer-aided control system design, is becoming more important in the process of making engine control systems today. In addition, the model-based development of the V-cycle helps to show how important control-oriented engine models are. Testing hardware-in-the-loop (HIL) is very important in this process. The mean value model (MVM) is often used in the control sector because it can tell when the engine is in different states and record how it responds to sudden changes. Historically, the mean value engine concept had a number of severe limitations that were recommended to boost engine response speed.

When doing acoustic characterization in production engine test cells, it is vital to use accurate measurement techniques. As seen in the prior chapter, sound pressure level (SPL) measurements done with a single sensor in the outlet or inlet duct are susceptible to reflection, standing waves, and other transmission effects, as well as pipe geometry effects. Simultaneously, acoustic intensity yields more consistent results.

When dealing with noise in gas ducts, the acoustic intensity was calculated using data gathered by arrays of pressure transducers installed flush in a straight duct section in both intake and output pipes, principally by an LCMV beamforming approach. In contrast to orifice noise measurements, the traditional Seybert's two microphone approach was also tried, and the LCMV beamforming worked better.

In the engine test cell described in section 3.1.3, acoustic measurements were obtained during an experimental campaign outlined in Chapter 5. The goal of this testing effort was to verify that the approach presented in Chapter 3 could be used in a real-world engine setting and that the findings and observations presented in Chapter 4 were still valid.

A. Setup of the engine cell

Because of measurement limitations and how difficult it is to run both the engine and the exhaust manifold together at the same time to get precise operating conditions, it is clear that there is a lot of noise coming from turbochargers. Most experiments are conducted using flow rig measurements.

Against this background, it may come as little surprise that studies on the acoustic performance of turbocharger compressors have also been carried out. Evans and Ward [30, 31] tested the effects of altitude and air-fuel ratio on turbocharger performance, finding a significant influence of altitude on specific thrust. Teng and Homco [16] explored the impact of engine speed and power on the acoustic characteristics of turbine stages in gas turbines. Pai et al. [40, 41] demonstrated that pressure perturbations from a turbocharger turbine affect cylinder pressure waves excited by exhaust pressure pulses, introducing an aeroacoustics interaction between the turbocharger's exhaust outlet flow field and engine intake flow field. Finally, Galindo et al. [69, 77, 106] measured at low frequencies (150 Hz) the evolution of interelement sound pressure level over time for a range of compressor speeds (2000 rpm to 4000 rpm) and inlet pressures (0 bar to 12 bar).

One method for determining turbocharger noise is to employ ambient microphones located within the engine test cell to detect radiated noise. However, it is hard to tell the radiation from the compressor group and pipes from the noise from the engine and other systems under these conditions. Furthermore, because engine test cells aren't always quiet, reflections will change the data gathered by ambient microphones, making an experiment go awry. Some researchers have used microphones or transducers to figure out the acoustic pressure in a compressor intake duct. These sensors aren't very good for this job. There are two things that happen when air flows through ducts: readings, making it unsuitable for this application. The project's objective is to adapt the beamforming setup for engine test cells, using pressure wave decomposition to calculate the Sound Intensity Level (SIL).

In an experimental installation, piezoelectric pressure sensors flush placed in the compressor input pipe were utilized to evaluate the beamforming approach and compare it to the two-microphone method. The comparison's findings may be found in the literature cited above. To assure the accuracy of the acoustic measurements, a commercial intensity probe (Brüel & Kjaer Type 4197) consisting of two phase-matched 1/2" microphones was mounted at the entrance orifice. Additionally, acoustic insulating mats were employed to eliminate reflections. When reviewing the literature on turbocharger noise presented in Chapter 2, it becomes clear that the majority of experiments employ flow rig measurements due to measurement limitations and the difficulty of operating the engine and exhaust manifold simultaneously to achieve precise operating conditions.

In light of this, it should come as no surprise that research on the acoustic performance of turbocharger compressors have been conducted. Evans and Ward [30, 31] investigated the effects of altitude and air-fuel ratio on turbocharger performance and found that height had a considerable impact on specific thrust. Teng and Homco [16] looked into the effects of engine speed and power on the acoustic characteristics of gas turbine stages. Pai et al. [40, 41] showed that pressure perturbations from a turbocharger turbine alter cylinder pressure waves stimulated by exhaust pressure pulses, resulting in an aeroacoustics interaction between the turbocharger's exhaust outlet flow field and the engine intake flow field. Finally, Galindo et al. [69, 77, 106] investigated the development of interelement sound pressure levels over time for a variety of compressor speeds (2000 rpm to 4000 rpm) and input pressures at low frequencies (150 Hz) (0 bar to 12 bar). The use of ambient microphones in the engine test cell can assist in determining the noise level of a turbocharger. Under these conditions, it is difficult to distinguish the compressor group and pipes from the engine and other systems. Additionally, because engine test cells are not always silent, ambient microphone data is affected by reflections introducing an experimental mistake. Although microphones or transducers have been employed to monitor acoustic pressure within a compressor intake duct by certain researchers, these sensors are not optimal for this application.

The microphone's measurements are affected by the flow of air interacting with the duct walls, making it unsuitable for this application. The project's purpose is to adapt the beamforming setup to engine test cells, using pressure wave decomposition to calculate the Sound Intensity Level (SIL).

The findings of this comparison may be found in the above-mentioned literature. To guarantee that the acoustic measurements were accurate, a commercial intensity probe (Brüel & Kjaer Type 4197) with two phase-matched 1/2" microphones was mounted at the entrance orifice.

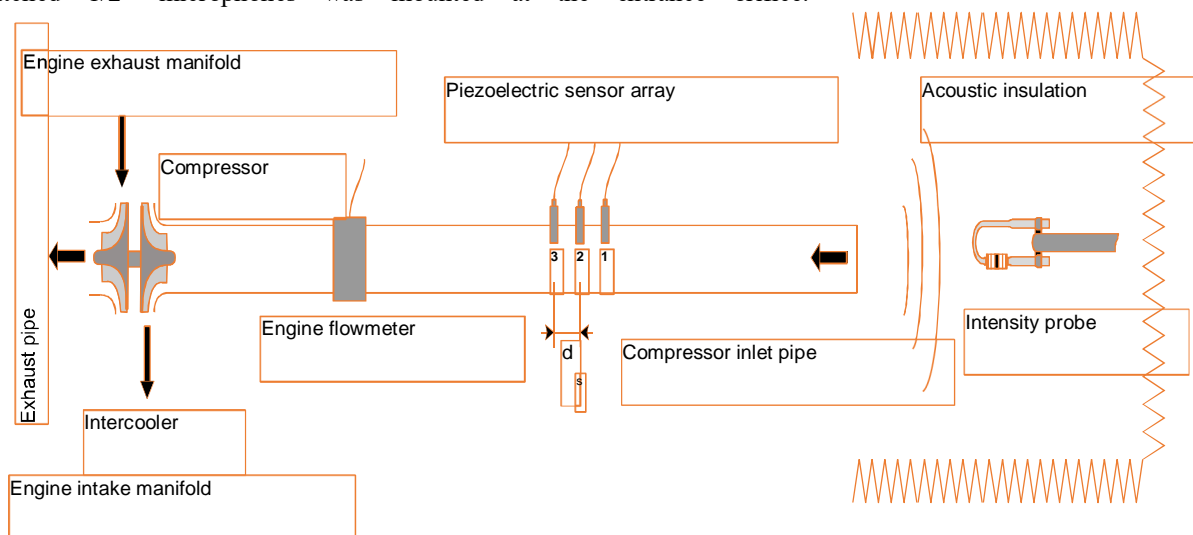


Figure 21: The turbine, which contains a moving set of airfoils (or blades), compresses the air as it passes between them. This causes the pressure and mass rate of the airflow to increase, which in turn provides more air to the cylinders.

This research used a 2-liter, 4-cylinder diesel engine that operates on diesel fuel. This engine has a maximum output of 120 kW and a maximum torque of 340 Nm at the crankshaft. It features a variable geometry turbine (VGT) turbocharger and 16 valves. To detect pressure drop across the compressors and gauge flow, a series of pressure transducers were inserted in the turbocharger's redesigned input duct. Some photos of the improved intake duct may be seen in Fig. 5.2. By regulating the compressed airflow's pressure and mass rate, the engine cylinders are fed with additional air. The compressor uses less air as a consequence of the variable geometry turbine's activity. The idea of our diesel engine model is presented in this section. It replicates the performance of a turbocharged 15.8 L electronic unit pump (EUP) diesel engine. Table 1 summarizes the essential features of diesel engines. The diesel engine model is separated into many blocks for HIL testing and control strategy development. Figure 1 depicts the model architecture, which is made up of many systems, each of which comprises one or more blocks. The air block, which exhibits nonlinear and dynamic behavior, is part of the air system (AS). The injection block is found in the injection system (IS). It is a unit injector in this study and has a quicker dynamic behavior than other systems. The cylinder block and accessory block make up the torque generating system (TGS). Torque, heat, and pollutants are produced by the combustion process in the cylinder. The cylinder block is in the TGS since this study is about torque. The starter and dynamometer are located in the auxiliary block. The auxiliary block is in the TGS because the starter creates torque and sends it to the crankshaft when the engine is started, and the dynamometer also generates torque on the test bench. The crankshaft block is part of the crankshaft system (CS). The cooling and lubrication blocks are part of the protection system (PS), which protects the engine from overheating and wear, respectively.

A dynamometer, or power and torque controller, is also included in the engine, enabling the engine operator to determine the appropriate operating conditions. The dyno demanded extending the input duct, which prompted the addition of a flexible piece to enable for small angling as needed. The engine test cell depicted in Fig. 5.2 has a feature that permits compressed air to be injected into the intake manifold after the intercooler. More information may be found in references 69 and 77, as well as a schematic of the setup in [69, 77]. The injected flow is smoothed down by a reservoir attached to the compressor. This reservoir may be seen in the bottom right corner of Figure 5.2.

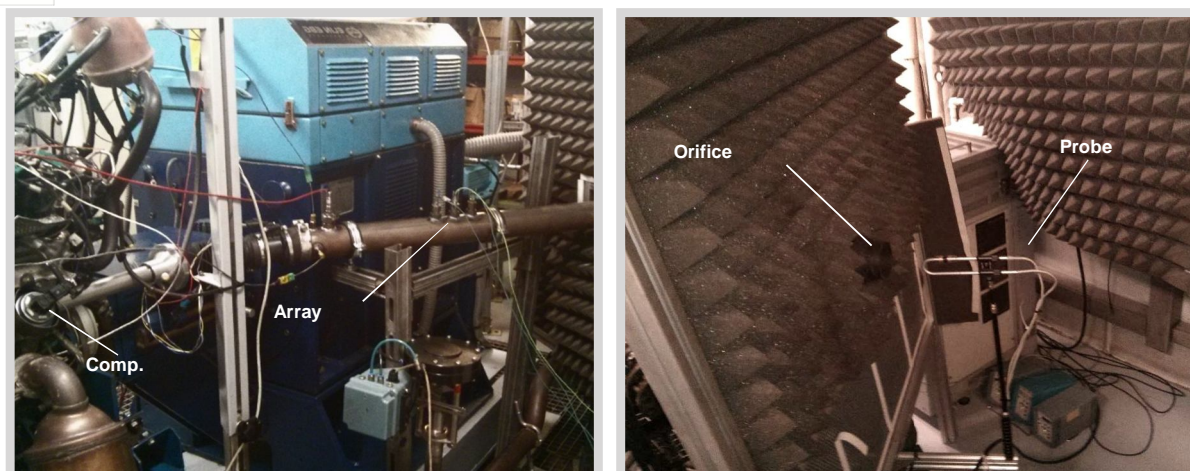


Figure 22: Images of the acoustic measures experiment, which includes the intensity probe and transducer array installed on the expanded intake pipe.

By regulating the compressed airflow's pressure and mass rate, the engine cylinders are fed with additional air. The compressor uses less air as a consequence of the variable geometry turbine's activity. This may enable adjustments to the compressor working conditions of a Diesel engine without compromising the engine's functioning. However, when constant pressure ratio lines are monitored rather than discrete constant-speed lines, pinpointing one specific operating state in the compressor map is more challenging.

The sound pressure level measurement is further limited by the microphone's frequency response and the decomposition algorithms. The microphone's frequency response restricts its capacity to detect high and low frequencies. The decomposition methods are intended to break down observed pressure data into signals that may be utilized to locate sounds. Both of these procedures were designed for plane wave propagation and are therefore limited to the frequency range below the cutoff frequency of higher-order modes, which may be calculated using Eriksson's formulas.

Another limitation is that the spatial frequency component is limited in some manner by the spatial resolution of the successive sensors—which are characterized as translating successive fixed-position components, which may be thought of as a Nyquist limit for spatial sampling rather than temporal sampling. The exact frequency of this cut-off is dependent on the spacing d_s between these sensor parts and is comparable in idea to the Nyquist limit. Above this frequency limit, spurious aliasing effects will appear.

B. Results of in-duct Measurements

The area of the compressor map closest to surge was established by varying the injected excess air mass at different pressure ratios during a measurement session using the given configuration. Low and high mass flow rates, as well as increased noise levels caused by the use of a faulty bearing material, were tested to assess the impact of noise created by the impeller at varied shaft speeds.

Noise levels are much greater at higher shaft speeds and lower mass flow rates, according to the findings. When comparing the noise level map to the flooding limit contours, it becomes clear that there is no direct link between the two, but that the contours are grouped in the top left corner.

All curves are reported as iso-speed rather than iso-pressure, according to the various measurement procedures. As a consequence, determining whether the rise is linked to the pressure ratio's highest point is impossible. Finally, the findings in terms of noise level distribution will be consistent with earlier data.

The engine's effect is recorded in one of the array sensors, indicating that the sensor's raw sound pressure level is comparable to those measured in the continuous flow test rig. In the plane wave range, the sound level is greater, and in the broadband range, it is lowest. Further investigation into the sound intensity at low frequencies shows a distinct peak at 12 Hz, which is accompanied by harmonics and other engine sounds. These noise events might be linked to other air management system problems.

C. Evaluation of the Methodology

The SPL with a single sensor, two-microphone technique, and LCMV beamforming was used. The sound pattern emitted by the input orifice could not be distinguished from the sound field inside the duct in the frequency range where the spectra were measured by the reference probe. As soon as the first radial mode appeared in expression 3.3.7, it was evident that the sound field generated by the intake orifice was distinct from the sound field generated by the induct itself.

This chart shows the sound intensity at three working conditions as a function of frequency. To create this image, we used the Fourier transform of pressure and plotted the intensity on the y-axis. We then computed SIL in three different ways. The intensity probe (red line) was used to measure UL and OL SIL, while the two-microphone method (blue line) estimates IL SIL. We also made a beamforming measurement using a program called FEA-SIL (black line). The correlation coefficient for each set of measurements is given on the figure and demonstrates that our beamforming measurement is best in the region where plane waves are present, which is from 0 Hz to 1 kHz.

D. Noise Produced

Aside from in-duct measurements, measuring noise generated by the turbocharger and its pipes is another approach for acoustic evaluation of a turbocharger. This approach enables real-world measurements without needing any pipe modifications. It has the extra benefit of allowing engine components to be tested in real space, but the test cell must be made anechoic to eliminate noise sources such as reflections in engine cell walls and resonances induced by engine or duct cavities. Engine components that are being evaluated in a lab should be near together. Because building an anechoic chamber is expensive, some test arrangements are simplified to simply the turbocharger group, which is driven by an external compressor or electric motor.

A technology for detecting acoustic particle velocity levels that was recently developed may be able to alleviate these problems and allow on-train testing in non-anechoic conditions. Two tiny filaments operate as hot-wire flowmeters in this approach, which was briefly described in Chapter 3. The acoustic particle velocity in the sensor plane may be calculated by measuring the modest voltage drop between them [101].

In the non-anechoic engine test cell, a novel technology based on acoustic holography was tried. (Acoustic holography is a three-dimensional reconstruction approach for mapping noise levels.) Particle velocity measurements are compared to typical free-field sound pressure level (SPL) measurements by scientists [102].

The turbocharger is easily identified as the cause of a 700–2000 Hz wideband noise (at this specific operating state), which sounds like a whoosh, using the pressure and particle velocity approach. The turbocharger is likewise identified as the source using the pressure technique, although its contribution is not as loud as the turbocharger's. The broadband particle velocity in both zones (turbocharger and intake) of a gas turbine engine is compared in this finding. The whoosh noise produced by a revolving blade stall, on the other hand, may be seen in spectra below 500 Hz, as illustrated in Figure 5.10, demonstrating the discrepancy between particle velocity and pressure measurements.

When it came to distinguishing whoosh sounds, the pressure strategy proved useless. It's worth noting that if you want to describe the whoosh sound by lowering pressure through the duct (rather than raising it, as with the pressure approach), you'll need to pay particular attention to the output pipe.

E. Conclusions

The test means for a compressor under engine conditions should be defined first. In the absence of a suitable anechoic chamber, anechoic measurements are advised.

Compressor noise can be measured with an inlet orifice intensity probe. Aside from their high cost, intensity probes aren't always the greatest solution. an acoustic spectrometer may be more desirable. Spectrometers allow for more efficient analysis of the internal field, but they do not detect sound waves that will not propagate externally.

In this chapter, we explained that measuring in-duct acoustic noise offers an inexpensive method of characterizing the sound field generated by the compressor. However, before using this technique to measure the sound pressure level (SPL) at various frequencies, one need to modify the air ducts so that straight sections of them can be used for testing. Using a single sensor for this sort of investigation tends to be limited in terms of accuracy and seems more accessible for most people to interpret. Sound intensity is a more accurate metric and gives a better representation of the acoustic power output of the source than SPL measurements.

The wave-intensity calculation using two consecutive sensors and the wave decomposition through the two microphone method (Beamforming method) can be more reliable in the low frequency range (250–1000 Hz). The wave-intensity calculation using an additional third sensor can be more reliable along the full plane wave range and especially in the lower frequencies.

VI. NUMERICAL SIMULATIONS

As the initial literature review showed, numerical simulations are valuable tools for analyzing and understanding physical phenomena. These simulations are also useful in developing prototypes, since they allow design variations and different operating conditions to be tested without the cost and risks associated with building physical test models.

It is, therefore, critical to ensure that these numerical tools are trustworthy. Small modifications to the geometrical model, boundary conditions, or numerical techniques used to solve the issue can have a big impact on the simulation's outcome. It may be required to double-check that the assumptions established in the simulation's physical models are correct for the phenomena of interest.

This chapter describes the experimental and signal-processing approaches used to validate a numerical model of a turbocharger compressor, including global variables, flow field measurements, acoustic output, and findings from various operating situations.

A. CFD Simulation Setting

In his PhD thesis, R. Navarro (2010) developed a model to account for a variety of physical phenomena associated with eel migration.

An overview of the model used to verify numerical findings and analyze physical events may be found in this section. Numerous approaches and methods have been used in the development of centrifugal compressors over the years. Computational fluid dynamics (CFD) and other one- and quasi-three-dimensional engineering software are included in this area. Centrifugal compressors tend to stall gradually, but axial compressors are more likely to halt abruptly. After experiencing an unexpected stoppage, Greitzer (1976) asserts that axial compressors may never restore their constant performance. In his work, Day (1994) states that the substantially different hysteresis loops between Greitzer (1976) and Day (1994) (C106) compressors allow Greitzer (1976)'s compressor to exit stall far more easily than Day (1994)'s (C106). While both the axial and centrifugal compressors studied by Emmons (1955) were able to enter surge, the centrifugal compressor showed a more progressive stall. Because they can't get out of stall, axial compressors frequently have stall operating points that limit their range of operation. Centrifugal compressors, on the other hand, typically have their operating range limited by the surge operating points since they can continue to run in stall conditions.

The centrifugal compressor discoveries, experimental facility design, and a model-to-model comparability analysis will form the basis for all future work on turbocharger surge. The only way to know for sure whether or not a compressor works is to put one through its paces using a replica. The RPA (Research and Production Association) "Turbotekhnika" and the Peter the Great St. Petersburg Polytechnic University's Research Laboratory "Gas Dynamics of Turbomachines" collaborated to develop a centrifugal compressor for an internal combustion engine turbocharger. Two impeller diameters of 175 (TKR 175E) and 140 mm (TKR 140E) were used to demonstrate the compressor's dimensionless capabilities (TKR 140E). An error of 0.89 percent in the design mode and a 1.55 percent error in the overall characteristic are predicted by the mathematical model for the Universal Modeling Method. ANSYS, a commercial CFD package, was used to calculate the properties of the TKR 140E compressor. Although the efficiency figure for the TKR-140E differed significantly from prior computations, there was a high degree of agreement in the operating area. A 9 percent overestimation of the work coefficient was found in the computations, which is in line with the authors' previous estimates. A significant Russian manufacturer of turbochargers for internal combustion engines, RPA "Turbotekhnika" produces a wide range of turbochargers. The turbocharger for the 8ChN26/26 gas engine, which was originally a diesel, is currently a hot topic. Initial estimates suggest that the highest degree of boost shouldn't go higher than 1.6–1.7. There must be a wide range of blower performance for this. Scientific school of compressor engineering (SPbPU) was created in 1960, and

currently "Gas Dynamics of Turbomachines" lab acts as a physical manifestation of the SPbPU scientific school. Centrifugal compressors can be designed for a wide range of applications by the laboratory's experts. The University of Michigan created the Universal Modeling Method (UMM), a set of specialized technical tools for calculating and designing centrifugal compressors. The Method is currently being improved by the writers. The TKR-140 radial turbocharger's normal diffuser and scroll proportions were used by researchers at the Laboratory of Gas Dynamics Turbomachines (LGDTM) built an ideal impeller and analyzed its gas-dynamic properties across a wide speed range. Personnel from RPA "Turbotekhnika" worked on the development, production, and testing of a turbocharger on their experimental test rig. Computational fluid dynamics (CFD) models of engine turbochargers (and other centrifugal compressors) are not yet capable of replacing engineering design and calculation methodologies.

RPA "Turbotekhnika" is a significant manufacturer of turbochargers for internal combustion engines, which are used in a variety of applications across Russia. The turbocharger for the 8ChN26/26 gas engine, which was converted from a diesel engine, is one of the most talked-about subjects right now, according to industry experts. Preliminary estimations indicate that the maximum boost degree should not be more than 1.6–1.7 degrees. This mandates the use of the broadest possible range of blower performance. Since the 1960s, the laboratory "Gas Dynamics of Turbomachines" has served as a representative of the Peter the Great St. Petersburg Polytechnic University's (SPbPU) scientific school of compressor engineering [21]. Designing centrifugal compressors for a wide range of applications [21–23] is something that the laboratory is quite experienced in. The Universal Modeling Method (UMM) is a collection of specialized engineering tools for the calculation and design of centrifugal compressors that was developed by the University of Michigan. In order to enhance the Method [24–26], the authors are now working on it. Using the usual diffuser and scroll dimensions of the radial turbocharger TKR-140 turbocharger, employees of the Laboratory of Gas Dynamics Turbomachines (LGDTM) built an ideal impeller and analyzed its gas-dynamic properties across a wide speed range. Personnel from RPA "Turbotekhnika" worked on the development, production, and testing of a turbocharger on their experimental test rig.

In order to understand the head loss model, you must first understand its basic qualities. - The head loss of a stage is equal to the total of the head losses of the intake nozzle, impeller, diffuser, return channel, and output nozzle. In the case of an inner blade or vane cascade head loss, the sum of losses on the suction and pressure sides of a profile, on a shroud, and on a hub is calculated. In terms of head loss, it is the sum of surface friction (which includes secondary losses) and separation losses, such as mixing and pressure losses. - Incidence losses are applied when flow rates are outside of the design range. In addition to the surface roughness criterion, the similarity criteria M , Re , and k are taken into consideration. Algebraic equations are created for each component of loss.... In the most current version of the Method, algebraic equations have sixty-four empirical coefficients that must be found before the equation may be solved. To identify them, the test qualities of hundreds of model stages are employed in conjunction with each other. At The Leningrad Polytechnic Institute in the late 1980s, Dr. D. Japikse presented a detailed description of the method's substantial deviations from the well-known Concept Agile engineering [39–43]. The following are the most important differences to make: - The parameters of the boundary layer theory are used to construct the concept loss model. It is possible to determine loss coefficients and drag force coefficients using this technique. - Test characteristics of stage components are used to determine the Concept loss model (impeller, diffuser, etc.). The test characteristics of a stage as a whole are utilized to determine the loss model for the

Method. Although there are differences between two engineering models, this does not suggest that one is valid while the other is erroneous. Several models may be beneficial in engineering applications, depending on the situation. When applied to this case, the Universal Modeling Method has been proved to be effective, allowing for the design of an efficient turbocharged compressor as well as the correct computation of its characteristics across the whole operating range. When selecting a turbocharger, consider the volumetric flow rate, pressure ratio, and turbocharger efficiency. Thermodynamics of the main engine's combustion chamber are also affected by ship speed. An application's pressure ratio and temperature can alter. Meratus Palembang's dynamic primary engine enables prompt cargo delivery. Thermodynamics is separated into four stages: charge, compression, combustion, and expansion. This method generates turbocharger operating line, turbocharger efficiency, and engine power output characteristics. When turbocharger pressure ratios are at their maximum, VTR 304, 321 and 354 have volumetric flow rates of 3,15 m³/s. The propeller's weight on the engine forces the turbocharger to work harder than the engine can. The volumetric value rises due to these dynamic conditions. The turbocharger on VTR 304 also runs at 80% efficiency at 11,1 knots and 78% at 10,4 knots. It is 78% efficient on VTR 321 at 11,1 knots and 79% efficient at 10,4 knots. The VTR 304's engines can produce 3220,595 kW (25889,903 kW) when all three are fully loaded.

1) Domain of Computer Science

Decide on the computational domain's size as the initial stage in numerical modelling. The turbocharger and the pipes fitted in the anechoic chamber rig mentioned in section 3.3 are the computational domains in this example. For reasons of accuracy, an actual compressor of the same exact model was disassembled and scanned with a structured-light 3D scanner to achieve the required level of detail. The digitized data was then processed using software post processing methods to create a smooth CAD model.

Only one primary blade and one splitter blade were included in the final model to ensure proper geometry; the rest of the blades were cloned. The computerized model also featured tip clearance and rear plate gap. By examining the voids between rebuilt surfaces, the fluid domain was recovered from the CAD model. In the diagram below, you can see an example mesh.

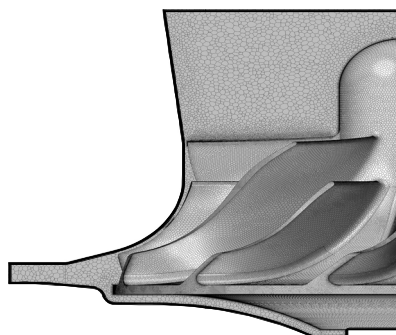


Figure 23: In the CFD model, a polyhedral mesh of the rotor walls (grey) and surrounding fluid (blue) was employed.

A mesh consisting of 9.5 million polyhedral cells arranged in a non-structured way was used to obtain high values for y^+ near the impeller walls. This mesh size was increased near the walls to increase the accuracy in this area and decreased farther from the wall to decrease the total size of the mesh. In boundary layer theory, the so-called y^+ is a dimensionless parameter. Some turbulence models function best when the first cell near to the wall is close to one.

By using the known diffusion coefficients for the compressor fluid, numerical calculations were performed to determine the volume of fluid that diffuses into and out of the turbocharger's compression chamber during each time step. Only pipes with a length of five pipe diameters were considered in these calculations to eliminate unnecessary calculation time. In Fig. below, the numerical simulations of these short inlet and exit ducts are compared to the actual experimental configuration deployed in the anechoic chamber test equipment. The real pipes were significantly longer than the simulated ones, as seen in the diagram.

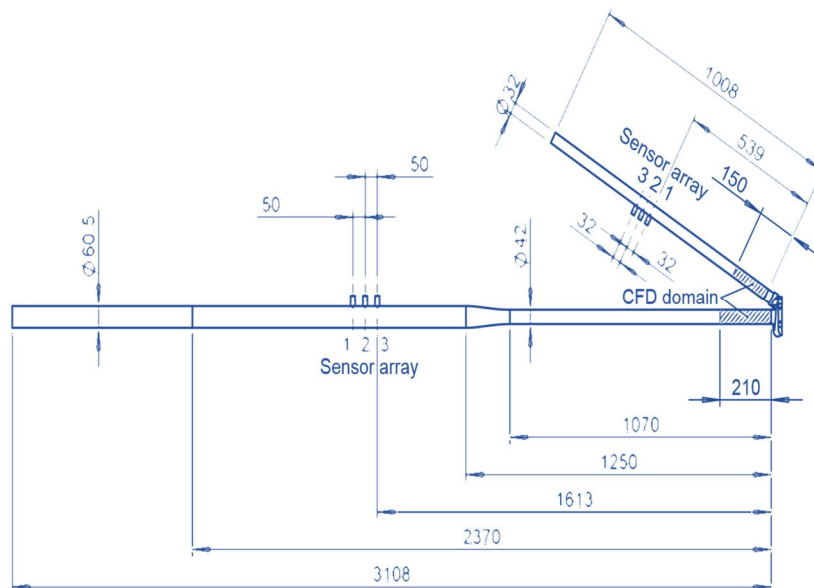


Figure 24 shows a schematic representation of the compressor's inlet and exit pipes, as well as the arrays of piezoelectric sensors that are used. The intake and exit pipes of the compressor are modelled using an experimental wave decomposition and computational fluid dynamics (CFD).

A mesh containing 9.5 million polygons was used to ensure that the y^+ values near the impeller walls were close to one, with the application of inflation layers near the walls to boost such values even further. The size of the polygons was increased as they got closer to the walls in order to lessen their overall size. Figure shows the results of the numerical simulations compared to the actual test setup in the anechoic chamber. The pipes installed in the test rig were much longer than those simulated in the model.

| | |
|---------------------------|---|
| Inlet boundary condition | $\dot{m} = 77\text{g/s}, T_T = 293\text{K}$ |
| Outlet boundary condition | $p = 223\text{kPa}$ |
| Rotational speed | $N = 158763\text{rpm}$ |

Table 1: The boundary conditions for the CFD simulation are taken from the experimental data taken in a small test rig in an anechoic chamber.

The diameter of the inlet pipe had to be lowered due to the pipes and flow meter that were accessible. Extending the CFD domain up to the limit of these ducts would have significantly increased simulation time, as seen in this picture.

2) Case Setting

The model was created in Star-CCM+ [108], a commercial CFD software tool that employed a segregated solver to solve the scenario. The SST k turbulence model was used in a DES simulation (Detached Eddy Simulation). When sub-grid-scale is practicable, taking grid size into consideration, and Reynolds-averaged equations when it is not [110], this hybrid technique is used. This should aid in the resolution of finer flow configurations that may contribute to noise creation. Mendonça et al. [45, 111] produced a similar solution.

The simulations' boundary conditions were set as outlet pressure and inlet mass flow rate, using values drawn from the experimental campaign detailed in preceding chapters of this thesis. To tackle the transient problem, a rigid body motion simulation was utilized, and a time step that equaled 10 of rotation was set to match the frequency in question. A stable solution was recorded at least 60ms after steady state was detected. The heat movement within the system was only examined adiabatic since it had no major impact on the results at high loads (112–114). For the sake of simplicity, surface roughness, dynamic shaft eccentricity, and mechanical deformations were not taken into account.

3) Solution Monitors

In addition to providing insights into the fluid field as a whole, some additional pressure sensors were added to monitor the acoustic behavior of the inlet and outlet ducts.

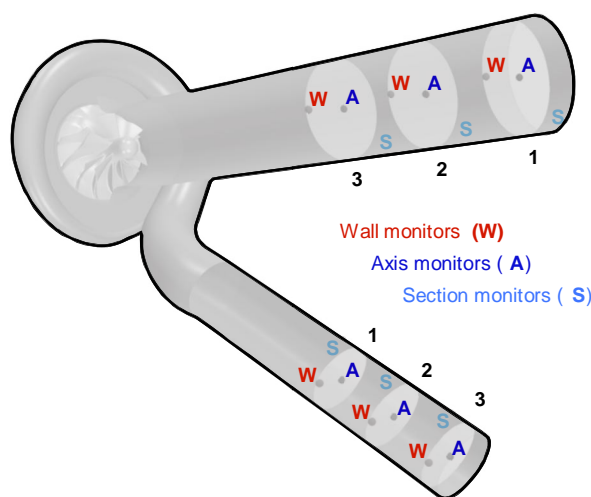


Figure 25: It shows the CFD domain, with a focus on the compressor wheel and three different types of pressure monitors that were chosen during the set-up process. It is important that they are not blocked by other things in the ducts.

When measuring the air quality in a room, a variety of techniques can be used. For example, one technique involves placing a single-point pressure recording flush against a wall, another involves placing a single-point pressure monitor in the middle of the room, and another involves placing an area-averaged pressure recording across the entire duct cross section.

Centerline monitors would have been required if piezoelectric transducers had been employed in the experimental campaign to analyze variations between data captured at this position, which could not be monitored experimentally without disrupting the flow, and data collected by wall-flush sensors.

Three pressure monitors were used to compare measurements in a plane wave frequency range. The monitors were produced at three different cross-sections in both the inlet and outlet ducts, to simulate how the real setup would work, and see if the longitudinal distance has an impact. It was only discovered that location had a minor impact.

B. Methodology

Validation tests were conducted to determine whether the numerical model could accurately represent the compressor's operation after a sufficient number of computational simulations were completed to ensure that the simulated pressure signal spectra had sufficient high frequency resolution for comparisons.

1) Global Variables

The compressor's overall performance results were to be compared to those given by established procedures as part of the validation approach. If they did not match, the simulation setting should be fine-tuned further. Under addition, numerous critical factors like as W_u and isentropic efficiency s may be used to determine the compressor's efficiency in real-world situations.

$$W_\mu = \frac{W}{m} = \frac{\Omega_T}{m} = C_p (T_{out,T} - T_{in,T})$$

$$\eta_s = \frac{W \cdot s}{W} = \frac{T_{in,T} (\Pi_{T,T}^{\frac{\gamma-1}{\gamma}} - 1)}{T_{out,T} - T_{in,T}} \dots\dots\dots 6.2.1$$

Here, Ω is the engine's rotational speed, T is the torque it produces, c_p is the amount of heat it absorbs, T is the pressure ratio between both sides of an engine and refers to a fixed variable used to compute a pressure ratio. Furthermore, an experiment may be carried out to see if the simulated forces are accurate. It was discovered in this experiment that as speed increases, so does torque.

Both experimental and computational findings were averaged over 5-second intervals to prevent tiny differences in time. The global variables for both examples are shown in the table below, demonstrating a good correlation between the two sets of values with a relative error of less than 10% for all measured variables.

The accuracy of global parameter prediction is good, with less than 1% relative error between CFD (computational fluid dynamics) and experimental findings, as seen in this data table. For the acoustic analysis, we may utilize averaged variables such as mean Mach number, temperatures, and pressures. This demonstrates that our compressor numerical simulation accurately reproduces the system's operational circumstances.

| | Π [-] | W_u [kJ/kg] | η_s [%] |
|------------|-----------|---------------|--------------|
| Experiment | 1.2 | 111.3 | 68.7 |
| CFD | 1.2 | 111.3 | 66.7 |
| r_r [%] | 0.9 | 0.7 | 0.4 |

Table 2: Comparison of global compressor variables observed in the experimental test rig and predicted by the CFD solution

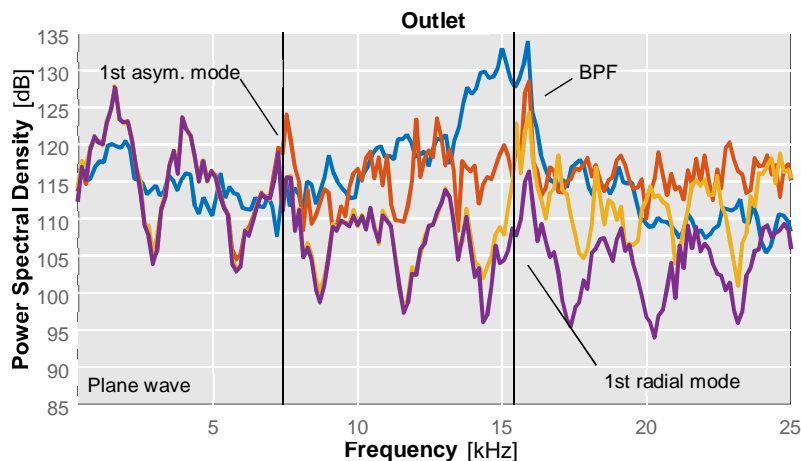
The accuracy of global parameter prediction is good, with less than 1% relative error between CFD (computational fluid dynamics) and experimental findings, as seen in this data table. For the acoustic analysis, we may utilize averaged variables such as mean Mach number, temperatures, and pressures. This demonstrates that our compressor numerical simulation accurately reproduces the system's operational circumstances.

2) Acoustic Result

The simulation findings, on the other hand, do not ensure that the setup is accurate enough to recreate transient flow events connected to the compressor's acoustic behavior. The fact that two alternative approaches, each based on different concepts and developed independently, produce identical trends does not mean that transient waves are not present in the compressor's acoustic wave generation. A link was discovered between pressure waves in both simulations and experiments after a reexamination of experimental data collected utilizing rapid piezoelectric sensors and simulation findings. This shows that the modeling design did not sufficiently simulate the transient waves detected with fast piezoelectric sensors.

a) Total pressure Spectra are a Type of Spectrum.

After applying the wave decomposition process to each signal, the original comparison of experimental and numerical data was done by comparing only the overall pressure spectrum. The three types of CFD monitors specified in Section 6.1.3 are taken into account in this comparison. After applying the wave decomposition process to each signal, the original comparison of experimental and numerical data was done by comparing only the overall pressure spectrum. The three types of CFD monitors specified in Section 6.1.3 are taken into account in this comparison. is presented in Figure below.



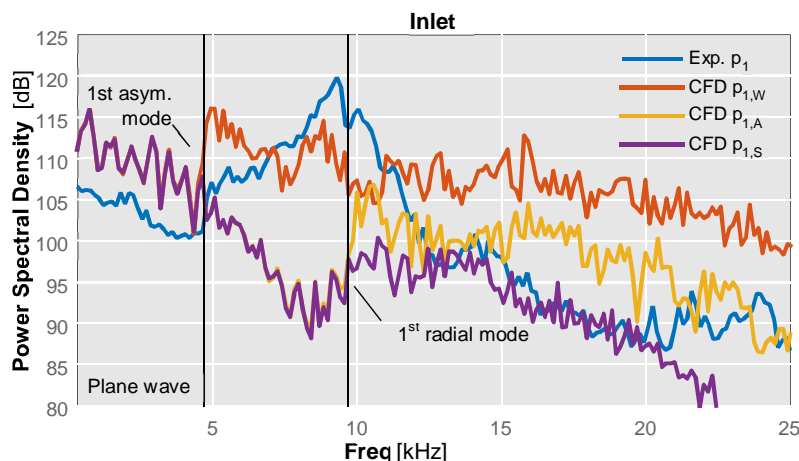


Figure 26: A comparison of the total spectral content of each monitor type will show that piezoelectric sensors provide superior performance.

The three separate CFD models indicate that when pressure is modulated over a cross-sectional plane wave, the three monitors will collapse in the frequency range of zero to one wavelength. When there is a cut-off frequency for each model at which the wall monitor indicates different spectral content than the theoretical forecast, the signals collapse. Each model predicts that a first asymmetric mode will propagate just above this frequency.

The area average monitor is situated in its characteristic line when the initial axial mode propagates, therefore it is unaffected by cross-section pressure changes. The axial monitor smooths out these swings, affecting just the displays closest to the wall.

Wall monitor Axis monitor

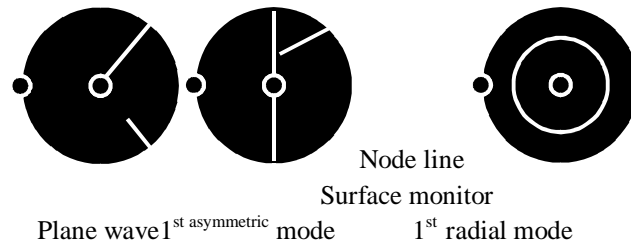


Figure 27: Two acoustic modes in a CFD monitor can be represented schematically by the solid lines, and the different types of monitors can be identified by the different line styles.

The axial pressure monitor is not in the line of modal propagation when the initial higher-frequency radial mode excites, thus it merely averages the axial variations. As a result, the frequency response of the axial monitor does not precisely mirror that of the duct, and the cutoff frequency is lower than anticipated by CFD. In the output findings, it can also be shown that BPF tonal noise levels are best predicted by the numerical model; this may be described as an example of wave phenomena. A definite BPF peak can be seen on the pressure monitor mounted on the wall, which is more evident in the exit instances than in the input ones. Although the findings of CFD-simulated spectra show some consistency with experimental observations, there is no strong connection for PSD levels and trends over the plane wave frequency range. This might be owing to the pipe's short length, which causes a standing wave pattern, as well as the lack of non-reflecting boundary conditions on the outlet walls.

b) Decomposed Spectra

Pressure wave decomposition (PWD) can provide crisper spectra by isolating different components of a signal, as described in the preceding chapter. The experimental data was deconstructed using the three-sensor LCMV beamformer described in section 3.3.1.2, but because PWD may be conducted on any waveform, additional approaches, such as the Method of Characteristic (MoC) [115–117].

$$P_{\text{back}} = \left[\frac{1}{2} \left(1 + \left(\frac{P}{P_{\text{ref}}} \right)^{\frac{\gamma-1}{2\gamma}} \right) \left(1 + \frac{\gamma-1}{2} \frac{u}{a} \right) \right]^{\frac{2\gamma}{\gamma-1}}$$

$$P_{\text{forw}} = \left[\frac{1}{2} \left(1 + \left(\frac{P}{P_{\text{ref}}} \right)^{\frac{\gamma-1}{2\gamma}} \right) \left(1 + \frac{\gamma-1}{2} \frac{u}{a} \right) \right]^{\frac{2\gamma}{\gamma-1}} \dots\dots\dots 6.2.3$$

P_{ref} is an appropriate reference pressure, and the heat capacity ratio is calculated using the instantaneous local values of sound and flow speed. The results of using this technique on a wall mounted CFD monitor are displayed in the diagram below.

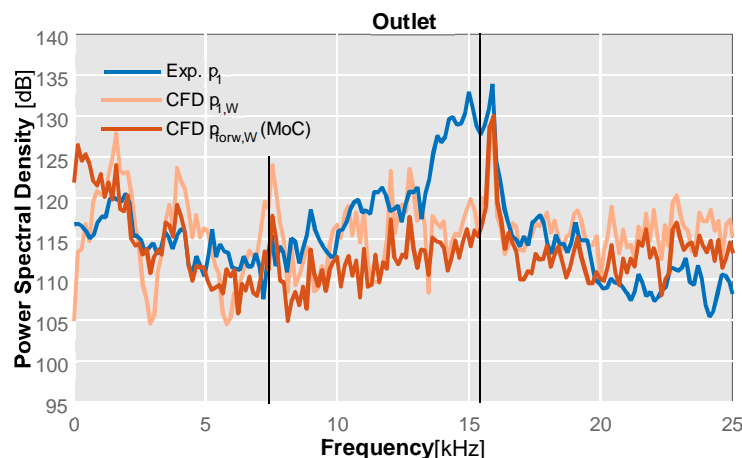


Figure 28: Comparison of experimental and model-simulated total pressure in the outlet case, using the wall monitor, shows that mode onset occurs at approximately 0.5% higher total pressure than simulated decomposed pressure.

The pressure spectra estimated with and without periodic oscillations match better with experimental data when oscillations are reduced, as indicated in the figure. Although there are differences below 2 kHz, the overall pattern of these two sets of spectra is comparable. Numerical models are better at reproducing Blade Passing Frequency (BPF) tonal noise at 16kHz, but they fall short of capturing broadband noise seen in trials between 13 and 17kHz. This might imply that numerical models are missing certain processes.

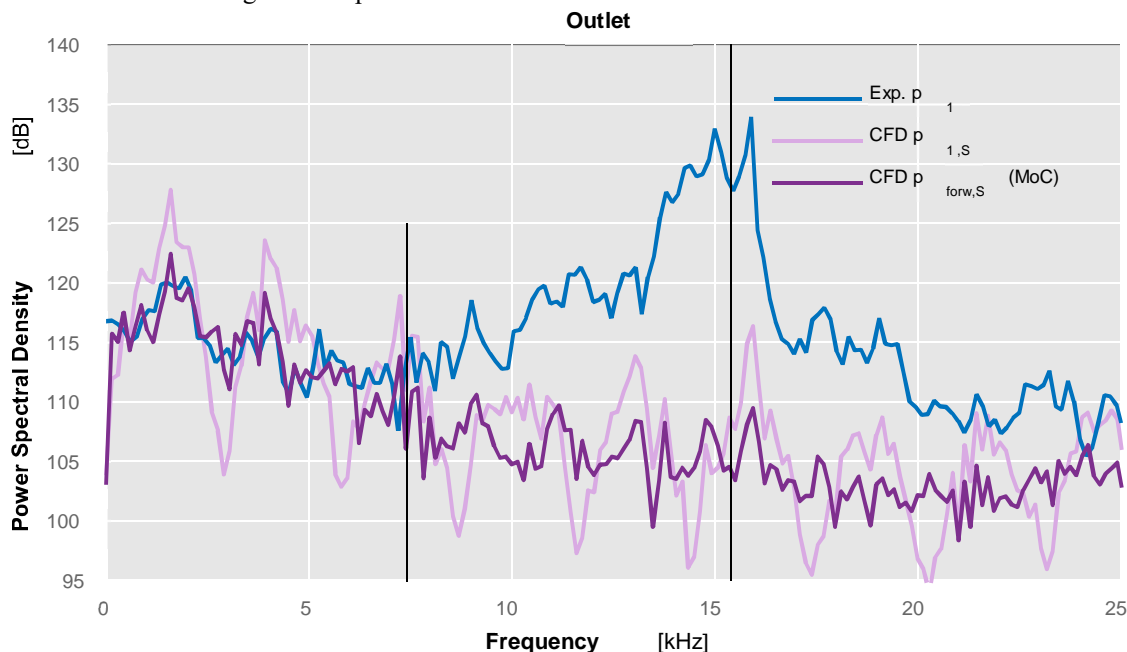


Figure 29: The experimental results were compared with those from a simulation of the outlet case, where pressure was decomposed into modes. In both simulations, pressure reached the same mode-onset value.

By utilizing a section monitor, which averages pressure throughout a whole region, the experimental and simulated data may be compared. In the region below the first asymmetric acoustic mode, which begins at 7.4 kHz, using the Method of Characteristics decomposition technique results in a better match between experimental and simulated spectral content. When applied to higher frequency ranges, the simulation, after modes begin to propagate, does not correlate well with the reference experimental data. Compared to a single-point wall monitor, tone noise at the Blade Passing Frequency (BPF) and bandwidth about 15 kHz are less effectively caught.

Further examination into the BPF tonal noise indicated that it might be caused by area averaging that ignores pressure changes across the duct's cross section. When one side of a flow control barrier is exposed to high pressure while the opposite surface is exposed to low pressure, area averaging fails to detect it. The pressure spectra in both the inlet and output ducts were properly anticipated by the CFD study.

3) DMD Results

Preliminary work involved implementing the SVD-based DMD procedure with coherence ranking and applying it to data from a small fraction of cells near the outlet wall to test the applicability of DMD to the CFD problem addressed in this chapter, as information about pressure at each cell is not saved in this CFD setup. Because of the POD/DMD attribute, which permits the selection of a subdomain rather than the entire domain, the results in those cells should be representative. Furthermore, data were down sampled both geographically and temporally by examining one out of every ten cells and one out of every ten pictures, yielding a spatial length of $M = 7103$ and a temporal length of $N = 103$.

Maximum coherence is at around 16,000 hertz and corresponds to mode 323, which is related to the blade passing frequency (BPF). Although the BPF occurs at around 16,000 hertz, there is another important DMD mode that exists in a range of frequencies that overlaps with the first asymmetric acoustic blade mode (7.4 kHz), tonal noise that overlaps with the BPF. This tonal noise dominates at the BPF. However, the whoosh noise that a distant car engine makes shifts in pitch as you pull off the road and into a parking space. The whoosh noise is low-frequency noise, usually around 1.7 kHz, which sounds more like an increasing whistle than a constant whoosh. TCN-like broadband noise is higher in frequency than the whoosh noise, but still low frequency compared to music or speech. It reaches its peak volume around 3 kHz and above. TCN-like broadband noise modes do not appear to be as coherent from one speaker to the next as modes linked to whoosh and BPF tonal sounds.

The distribution of the three lower-frequency modes (0.8 kHz, 1.6 kHz, and 2.1 kHz) is connected to plane wave propagation; the distribution of the higher-frequency modes is more complicated as a result of acoustic mode propagation in the outlet duct. The effect of mode frequency on acoustic propagation and spatial composition of DMD modes.

The mode corresponding to a frequency of 0 kHz has been selected in the simulation on the left, resulting in a uniform distribution along the duct. A standing wave pattern forms as the frequency rises. The pattern alters when higher frequency modes occur in the simulation. Mode 11.5 kHz is influenced by mode (0,1) since the information is no longer homogeneous throughout each sector and instead varies depending on the angle. Finally, because numerous modes are present at 25 kHz, the pattern is rather complicated.

C. Conclusions

Due to the fact that many writers did not study them in detail, this chapter explores the validity of numerical models of automobile compressors from Chapter 4, which were produced from an acoustic perspective.

When using computational fluid dynamics to model compressors, the domain and boundary conditions must be carefully defined, since this has a substantial impact on the spectrum information that can be extracted from the simulation. Pressure wave decomposition is one technique to deal with this problem while keeping the CFD domain and mesh within normal computational constraints. This strategy has been demonstrated to improve the separation and recovery of spectral information coming from the compressor in both computational and experimental findings; however, spurious interferences must be filtered away as well.

Placing an acoustic parameter monitor close to the operational fluid stream should produce better results than keeping it further away. It is critical to position the sensor on a wall-flush monitor so that higher order modes aren't triggered. The results of a wall-flush monitor should give further information regarding the compressor's acoustic behavior.

Using computer simulations, researchers could investigate the effects of pressure and velocity on the sound generated in the engine of a motorcycle. They found that the acoustic output observed in internal combustion engines can be caused by the flow phenomena identified by their analyses. They used contours of pressure to predict the evolution of backflows in fluid dynamics simulations. They saw increased velocities at the point of maximum pressure ratio when compared with steady-state simulations. Peak spectral densities from velocity signals in the diffuser pointed to areas where whooshing occurred during engine operation at high mass flow rates.

When a turbofan engine moves from normal operation to an unstable state, its acoustic output (how loud the engine is) increases. Computational fluid dynamics models have shown that rotating low pressure "bubbles" form and move in the direction opposite the air flow. If an engine is operating with less air flow, these bubbles appear in a part of the diffuser near the volute tongue. When these bubbles appear, backflow can be predicted to occur at point P in the diffuser. The highest-pressure ratio occurs during this point and shows where backflow initiation occurs within the wheel. Except in two situations when larger mass flow rates were simulated, both velocity and pressure information indicated areas of increased velocity in the diffuser near the volute tongue. These models might reveal how turbofan engines' acoustic output can be enhanced when they run outside of their typical operating range.

Acoustic emissions were observed in all three simulated conditions. These emissions may be linked to vortex shedding from the compressor blades. One postprocessing technique is to inspect the location of acoustic-relevant flow features at several frequencies using a Fast Fourier Transform (FFT) on the pressure signal at different locations on the blades and diffuser. An example has been presented regarding the 3 kHz frequency. Another postprocessing technique would be to decompose each one of the modes of vibration into eigenfunction modes, which can then be mapped with a Fast Fourier Transform (FFT). The use of modal decompositions provides a means of analyzing sound-producing events in rotating machinery without having to guess which are the relevant frequencies and spatial locations. The Dynamic Mode Decomposition, for example, is a relatively new method that is not yet widely used but shows considerable potential. This technique's formulation and implementation have been demonstrated in a limited-scope example. This example demonstrates the model's capacity to detect key flow frequencies and their spatial distribution on outlet duct wall cells, with a focus on whoosh noise and pre-mature turbulence production known as BPF tonal noise.

The application of spatial filtering in the study of both linear and nonlinear convection-diffusion equations has been demonstrated. Spatial filtering on a wider scale is outside the scope of this research since it necessitates computing methods capable of handling big data sets (i.e., manipulating data in the order of gigabytes). Further study of spatial filtering might lead to a more accurate identification of key frequency components.

VII. INLET GEOMETRY EFFECT

To minimize flow instabilities, geometric modifications of the input line near the impeller were proposed and evaluated in the literature study conducted in Chapter 2. The fundamental goal of these changes is to postpone the onset of deep surge or completely eliminate it, so keeping the map's useable zone (the amount of load and efficiency that can be used) broad and enhancing compressor thermodynamic efficiency during low air mass flow operating circumstances. It is important to remember, however, that these changes have an impact on carbon emissions, noise emissions, and compressor wear and tear.

This chapter details geometric configurations that were evaluated in a flow rig and under real-world situations. The geometries that were evaluated were those that were most often recommended in the literature.

A. Geometries

We employed basic geometries to measure acoustic emission in an experiment conducted using the anechoic chamber flow test apparatus described in Chapter 3. To evaluate acoustics, we employed a reference pipe, an orifice noise measuring free-field microphone, and a radiated noise system with four evenly dispersed free-field microphones. Researchers used three piezoelectric pressure sensors in a short length of pipe upstream of four distinct tested designs to confirm their computational fluid dynamics (CFD) calculations. To imitate more realistic entrance circumstances, a straight pipe was employed instead of a U-bend.

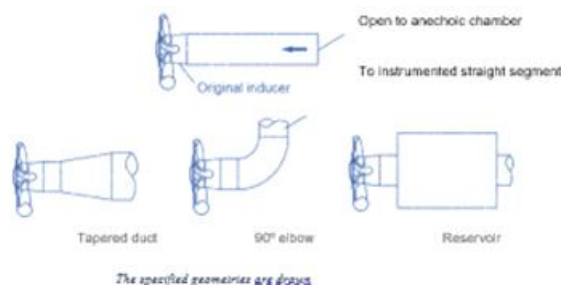


Figure 30: The specified geometries are drawn

1) Surge Margin

The acoustic output of each form was evaluated using raw pressure data from a fast sensor, which measured the air mass flow at where the compressor achieved deep surge conditions. After determining the influence of each shape's acoustic output on flow stability, the allowable operating parameters may be expanded.

Experiments on turbochargers revealed that Yokogawa digital oscilloscopes collected pressure data as well as mass flow and shaft speed information, while a custom-written software application recorded the rest of the ancillary data. From higher to lower mass flow, measurements were made at varied air mass flow levels with a constant shaft speed of 160 krpm.

We obtained the violent oscillations of deep surge when they reduced the mass flow to a level near to that of deep surge and began a continuous monitoring of variables such as turbine speed, engine speed, intake temperature, and backpressure. An approach similar to that described in Chapter 3 was used to evaluate the pressure recording. By dividing the power of the 0–50-Hz pressure spectrum by the power of the 50–100-Hz pressure spectrum, frequency ratios R_f were calculated.

$$R_f = \frac{\sum_{f=0}^{50} |P(f)|^2}{\sum_{f=50}^{100} |P(f)|^2} \dots\dots\dots 7.1.1$$

Below are graphs that shows pressure being gradually reduced and the air mass flow gradually dropping to a deep surge condition, the different geometries each recorded non-dimensional pressure.

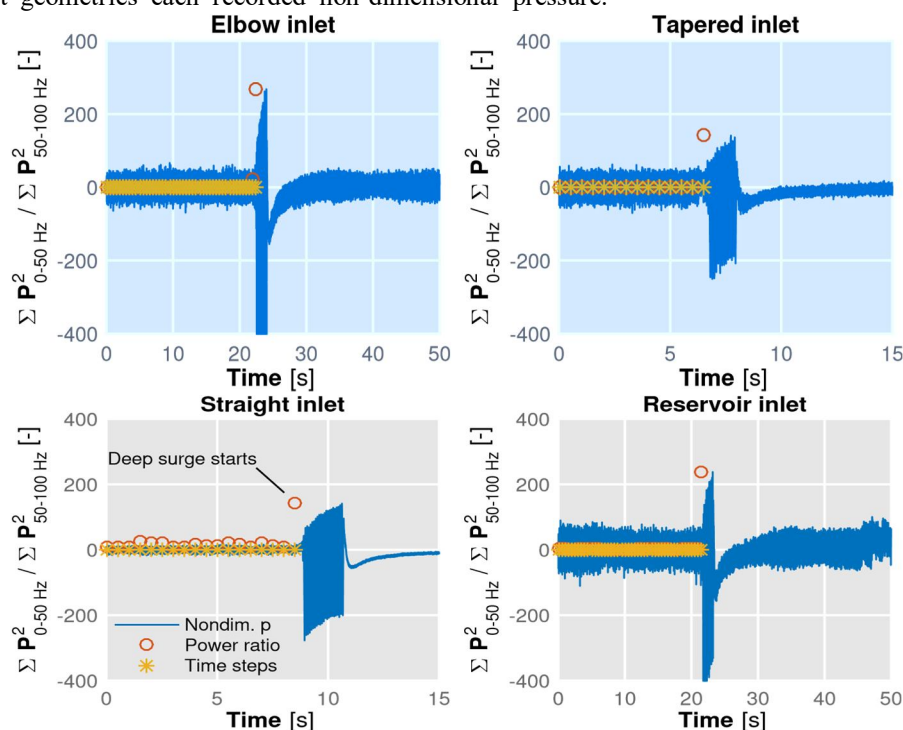


Figure 31: With pressure being gradually reduced and the air mass flow gradually dropping to a deep surge condition, the different geometries each recorded non-dimensional pressure.

Low surge was thought to have started when the power ratio hit one hundred. Averaging the data from the two preceding time steps yielded the lowest allowed mass flow. Non-dimensional pressure traces can be mixed with time steps and power ratios as shown above. The lowest permitted air mass flow is depicted in the diagram below.

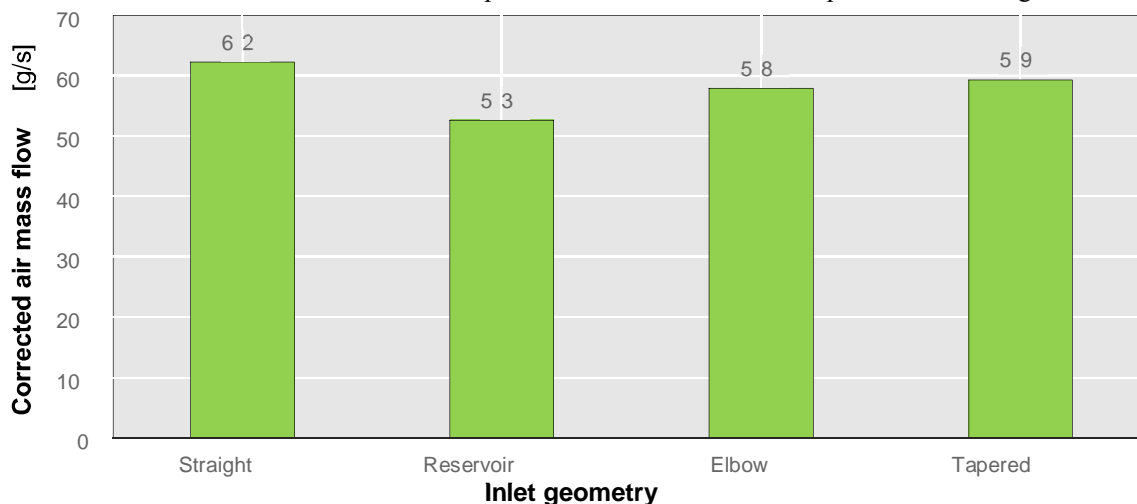


Figure 32: The presented approach yielded the lowest permitted air mass flow for the various basic geometries examined.

As seen in this picture, the straight conduit is the first to experience deep surge conditions. Until the surge occurs, the edges of the tapering duct and the 90° elbow pipe are identical. At the same time, the reservoir prolongs the damaging scenario even more, allowing for a ten-g/s reduction in air mass flow to be achieved.

2) Levels of Background Noise

In addition to assessing the impact on surge margin, the levels of external noise were also measured. Two unique measurement procedures were available in the anechoic chamber, as previously mentioned in the chapters on the subject. We used a single free-field omnidirectional microphone, which was situated 10 mm distant from the intake aperture, to gather orifice noise. Each time a new form was created, the microphone had to be adjusted to accommodate the different lengths and orientations of the orifices. This was especially true in the case of the elbow.

It was decided to keep the second system in the same location for all of the geometry studies since it detects externally radiated noise and consists of four equi spaced free-field microphones situated one meter from the center of the intake assembly. Both cases included the use of a PULSETM DAQ system to acquire data from the microphones, which were calibrated before to the tests using a Brüel & Kjr pistonphone. In the figure below, the results of both measurements taken at the stable operating point closer to surge, as stated by the approach described above, are shown since here is where the highest amount of noise may be found.

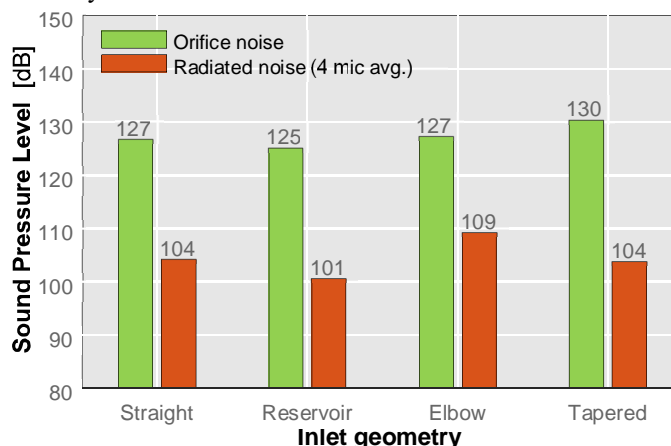


Figure 33: For each intake geometry at the stable operating point closer to surge, noise is radiated to the anechoic chamber in the form of sound waves.

This experiment has revealed that the intake geometries studied here have a significant impact on the perceived loudness of radiated noise. When compared to the reservoir, the straight duct generated greater noise levels, with a reduction of up to 3 dB in the case of the average recorded from the four microphones.

In comparison to the straight entrance, the 90° elbow inlet yielded a 5 dB increase in sound level. The fact that the orifice was not perpendicular to the plane of the four microphones employed may have impacted this finding. Finally, tapered ducts appeared to emit sound at the same volume as straight pipes. The reservoir's orifice noise was reduced by additional two decibels. The straight reference pipe had the same level as the elbow, but the tapered duct had a higher level of 13 dB, which was 3 dB higher than the reference geometry.

To investigate these level disparities in further depth, Fig. above shows the varied spectra acquired by the orifice microphone in each geometry test. The levels for the tapered duct are higher, as are the levels for the full frequency range, but the inlets with the elbow and reservoir remain closer to the straight reference pipe.

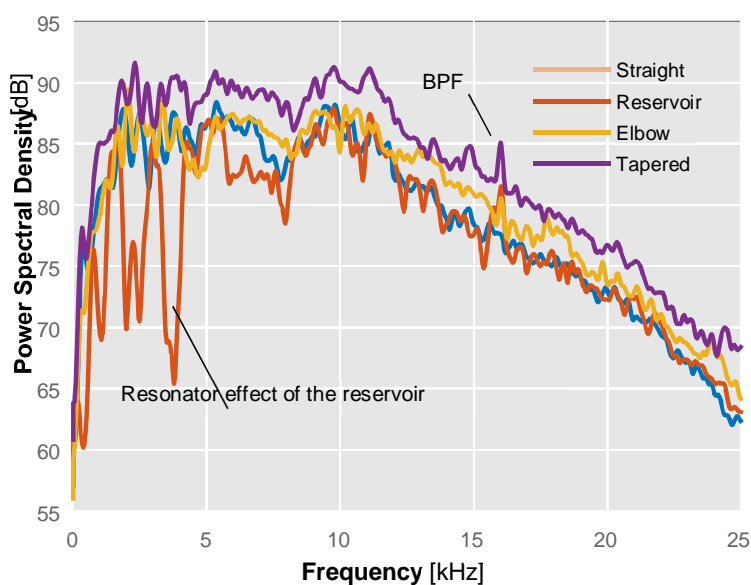


Figure 34: A comparison of sound spectra for each of the simple inlet geometries is given for the configuration with the highest amplitude at the stable operating point.

But the most noticeable distinction between the tapered duct spectrum and the reservoir spectrum is attenuation at frequencies in the plane wave zone, which is present in both spectrums. This is due to the fact that the reservoir provides a critical resonator effect. The tapered duct spectrum, on the other hand, boosts levels over the whole electromagnetic spectrum. In addition to this, there is a minor peak at 16 kHz, which corresponds to the blade passing frequency associated with the 160 krpm shaft speed used in these tests.

B. Engine Testing are Performed While the Vehicle is Running.

The findings of our on-engine testing were presented in Chapter 5. We investigated the impact of several geometric modifications of the turbocharger inlet line on performance, surge margin, and noise emission in our follow-up experimental session.

1) Setup Measurements

Because the reservoir case could not fit into the available compressor inlet, the required geometric adjustments in the intake line were made to account for realistic packing size constraints of commercial vehicles. As a result, the reservoir case was not tested in this scenario. Similarly, elbow inlets were not tested since rerouting the intake line would be required. The influence of tapered ducts, spinning devices, and nozzle-like additions on the system was next investigated.

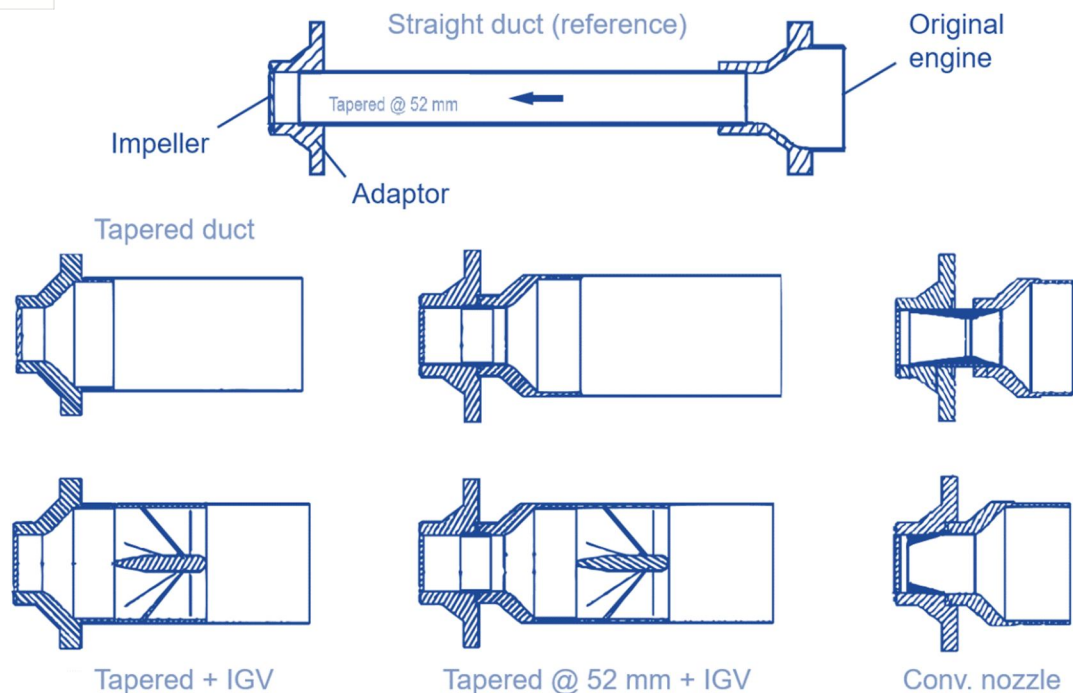


Figure 35: The cross-sectional view of the inlet geometries considered for the on-engine campaign.

In the diagram above, the selected geometry varies as a result of these selection criteria. On top of the figure is the reference geometry. The turbocharger inducer was removed and replaced with a straight duct and an adaptor. At the duct's terminus, a pipe with the origin.

A tapered transition was used to connect all of the diameters. In order to achieve the shortest possible inlet duct form, a tapered duct was installed directly in front of the compressor impeller leading edge. This is portrayed in the figure's central portion, as well. In conjunction with the tapered duct, an IGV device was utilized.

To make the entering airflow more erratic, this was done to increase the spinning of the flow. Using a 3D printer, the device stators, which have zero-degree leading edge angles and seventy-degree trailing edge angles, were 3D manufactured from the CAD design. The device that was installed in the intake pipe is seen in the diagram below.

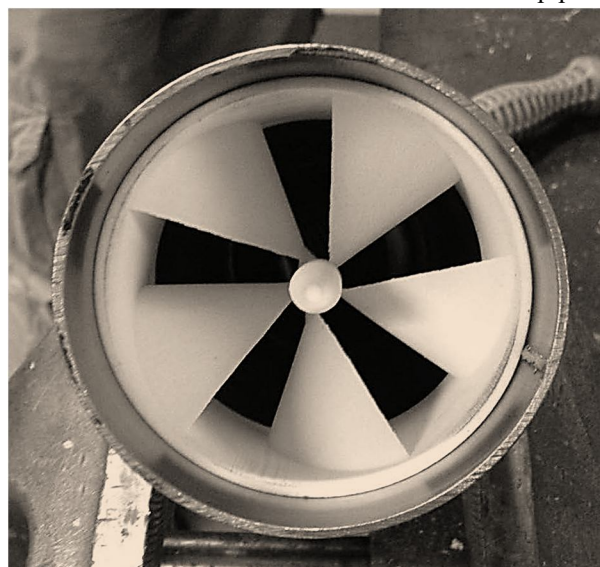


Figure 36: The image below shows a 3D-printed IGV device is fitted to the inlet duct of a compressor, revealing the inlet and impeller.

Except for the distance between the impeller and tapered duct, which was enlarged to 52 mm to see how the proximity of the tapered duct to the impeller impacts the compressor's performance, the two subsequent geometric adjustments (middle column of Fig. 21) were similar. One measurement was carried out using an IGV, whereas the other was carried out without one. Finally, a convergent-divergent nozzle was tried between a tapered adapter and the impeller, as well as a convergent nozzle directly after the tapered duct, with its throat as near to the impeller wheel as feasible. An acoustic measuring setup was built to assess the effectiveness of this design, similar to the one used in Chapter 5 to measure the compressor's noise levels. The intensity probe was positioned one inch from the intake orifice, and the pressure decomposition array was linked to the straight inlet extension. We investigated noise production under numerous scenarios, including both cautious and severe settings, to confirm that the results from the noise characterization campaign were relevant to real-life conditions.

2) Results

The goal of this experiment is to compare the acoustic findings from various channel geometries, this part will focus on the orifice intensity probe data, which were found to be well associated with in-duct noise in section 5.3. An intensity level map is shown below, highlighting the locations where measurements were made. The strength of sound was interpolated between frequencies of 1 and 3 kHz, which are particularly essential for the "whoosh" problem.

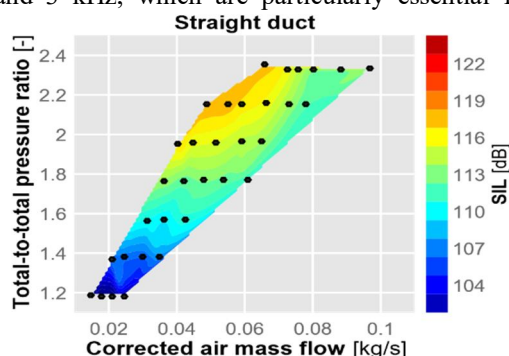
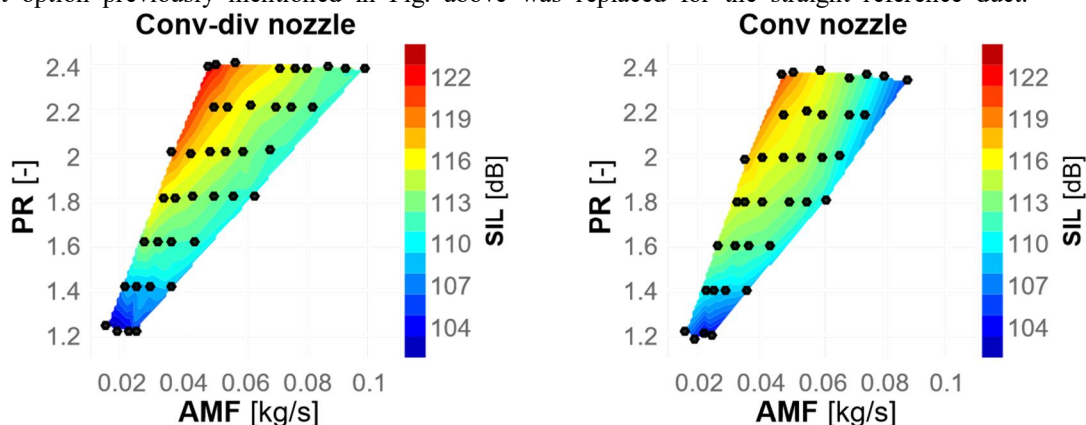


Figure 37: The straight intake utilized as a reference in the on-engine inlet geometric variation test has a loudness level map between 1 and 3 kHz.

Note that the displayed operating circumstances do not reflect constant shaft speed lines due to the facility's unique regulating method based on compressed air injection into the inlet line; therefore, no judgment regarding the slope of these lines. This graph shows that noise levels in the selected band behave as expected while also showing a dependency on air mass flow. The graph indicates a higher noise level at higher pressure ratios and a greater dependency on air mass flow at higher pressure ratios. The figure below shows the findings for the same frequency range when each geometric inlet option previously mentioned in Fig. above was replaced for the straight reference duct.



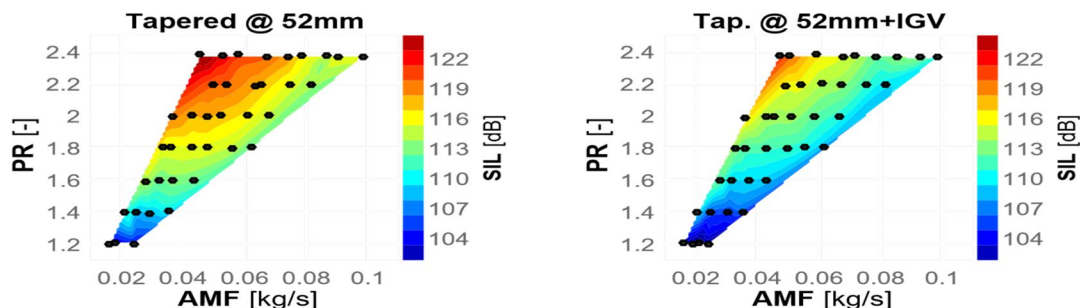


Figure 38: The figure shows the sound intensity level maps for the several geometries utilized in the on-engine test between 1 and 3 kHz

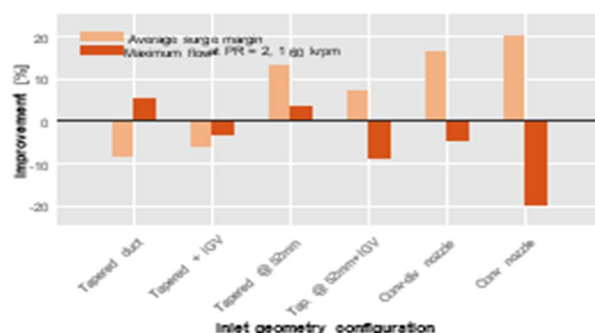


Figure 39: Performance fluctuation for various intake geometry over the engine's usual operating range.

To maximize surge margin and avoid compressor surge, the effect of geometry modification on air flow must be investigated for maximum flow at 160 krpm. The performance of each geometry was found to be affected in different ways by the duct inlet cross section. The figures above show a comparison of straight ducts along with those featuring an IGV and tapered ducts featuring various outlet sections. These show that there is a trade-off whereby the maximum flow rate is maximized when the straight duct is used but the surge margin is reduced. A better surge margin can be achieved by using a tapered duct, most effectively at 52 mm from the impeller.

In order to use a convergent nozzle in a real-world application, the nozzle throat must be mechanically opened at high flow rates. At the same time, if this is done, at $TT = 2$ and 160 krpm of shaft speed, an equally great air mass flow decrease will occur. The average sound intensity level (SIL) at a given frequency range as measured by the Brüel & Kjaer intensity probe pointed directly at the entrance orifice is shown in the diagram below.

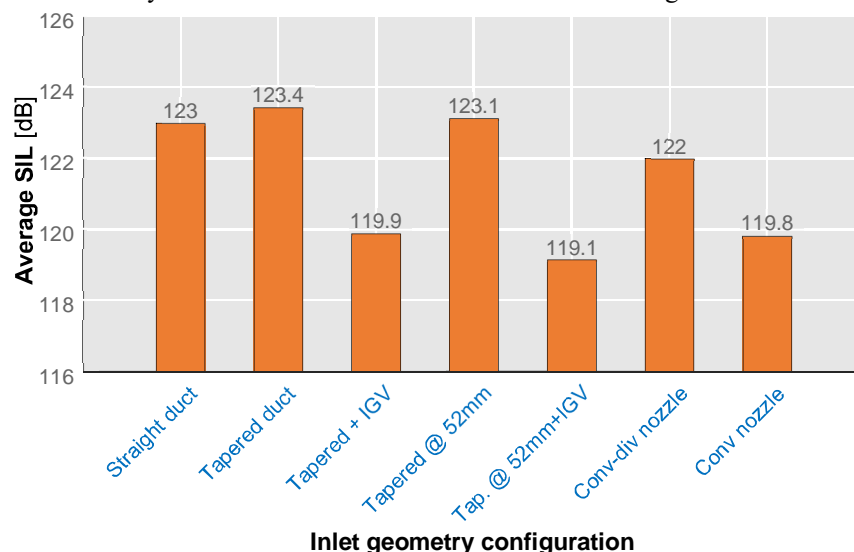


Figure 40: Comparison of mean sound intensity levels for various intake geometries across the engine's usual operating range.

C. Parametric Analysis of the Elbow

The turbocharger test rig utilized for the inlet local flow measurements detailed in Chapter 7 showed not only global features of sound intensity and air mass flow, but also local factors such as temperature distribution, skewness, and other variables. Because sound intensity could not be accurately quantified using both approaches during the previous experimental campaign or in the preliminary testing phase, it was decided to begin research on this issue by looking at this specific variant of elbow shape.

This shape would generate non-uniformities in the flow field that circumferentially tapered ducts and nozzles do not, providing a great contrast for evaluating the impact on circumferential temperature distribution skewness and association with noise production. As a result, a parametric campaign was created to assess the impact of three 90° elbows with variable radius on inlet-induced flow distortion and temperature skewness. Given the wealth of data on the link between these parameters and noise generation, it was hoped that the parametric campaign would indicate which parameter values were most likely to result in effective designs. The campaign's objectives were twofold:

1) Designing Geometry

During the installation of the elbow inlets, three types of elbows were used. The very tight elbow had a radius of 0.75 times the diameter (D). The medium elbow had a 1-inch radius. The third elbow had a radius of 1.5 inches, which was smoother and created less distorted flow than the previous two elbows. The elbows needed to set up in a way that the thermocouple arrays could be attached easily to heat sensors already previously installed. The pipe needed to house the arrays in a way that would allow them to be secured once again and provide similar spacing between tips and the wall of the tank as in the straight pipe experiment. Three different elbow types were chosen: zero point seven five diameter (tight), point one diameter, and one point five diameter, which would provide a smoother transition and less distorted flow.

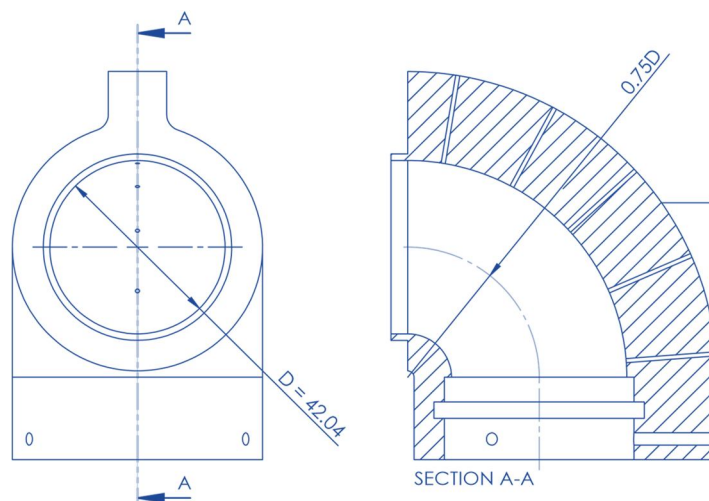


Figure 41: The 0.75D elbow inlet is meant to fit into the compressor intake adapter and contain the linear thermocouple array, as shown in this mechanical drawing.

Because the thermocouples had to fit tightly, the researchers opted to make numerous elbow prototypes using 3D printing. The thermocouple and retention screw guiding holes, as well as the sealing O-ring slots, may all be included right into the design. The mechanical drawing of one of their prototypes, with a radius of 0.75 D , is shown above.

The CTC project team designed an elbow that could simply be fitted to a compressor to improve the accuracy of thermocouple data. Engineers would not need to drill into the compressor to install a thermocouple if they used this elbow; instead, the thermocouple could be installed by a manufacturer or engineer before the elbow was fitted. An industrial partner was recruited to build molds so that these elbows could be mass-produced after three variations of the design were constructed by gluing together a sheet of metal over a smaller portion of pipe and rolling each junction on an industrial metal bender.

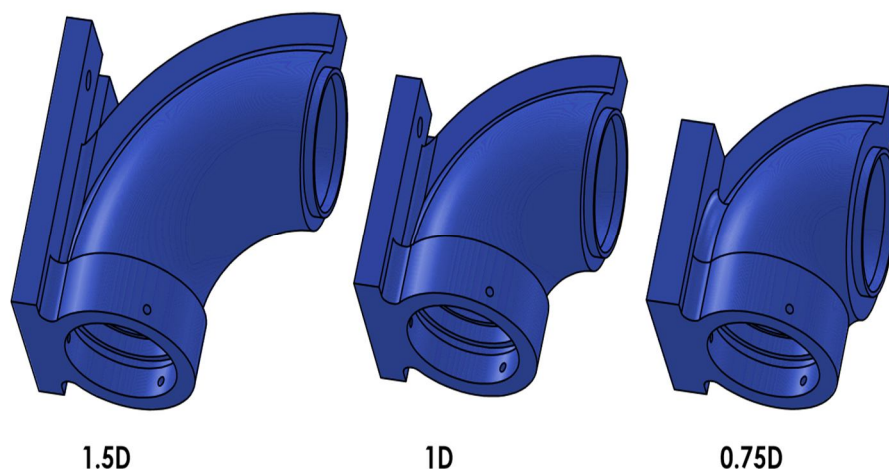


Figure 42: The 3D-printed prototypes were created using CAD models of compressor elbow inlets of various radius (decreasing in radius from left to right).

In light of these issues, the elbow prototypes were created utilizing a technology known as Selective Laser Sintering (SLS). It entails focusing a laser beam onto the surface of a tray containing powdered material and binding it together in layers to create the desired shape. Table 8.1 contains the technical specifications for the material that was selected. The heat deflection temperature, sometimes referred to as the heat distortion temperature, is crucial in determining the outcome. It refers to the temperature at which a sample is taken. starts to deflect at least 0.25 degrees. mm under the stress of 1.82 MPa. Because the intake line is close to ambient pressure in this situation, no problems are predicted until the temperature rises.

| Property | Normative | Unit | Value |
|----------------------------------|------------------------|-------------------|-----------------|
| Tensile Modulus | DINENISO/527 | MPa | 38003.548 |
| Tensile Strength | DINENISO/527 | MPa | ±±±15031501 |
| Elongation at Break | DIN/ENISO/527 | % | |
| Flexural Modulus | DINENISO/178 | N/mm ² | |
| Impact strength (Charpy) | DINENISO/179 | MPa | |
| Notched Impact Strength (Charpy) | DINENISO/179 | MPa | |
| Shore-D/A-hardness | DINENISO/179 | | 36004.6D |
| Heat Deflection Temp | DIN53505 | °C | 7629130±±±0.322 |
| | ASTM/D648 (1.82MPa) | | |
| Vicat Soften Temp B-50 | DINENISO-306 | °C | 169 |
| Density | N/A | g/cm ³ | 1.36 0.05 |

aluminum-filled polyamide utilized in the laser sintering of prototype elbow inlets.

Table 4:
Specifications for the

2) Setting

The prototype elbows were mounted with thermocouples and inserted into the anechoic chamber test apparatus after SLS fabrication and delivery. The construction of the narrower elbow version is shown in the diagram below. During the sintering process, the little holes for the thermocouple alignment became plugged with remaining dust and had to be finished using a hand drill. This was not a concern because the material used is easily automated.

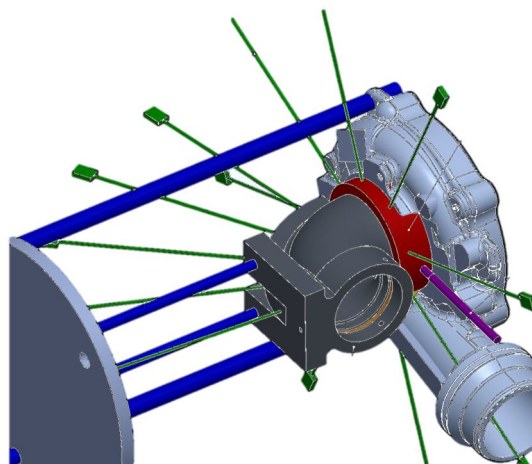


Figure 43: CAD model of the compressor assembly, such as the temperature and pressure instruments, as well as the mounting system, with the 0.75D elbow intake attached to the common adapter.

In Fig., a drawing of the adapter piece holding the circumferential temperature array, the inducer micro pressure probe, and a sealing O-ring, we can see how this portion was retained in place and how perforations in the flat surface were used to position the elbow parallel to the outlet.

3) Results

This test campaign for the local flow characterization chapter was carried out utilizing straight intake pipes that were comparable to those used in the original reference map in order to establish how precise the interpolated maps were. The operating circumstances of each measured data point for both the straight input pipe used as a reference and the three mentioned elbow prototypes are shown in the data above. It can be shown that consistency was reached in the majority of settings, though not at the maximum flow rates. This was most likely owing to turbulence caused by the elbows, which increased friction. When the flow rate was high, especially at greater pressure ratios, the most hazardous situations occurred.

To determine how accurate the interpolated maps were, this test campaign for the local flow characterization chapter was conducted using straight intake pipes that were equivalent to those used in the original reference map. The data above shows the operating conditions of each measured data point for both the straight input pipe used as a reference and the three elbow prototypes indicated. Consistency was achieved in the majority of settings, but not at the highest flow rates, as illustrated. This was most likely due to the elbows' turbulence, which enhanced friction. The most severe scenarios occurred when the flow rate was high, especially at higher pressure ratios.

a) Sound Amplitude

Sound intensity levels were calculated for each operating condition utilizing in-duct piezoelectric sensor arrays and the wave decomposition technique outlined in Chapter 3 to determine the sound pressure levels. After taking an average of the sound intensity level between 0.7 and 3 kHz in order to concentrate on the previously stated whoosh noise issue, a noise map for each geometry was generated using the interpolating technique.

To evaluate the several elbow prototypes, tiny discrepancies between operations under different situations were employed to compare the different designs. Difference maps were constructed by subtracting the reference straight duct noise map from each of the newly acquired elbow noise maps in order to emphasize the differences between the reference straight duct noise map and the results obtained for each of the elbow prototypes.

The flow intensity maps produced by the three elbow designs are clearly different; the maps demonstrate that the elbows' inlets and outlets, depending on their arrangement, may obstruct the passage of the fluid through the elbow. Despite the fact that the interpolation approach produced high mass flow rates along a number of the lines, the black dot indicates the actual measurement site, and it is clear that some information is missing in the area surrounding this location. A few slight measurement errors happened between the time these patterns were taken and when they were compared, which resulted in some data being left out of the analysis.

As the radius of the elbow grows, the fluctuations in sound intensity at the inlet seem to be greater than those at the exit. This surge is most visible at lower flow rates and medium-low shaft speeds, with a level increase of up to 6 dB occurring under these conditions. The value of the point with a minor increase in level for both inlet and exit ducts seems to decrease when the elbow radius is reduced for medium to high air mass flow and medium to high shaft speeds, according to the data.

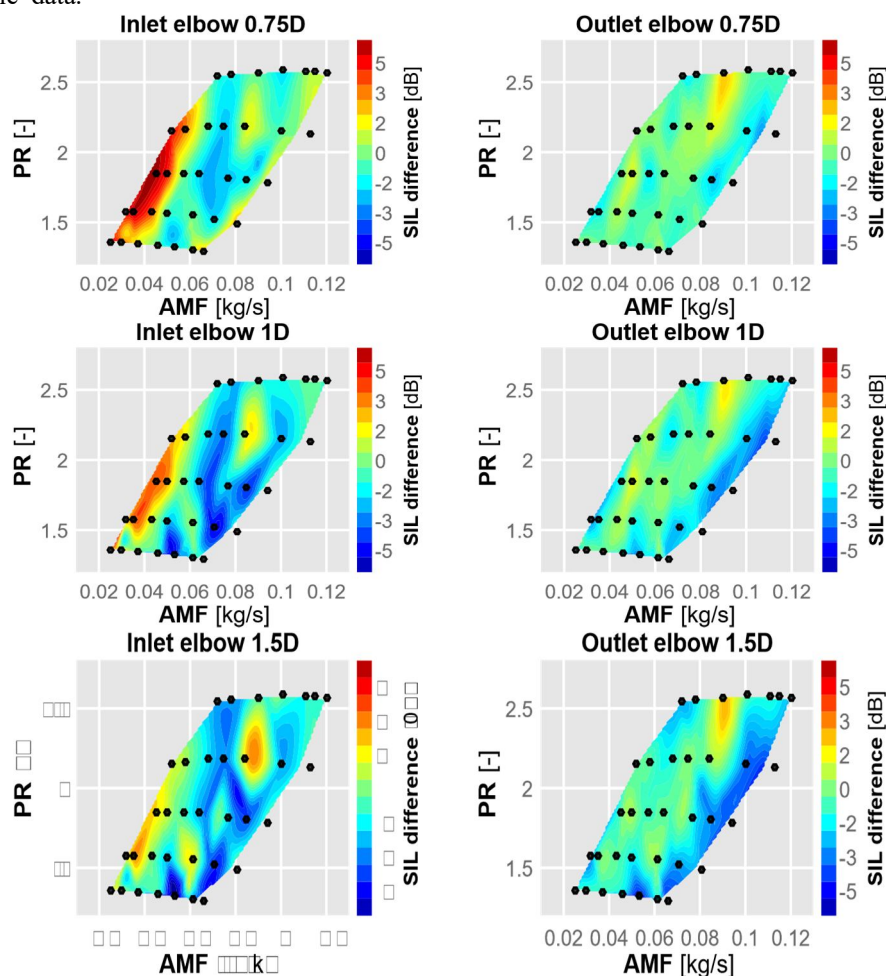


Figure 44: In-duct sound intensity levels at the inlet (left) and exit (right) for each of the specified inlet elbows compared to the reference straight duct. 1.5D, 1D, and 0.75D, from top to bottom.

Finally, operating parameters at both the inlet and outflow, especially for medium greater mass flows and lower shaft speeds, limit noise output in the given frequency range. In the input duct, these drops, like the rises, are more noticeable, while positive and negative oscillations in the output duct are less.

To better quantify the effects of elbow configuration on sound intensity, histograms showing the distribution of differences between sound levels in inlets with different elbows were computed. Intensity level differences range from -1 dB to +1 dB. It can be seen that the two wider elbows (1.5D and 1D) have a mean of around -1 dB, similar to the mean for the less wide elbow (0.8D).

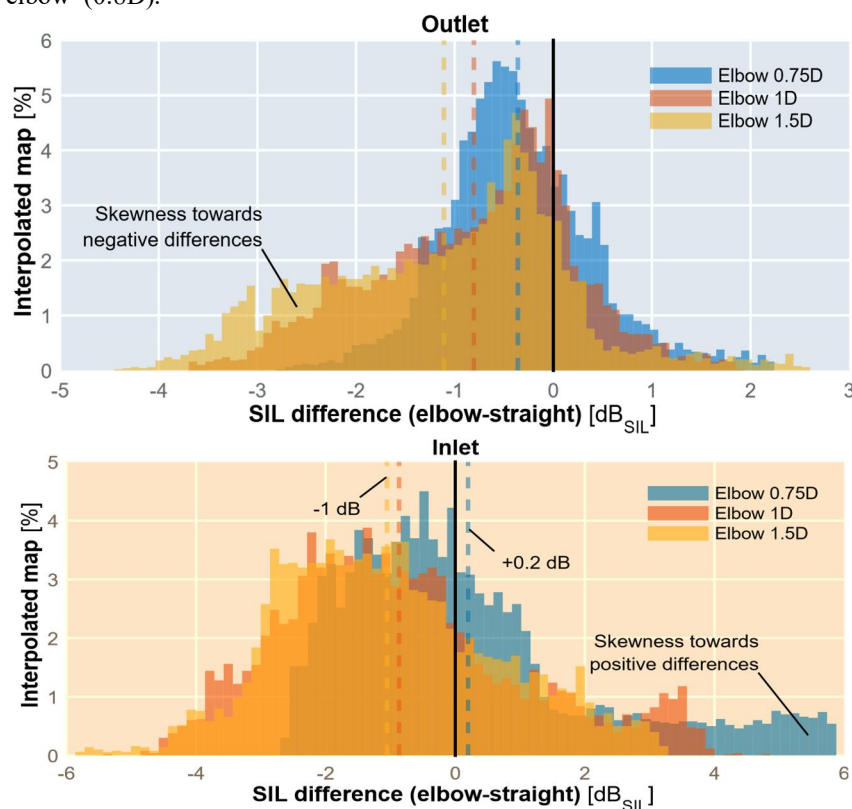
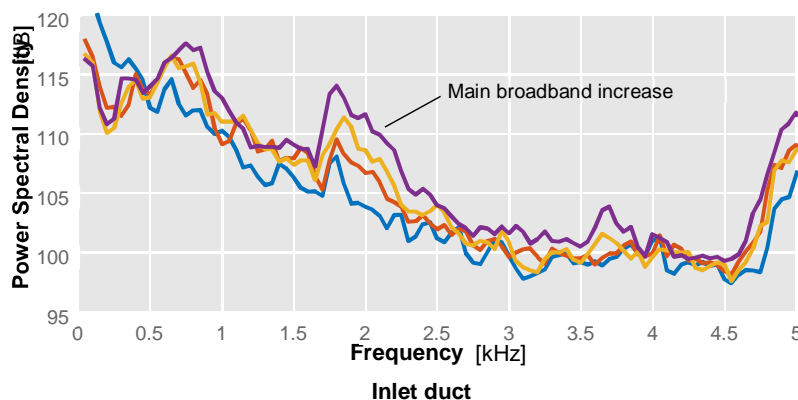


Figure 45: The results of the sound intensity level differences for both inlet and outlet sound pressure levels were compiled into histograms that illustrate the percentage of the compressor map at which each different level occurred for each tested elbow configure

The narrowest elbow (0.75D), which corresponds to the low flow, medium-low speed zone depicted in the intensity maps above, appears to exhibit a large skewness toward positive differences of up to 6 dB. These points add about 0.2 dB to the average. When looking at the outlet difference distributions, it appears that the narrower elbows have a more symmetrical distribution than the larger elbow or the 1.5D elbow. The narrowest elbow has a mean of about 2 dB, which is less than the other two variations.



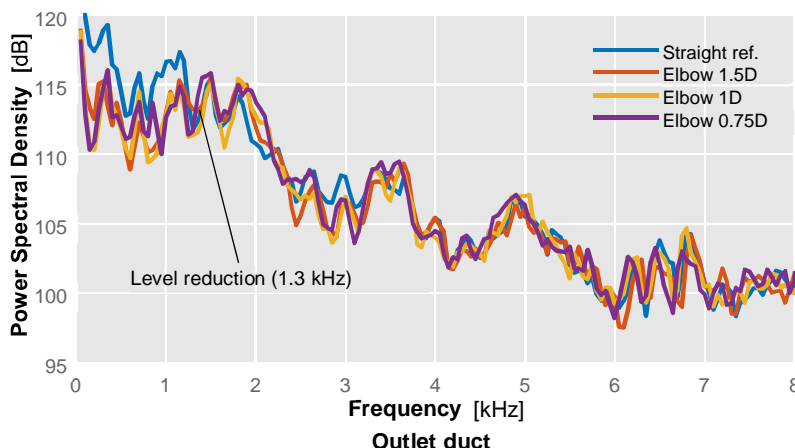


Figure 46: In the 45 g/s plane wave range spectra at both inlet and exit, variations between the straight reference duct and each of the elbow arrangements may be seen, pointing to the efficacy of a specific elbow.

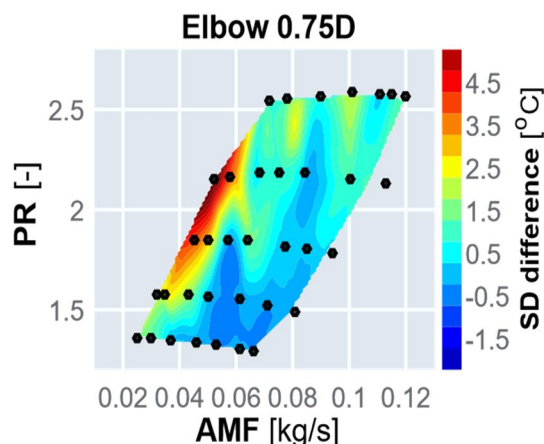
Figure shows the frequency spectrum of a plane wave. A comparison of the spectrum with the random fluctuations in pressure recorded by inlet and exit piezoelectric sensors in the turbulent flow zone shows that the two spectra are quite similar. The PSD in the plane wave zone, for example, was identical to that in the turbulent region when operating conditions were high (140krpm, 45g/s).

The spectrum generated by the straight duct is comparable to those of the elbows—which are smaller in size—up to 1.3 kHz. Above 1.3 kHz, the straight duct exhibits higher levels than all of the elbows, which is also evident from the maps and graphs provided. The increase in frequency is not uniform; observe how the tiny peak at 1.7 kHz grows as the elbow radius decreases, eventually reaching a broadband frequency above 2.5 kHz for the smallest radius elbows.

Between 0.75 and 3.6 kHz, there are two minor broadband elevations in the outlet spectra that are likewise apparent in the pressure spectra collected by the diffuser pressure probe. The smaller of these is seen at 2.3 kHz and is a consequence of an increase in the upstream transmission at this frequency because of the small tube attached to the diffuser inlet manifold during experiments with the so-called whoosh broadband noise.

b) Temperature

Aside from the changes in sound intensity created by the various inlet designs, a similar processing approach may be used to evaluate the differences in temperatures in the intake section that are connected to the hot reversed flow coming from behind the compressor impeller. Analysis of thermocouple data from two arrays (circumferential and longitudinal) produced maps of backflow length and flow temperature skewness.



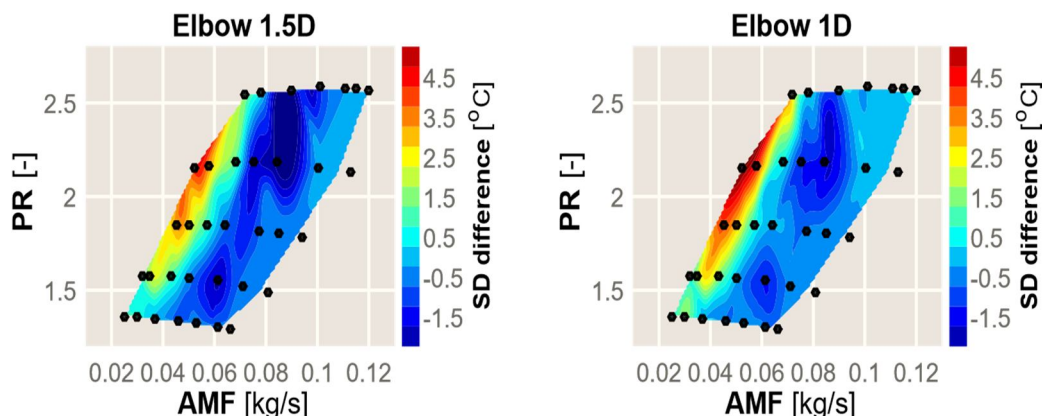


Figure 47: Use this map to show the differences in the temperature of circumferential segments for each of your selected elbows vs. the reference straight section.

The difference maps for each elbow variant were then compared to the original reference map, which was measured using a straight input duct. Figure above shows the difference (elbow minus straight) maps that resulted. To provide a fair comparison, the same color scale was used.

Similar patterns may be identified in each of the three examples. Lower air mass flow levels show a gradual increase in temperature skewness, especially when working at medium shaft speeds. A minor reduction in flow temperature skewness can be detected at higher air mass flow levels, which is much more visible with the less narrow elbow arrangement (1.5D, top left map). This reduction zone is similar to the 1D elbow in terms of conditions. Nonetheless, the temperature skewness difference is smaller than in the previous example, and in the case of the most reduced elbow form, it is almost negligible (0.75D).

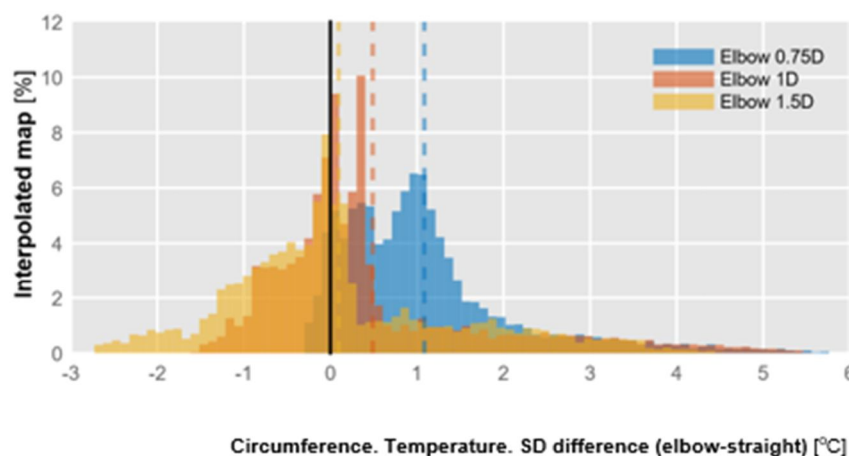


Figure 48: Histograms show the temperature standard deviation differences between each of the tested elbow modifications and the reference straight inlet pipe. The percentage of the interpolated compressor map where each different level was found indicates

As the graphs show, there is a jump from low ILDs to high ILDs in a very small part of the map, which can be seen in both figures as an indentation on the right side. An increase follows this in sound levels that span a greater range than the change from low to high ILDs. The left tails of the distribution curves are shorter but more populated, indicating that most compressors have small changes in ILD compared to the average. The average ILD difference for compressors with the narrowest elbow design is roughly 1.0 dB, whereas it is nearly negligible for compressors with broader elbows. By examining the temperature profiles produced by the longitudinal thermocouple array that was incorporated in the design of each elbow prototype, we can estimate the length of the hot reversed backflow that flows upstream of the impeller and into the intake.

c) *Correlations between temperature and SIL*

As we saw in Chapter 7, when we studied the effects of elbows on sound propagation, there is a correlation between the skewness of circumferential temperature profiles and sound intensity. This figure shows the correlation for three different elbows. In general, large changes in noise level are seen at high flow rates; however, no apparent change may be seen at low flow rates. Using the same axis limits as for a straight pipe, a correlation between the degree of sound intensity and circumferential temperature skewness was calculated for the three elbow-inlet instances. The correlation can be seen for both the straight pipe and the straighter elbow (the one with a central radius of 1.5D), separating higher flow rate conditions (indicated by blue circles) from lower flow rate conditions (indicated by red circles), where skewness is well correlated with increased noise levels. When designing elbows with narrow inner diameters, it is difficult to control temperature and sound intensity. When the inner diameter of the elbow is large enough to accommodate a larger flow rate, the temperature and sound intensity curves can be manipulated so that they are similar across all flow rates; when flow rates are small enough and the elbow radius is narrow enough to generate large turbulence levels, no amount of manipulation can reduce the difference between the hottest and coolest points around the elbow.

When the radius of a pipe elbow decreases, the temperature fluctuations at the pipe entrance and exit increase even when the flow rate is held constant. Temperature fluctuations can be seen in the bottom plots of the figure. In addition, sound intensity and frequency are increased across all four plots, as was previously shown in the figure by the “hump” of whoosh noise at lower frequencies.

D. *Elbow Parametric Study*

The turbocharger test rig described in Chapter 7 was used to investigate the effects of inlet geometry on the local flow pattern. Temperature distribution, skewness and other such characteristics were measured. The data gathered by the CFD simulations will be useful if laboratory experiments are conducted to study the performance of local modifications to inlets. The study investigating the influence of elbow geometries on noise generation and flow distortion started with this 90-degree geometry variation because measurements during the previously described on-engine experimental campaign showed that characterization of the sound output was not straightforward. Even though a variety of different 90-degree tapered ducts and nozzles were tested, it was impossible to unambiguously link noise generation to flow distortion in these variations. On the other hand, flow distortion is an important factor when trying to explain the mystery behind aerodynamic sound generation, so it seemed like a good idea to look at the influence of different elbow geometries on this phenomenon.

E. *Conclusions*

The chapter has presented three different experimental campaigns, each designed to investigate the influence of different inlet geometries on turbocharger acoustic output. While different in scope, all three experiments resulted in similar conclusions. First, a series of tests was carried out to investigate the noise characteristics of various geometric forms added to the inlet of a compressor. The straight duct used as a reference had the same diameter as that of the inlet. Orifice noise was recorded using both a free-field microphone and an orifice micrometer that averaged four orifices.

VIII. EFFECT OF INTAKE FLOW FIELD

Although Turbo compressor have been installed in a large number of engines in an attempt to improve economy, there have been concerns voiced about the disruptive impact of noise and vibration on passenger comfort. According to a review of the literature, the flow field immediately upstream of a Turbo compressor can have an impact on the engine's performance. Based on computational fluid dynamics (CFD) studies of the flow field around a turbocharger operating in unstable conditions at the marginal surge area of the map described in chapter 2, this conclusion can be supported. Based on the modelling findings, it was discovered that when the turbocharger runs at high rotational speeds approaching its surge limit, a complicated flow field form. Researchers have been studying the reversed flow that is often associated with natural gas engines in laboratory settings for years, and while some researchers believe that an accurate model can be generated by measuring variables such as pressure and temperature, CFD theorists such as Smith believe that a more thorough approach would use a three-dimensional volume of data that includes pressure, temperature, velocity, and density.

A. Methodology for Local Measurements

The methods used to comprehend the process of gas being pushed backward via a channel is described in this section.

1) Modifications to the Turbocharger

The chosen compressor was modified (as in earlier chapters) to accommodate the temperature and pressure sensors required to monitor these variables. The original inducer was removed up to the plane of the blade leading edges and replaced with a detachable adapter piece featuring thermocouples in the compressor housing.

The straight pipe section affixed to this adaptor is detachable, and a linear thermocouple guide which facilitates the measuring of temperature, can be inserted into the pipe. This enables users to replace the straight pipe section for others with different geometries in order to create elbows or tapered ducts.

2) Temperature

Backflows from after the impeller, according to [106 and 133], are one of the first signs of approaching instability and stall. Flow reversals from immediately downstream of the impeller are the most common precursors of compressor stall. Because the flow reversals are coming from a hotter region, they tend to be wetter than the remainder of the gas due to the non-isentropic compression process.

As a result, both pressure and temperature readings should be used to pinpoint the start of deep surges. For example, Liu et al. (52) discovered that both pressure and temperature standard deviations are excellent markers of deep surges.

Two 1.5 mm type K thermocouple arrays were installed on the compressor inlet to capture the temperature impact of this backflow. A circumferential array that spans a cross section of the pipe just 14 mm from the compressor wheel plane measures the temperature every 45 degrees. In the longitudinal direction of the pipe, the second array is linear, reaching up to two inlet diameters.

To describe backflows, Andersen [51] and Lang [49] employed thermocouples in the center of the pipes and a single one 14 mm from the blade tips, projecting 4 mm. Different solutions are used by compressor manufacturers to prevent gas recirculation in the intake pipes. Backflows are thought to be up to three diameters long and half the diameter of a pipe radius thick. Several thermocouples should be placed in the center of the ducts, while recirculation's should be identified by thermocouples positioned 4 mm from the blade tips emerging out of the pipes.

Temperature data were collected once again in order to create reference points for the two arrays of sensors. The temperature of the air consumed by the intake flows was used to determine the temperature of the ambient air in the testing room. Additionally, an external thermocouple was mounted to the exterior wall of the circular array adapter, as was previously described. It was also mounted on the turbocharger assembly, with its view field covering both the compressor volute and the input pipe duct. A thermographic camera was also installed on this assembly. This allowed for the assessment of the outside temperature distribution, which demonstrated that the temperature profiles observed by the linear thermocouple array were not generated by heat transfer from the engine's pipes as had been suspected before.

3) Pressure

To evaluate compressor pressure distributions, temperature compensated Kistler probes were utilized in two sites. The inducer, which is upstream of the compressor wheel, and the diffuser, which is downstream of the wheel, were the two places. More accurate readings for monitoring air turbulence can be obtained by placing the inductive probe 6mm away from the wheel's leading edge and the diffuser probe 5 mm from its starting and 34.5 mm from the turbocharger axis line.

4) Velocity

Validating computational fluid dynamics (CFD) estimates of the joint flow of two fluids requires detailed flow-field observations. Understanding how backflow obstructs the overall flow of the surrounding fluid is just as important as analysis of flow parameters. This essential information will contribute to CFD's wider acceptance as a forecasting tool.

a) Laser PIV Measure

A Particle Image Velocimetry (PIV) system was placed in the anechoic chamber to enable for the visual observation of flow fields and particle paths, among other things. The Qswitched Nd:YAG laser lights the measurement zone, which has been seeded with particles, with two consecutive laser beams, and captures the movement of the particles over the course of two frames using the Qswitched Nd:YAG laser.

Cross-correlation techniques may be used to identify the location of the particles, and velocity estimation methods can be used to estimate the velocity of the particles. A typical PIV setup includes a laser sheet for measuring particle displacement, a straddle CCD camera (from the TSI 9306A Six-jet atomizer) for capturing images of particle groups in motion at 15 Hz, and a two-dimensional velocity field calculator for calculating instantaneous two-dimensional velocity fields based on the positions of moving particles.

When combined with shadowgraph, particle image velocimetry (PIV) may be used to calculate flow velocity in subsonic and transonic flows in real time. Particle image velocimetry (PIV) is a non-intrusive, two-dimensional imaging method. The combination of PIV with shadowgraph, as established by Fitts et al. [1], is a very successful approach of measuring the speed and directionality of subsonic wind tunnel flows. Currently, the study is focused on the possibility of merging PIV with shadowgraph to measure flow velocity in a transonic wind tunnel, but it does not investigate methods for improving the accuracy of PIV data.

Flow fields were photographed at a rate of 1,000 frames per second using a 10-millisecond exposure period to conduct a correlation study between the images collected. The total number of pixels in images varied depending on the spatial resolution, ranging from 216,720 to 562,240. Velocity estimators were tested for accuracy using the standard deviation and maximum absolute deviation from mean measurements, which served as the validation criterion (cross-correlations). These criteria were used to demonstrate the algorithm's capacity to discover relevant results for use in experimental analysis, as well as to verify its overall performance, and to demonstrate the algorithm's ability to find relevant findings for use in experimental analysis.

When measuring airspeed in an aviation engine, it's typical to assume that the airflow is moving at a constant rate through the engine. This assumption is incorrect. However, under rare conditions, the airflow might get clogged, resulting in a back-up of more exceeding two feet in height.

These occurrences may impair researchers' perspectives while they are trying to observe the longitudinal movement of a plane, leading in incorrect data being produced.

The fluid ring, which is composed of minute particles, may cause the blades to become obscured from vision. Because of the high transversal velocity, the particles are driven to collide with the inner wall, resulting in the formation of apparent helicoidal tracks over the surface's surface. When trying to check the blades, this causes a challenge for the inspector. For example, you may utilize a procedure that consists of settling the turbo to suitable operating conditions and then seeding it for at least 1 second. It is recommended that you have around 10 pairs of useful shots before stopping the turbo and cleaning the glass pipe in preparation for the next run. Instead of recording through the glass layer, you may measure each plane directly on the compressor by directing your camera right at it from above.

It is necessary to develop a method for rotating the rotor and camera assembly in order to compare the cross-sectional photographs with their corresponding three-dimensional models. In order to keep the brightness of the light source to a minimum, each pair of images was taken at almost the same blade position, which was achieved by a mechanism. This made it possible to use a postprocessing approach to subtract the average intensity of many non-seeded photographs from each seeded image, resulting in a significant reduction in the brightness of the lit rotor and an improvement in particle correlation overall.

Considering that the back of the glass was painted matte and that there was no other surface to reflect off, laser pulses reflected by the back of the glass presented an issue in this situation. We opted to use it for measurements since the back of the glass was painted matte, which helped the clarity of the fields we replicated on the computer screen. Fortunately, our reconstruction contains just a few flaws, such as a slight notch that can be seen at different points around the axis nut's circumference. In addition, several small sensor faults resulted in the inclusion of pairs of laser pulses in the first frame on occasion, which was not intended. These cases, on the other hand, are simple to identify and exclude from consideration.

A transverse flow's velocity field is less well illuminated by snapshot pair correlations than it is in a longitudinal flow because the transverse flow's velocity field is more chaotic than in a longitudinal flow. Despite this, there are more snapshot pairs for the transverse flow than for the longitudinal flow since oil soiling is less of a concern there. Therefore, the snapshot pair correlation method can still successfully reconstruct the vast majority of the velocity field data.

B. Correlations

Comparing pressures from different compressors—all of which had equivalent straight ducts—reveals a correlation between temperature and velocity.

1) Sound Intensity and Backflow

If you want further evidence that there is a relationship between the thermal processes discussed above and whoosh wideband noise, consider the following: Using the circumferential thermocouple array, we can plot the entire sound level in that frequency band against the temperature standard deviation, which shows an increasing trend followed by a plateau below roughly 1.1 degrees Celsius deviation. When low mass flows are present and there is no evidence of hot backflow, the sound levels seem to increase with shaft speed. This suggests that there is some form of flow disruption that cannot be explained by temperature variations.

Following linear least squares fit to the data for the selected frequency range, it was discovered that there was an association between sound intensity and skewness of the circumferential temperature distribution at the entrance. This discovery reveals that there is a connection between the two occurrences.

Even though the backflow carrying the bulk of the skewness has not yet reached the thermocouples, the sound level increases, showing that whooshing is happening after the impeller rather than inside it, as previously stated. It was discovered that a linear relationship between circumferential standard deviation of temperature and maximum temperature of the backflow was fairly consistent, indicating that a relative or dimensionless standard deviation (raw standard deviation divided by a representative temperature) is roughly constant, as follows: As temperature rises as a result of increasing pressure ratios, backflow is skewed in a similar manner throughout the compressor map, and it increases linearly as temperature increases.

2) Temperature Profiles and Velocity

A comparison was made between the profiles of temperature and velocity obtained through PIV and those observed by thermocouples. To accurately measure the velocity of air flowing over a curved surface, an experiment was performed in which PIV was used to take a picture of the movement of particles in the airstream. This test was performed at a certain operating point and at a different temperature than the operating point of another experiment. Thermocouple array data from the latter experiment were then normalized with respect to that from the former experiment, so that velocity magnitudes from both experiments could be directly compared. It is important to note standard deviation values for each thermocouple array data point.

A backflow occurs in a turbocharger when the air from the intake manifold circulates back towards the compressor. The flow of air through the turbocharger is divided into several zones by velocity and temperature changes. While the center of the turbocharger has a high velocity, it also has a high temperature. The profile of the centerline of a turbocharger is relatively uniform, with few variations both in terms of velocity and temperature. However, at a distance of a half radius from the wall, as speed increases towards the compressor, there is more variation. There is also less overall difference between the centerline and backflow profiles than in the normalized profile at these points, which contains more significant deviations from an average condition than when looking at average measures of temperature and velocity throughout.

The turning point of the centerline profile of flow back into the compression space can be seen to occur between 0.7 and 1.4 diameters from the compressor wheel depending on pressure ratio, which is located at a position where the velocity increases sharply towards the impeller. This effect is less noticeable in the temperature and profile measurements taken by a thermocouple array closer to the compressor wheel, but when normalized over the radial extent of flow in front of the impeller, it can be seen that there is good agreement between normalized or back-calculated temperature profiles and experimentally measured data.

This means that the temperature and velocity profiles in the cross-section of the channel, when plotted by depth, will display a pattern of oscillation from maximum values to nearly zero. A stable oscillation occurs near the core flow at $\pm 1/4$ of the radius away from the centerline.

As a result, the comparison of mass flows derived from the two datasets reveals a very excellent match and gives information on how backflow influences flow-field velocity variability. This conclusion is consistent with Liu et al[52] 's findings, which demonstrated that the standard deviation of temperature, pressure, and mass flow recorded at specific places increases dramatically towards deep surge conditions. This may be explained by the fact that as the backflow advances, it raises the amplitude of the velocity field by extending its deviation further upstream.

C. Conclusions

In this chapter, the authors address the problem of acoustic noise generated by a turbocharger compressor when a marginal surge occurs by conducting a novel experimental investigation. The researchers concentrated their attention specifically on the flow instability that extends into the input duct and causes backflow upstream of the impeller. They discovered that there are two sorts of flow patterns that might occur: rotation, vortex shedding, and reintegration (or reintegration). There have been many suggestions for reducing backflow. For example, one potential solution is to add ports or a shroud to the entrance duct to prevent it from entering.

The current chapter describes research on the intake flow instability of turbocharger compressors, which was conducted by the author. When marginal surge conditions were achieved, the goal was to define the flow behaviour and determine its characteristics. In particular, when marginal surge conditions were achieved, attention was drawn to the high-temperature flow that reversed direction and extended upstream of the impeller and into the last segment of the input duct. Backflow, together with rotation and vortex shedding, was considered to be the source of acoustic noise, according to the researchers. In order to lessen the likelihood of this backflow occurring and the amount of noise produced, many approaches have been suggested [135, 136].

We employed array thermocouples to assess the temperature distribution in a compressor in order to establish if a surge control mechanism influenced backflow in the compressor. It was possible to record the temperature distribution and variability in both the axial and circumferential directions because we used two independent arrays. We were able to demonstrate by thermography that the temperature data were not considerably impacted by radiation from the pipe walls.

Two arrays of thermocouples were installed within the compressor inlet to better understand the temperature distribution associated with marginal surge—that is, the temperature distribution when air flow through a compressor is low but greater than the temperature distribution associated with deep surge. The arrays were used to measure the axial and circumferential temperature distributions under a variety of different situations. An array of thermocouples was inserted inside the input pipe in order to quantify the radial distribution of temperature generated by hot backflow during the testing process. Temperature imaging outside the compressor assisted in determining where internal thermocouples should be placed and ensuring that radiation from pipe walls did not interfere with measurement results. The examination of these temperature distributions, as well as the temperature skewness within the circumferential temperature profile, were used to calculate the duration and amplitude of intake backflow over the experimental period.

Mass flow rate is the most important component influencing the extent of hot backflow under high-speed operating circumstances since it determines the amount of heat transferred. Surge is shorter and less severe at higher mass flow rates, but backflow has a higher temperature because of the increased mass flow rate. Circumferential skewness grows at a linear rate with rising backflow temperature, as seen in the graph below. These properties may be utilized to understand the behavior of localized flows. To investigate the flow behavior at the local level, miniature pressure probes were utilized. Using a pressure probe connected to the inducer, it was discovered that when the impeller suffered backflow, the pressure on the upstream side of the impeller changed quickly. This corresponded to the results from the temperature probe, supporting the prediction that, when exposed to a backflow, the liquid would not all depart via the inducer.

In addition to being noticed at their regular frequencies, whoosh noise humps were also found in a higher-frequency wideband that had large frequency changes. Large changes in thermodynamic conditions at the specified measurement sites might account for the observed bandwidth shift in sound speed. For its part, the plane wave frequency seems to be able to keep the broadband change under control.

Some data shows that whoosh noise—the characteristic sound of turbochargers—may be enhanced by the input flow structures that have been reversed during marginal surge conditions: It's possible that the reversed airflow is effectively increasing the whoosh. However, it is possible that the reversed flow is not the source of the whoosh.

The researchers in Taiwan tested this notion by conducting a series of tests to quantify the reversed flow at the turbocharger compressor in unstable situations when the backflows are completely formed and limited. It was decided to construct a clear glass pipe in order to enable researchers to see what was going within. It was decided to picture the lighted particles after seeding circumstances with non-toxic fluorescent dye and lighting the flow with a laser sheet. After that, it was decided to image the particles using a camera.

The results of the experiment clearly demonstrated that the reversed flows were not completely established and, as a result, could not be the source of the whoosh but could only contribute to it. These findings show that methods aimed at reducing backflows might assist to enhance whoosh while also reducing the negative impacts of whoosh on vehicle noise and vibration perception.

The first experiment was an attempt to test the flow parameters of a single turbocharger by shining laser light through a clear duct and capturing the photographs using a digital camera.

Oil particles in the backflow obstructed the backflow duct, making it impossible to determine precisely what was going on in certain regions of the system.

The turbfan engine created backflow as running circumstances became difficult, which drove additional oil into the blocked sections as the situation worsened. It is reasonable to question the seeding process utilized by Wernet as well as the pipe coating used by Gancedo et al. based on the fact that just a few images of the longitudinal plane were acquired. If a greater number of photos is necessary, researchers could explore doing more study into other seeding processes or alternative pipe coatings.

It was discovered that the reversal of flow around the periphery indicated by Lang's models was occurring at greater flow rates, despite the fact that the rise in core speed was found to be consistent with the decrease in usable diameter and earlier temperature observations throughout the study. This implies that the differences between stable axial flow and unstable circumstances induced by reversed flow in a restricted pipe may be distinguished using PIV, but it may be difficult to discriminate between the two at large flow rates. It is possible for a jet of liquid to develop and flow back down the pipe when the flow is unsteady.

It is possible that a more rotating flow will develop. For the purpose of determining whether measurements taken in the transversal plane provide reliable estimates of this phenomenon, a laboratory experiment was conducted in which three cross sections of the flow field were measured: two inside and one outside the length to which the backflow had progressed.

In order to evaluate how fluid velocity changed between two distinct parts of a highly rotating vortex, researchers performed an experiment, which they concluded may be a useful method for measuring the length and radial dispersion of a restricted backflow.

Using a faster backup, the researchers discovered that the whirling water spread uniformly over the glass surface and did not cling or clot, making it simpler to perform measurements than with a slower backup. In order to guarantee that the PIV findings and the preceding temperature measurements were in accord, a comparison between the two techniques was performed last. The measurements were standardized in order to allow for comparisons to be made between the two sets of information.

A comparison was made between the measurements taken along the inlet duct axis and the measurements taken at the nearest thermocouple; a good agreement was found between the two results, reinforcing the conclusion that a high transversal speed profile is caused by hot reversed flow, and that the velocity distribution captured by PIV is accurate. As the temperature rose, the standard deviations of velocity profiles increased as well, making axial flow data more consistent with one another.

IX. SYSTEM DESIGN

A. Design Constraints

Students in New York City are frequently confronted with the scarcity of parts in the accessible marketplaces necessary for projects. As a result, we cannot produce the turbocharge; we will preserve the car's original body. As a result, we challenge with the turbocharger's placement. Due to the time constraint, we will not produce it abroad. These are constraints that we face. The turbocharger is selected by how many hours of power you want. We selected the turbo size and system design because the throttle inlet plays a vital role.

1) Standards



| Standards | Codes |
|--|----------------|
| Level Two J1349 Certified Power Engine Data for the 5.7L V8 found in the 2016 MY Dodge Charger R/T AWT | CPFC209MYCHATX |
| Engine power measurement — Calculation and approach — General specifications for internal combustion engines | ISO:155502016 |
| Turbocharger Connections | J1135197607 |
| Coolant System Hoses | J20201503 |
| Turbocharger Gas Stand Test Code | J1826 |

| Standards | Codes |
|--|----------------|
| AS6300 Valve Spring | AS63001 |
| Flange-Two-Bolt Exhaust | AS222B |
| Automotive-Pipefittings | J530201803 |
| Engine-Charge-Air-Cooler (CAC) Nomenclature | J1148200405 |
| Exhaust Manifolds Made of High- Temperature Materials | J2515201712 |
| Aluminum alloys and wrought Aluminum-- Cold-drawn bars/rods, wires/tubes -- Part 5: Drawn square and hexagonal wires and bars -- Tolerances on dimensions and form. | ISO 63635:2012 |

The technique for accomplishing the project's goals must go through a few essential stages. The outcome will be based on what was used effectively in the design method to create the project's final prototype. To obtain the final prototype, we must complete the following steps

- To ensure the first step is accomplished, have a background in IC engines and good related research.
- Using SOLIDWORKS, create the system's draft designs.
- Choosing a turbo compatible with the chosen engine, the 5.7 Dodge Charger Hemi.
- As the exhaust creates heat, an adequate Intercooler should be used.
- Produce and assemble the system's components.
- Dynamometer testing before and after the turbocharger indicates the change in results and determines if it is relevant.
- Investigate the Turbocharger Compressor Acoustics in the future.

B. Theoretical Calculations and Theory

The broken power W_b is the engine's power output as measured by a dynamometer. Another consideration is the Mach number, which should be less than one since a Mach value of 1 will result in a constricted flow.

| ENGINE RPM | Torque | Volumetric efficiency | Pressure inlet | Pressure ratio | Inlet temperature | Volume displacement | Stroke | Valve diameter |
|------------|--------|-----------------------|----------------|----------------|-------------------|---------------------|--------|----------------|
| RPM | Nm | % | KPA | | K | Letter | m | mm |
| 4250 | 503.80 | 101.10 | 101.30 | 0.98 | 301.0 | 5.70 | 90.0 | 50.0 |

Table 5: Data for the automobile is gathered via an Excel data log.

1) The Brake Mean Effective Pressure b_{mep}

$$b_{mep} = \frac{4\pi\tau}{V_d} \dots\dots\dots \text{Eq. 9.1}$$

Where: b_{mep} : The Brake Mean Effective Pressure τ : Torque

V_d : Volume Displacement.

When: $\tau = 503.8 \text{ Nm}$, $V_d = 5.7 \text{ letters}$

$$b_{mep} = \frac{4\pi(503.8)}{5.7/1000}$$

$$b_{mep} = 1110.7 \text{ KPa}$$

2) The Brake Power, W_b

$$W_b = 2\pi\tau N \dots\dots\dots \text{Eq. 9.2}$$

Where:

W_b : Brake Power

τ : Torque

N : Mean Speed(rpm)

When:

$$\tau = 503.8$$

$$Nm \ N = 4250 \text{ rpm}$$

$$W_b = 2\pi(503.8) \frac{4250}{60}$$

$$W_b = 224.220 \text{ KW}$$

3) The Mean Piston Speed (\bar{U}_P)

9.9.3 The Mean Piston Speed (\bar{U}_P)

$$\bar{U}_P = 2NS \dots\dots\dots \text{Eq. 3.3}$$

Where:

\bar{U}_P : Mean Piston Speed

N: Mean Speed(rpm)

S: Stroke (four Strok)

when:

$$N = 4250 \text{rpm}$$

$$S = 90.0 \text{mm}$$

$$\bar{U}_P = 2 \left(\frac{4250}{60} \right) \left(\frac{90.5}{1000} \right)$$

$$\bar{U}_P = 12.82 \text{m/s}$$

9.2.4 The mass Airflow rate (\dot{m}_a)

$$\dot{m}_a = \eta_v \rho_i V_d \left(\frac{N}{2} \right) \dots\dots\dots \text{Eq. 3.4}$$

where:

\dot{m}_a : Airflow rate

η_v : Volumetric

Efficiency ρ_i :

Density of the air

V_d : Volume Displacement

N: Mean Speed(rpm)

4) Density of the air

$$\rho_i = \left(\frac{p_i}{RT_i} \right) \dots\dots\dots \text{Eq. 3.4.1}$$

Where:

ρ_i : Density of the air

p_i : Pressure inlet

R: Gas constant

T_i : Inlet temperature

9.2.5 Mass flow rate (\dot{m})

$$\dot{m} = \rho_i A_f C_0 \left[\frac{2}{\gamma-1} \left(\left(\frac{p_2}{p_1} \right)^{\frac{\gamma}{\gamma-1}} - \left(\frac{p_2}{p_1} \right)^{\frac{\gamma+1}{\gamma}} \right) \right]^{\frac{1}{2}} \dots\dots\dots \text{Eq.3.5}$$

where:

$\frac{p_2}{p_1}$: pressure ratio

γ : 1.4

9.2.5.1 Sound speed

$$c_0 = \sqrt{\gamma RT_i} \dots\dots\dots \text{Eq.3.5.1}$$

where:

γ : 1.4

T_i : Inlet temperature

R: Gas constant

9.2.5.2 Effective area

$$A_f = C_f A_v = C_f \frac{\pi}{4} d^2 (\text{seat}) \dots\dots\dots \text{Eq.3.5.2}$$

Where:

C_f : flow coefficient

A_v : Valve area

d: Diameter

9.2.6 The Mach number (M)

$$\frac{p_2}{p_1} = \left[1 + \left(\frac{\gamma-1}{2} \right) M^2 \right]^{\frac{\gamma}{\gamma-1}} \dots\dots\dots \text{Eq.3.5.6}$$

where:

$$\frac{p_2}{p_1} = \frac{p_{low}}{p_{high}}$$

9.2.7 The critical mass (\dot{m}_{cr})

$$\dot{m}_{cr} = \rho_i A_f e_0 \left(\frac{2}{\gamma+1} \right)^{\frac{(\gamma+1)}{2(\gamma-1)}} \dots\dots\dots \text{Eq.3.7}$$

where:

\dot{m}_{cr} : Mass critical

A_f : Effective area

ρ_i : Density of the air.

γ = 1.4

c_0 : sound speed

A dynamometer is used to measure torque, a moment of force (torque), or power before and after a turbocharger is installed. For example, the power generated by an engine, motor, or other rotating prime movers may be measured by measuring both torque and rotational speed at the same time, as shown in Figure 1. (rpm). It is possible to determine the volumetric efficiency, intake air temperature, pressure ratio, and manifold absolute pressure with the help of this equipment. Table 1 has a detailed description of the dynamometer [1].

| | Specification |
|-----------------------------|----------------------------|
| Max. spd | 200MPH/322KPH |
| Max. torque horsepower | 2000HP/2000FT LBS |
| Drums | 1 |
| Drum-diameter | 24IN/61CM |
| Drum-weight | 81IN/205CM |
| Max. axial weight | 3000LBS/1361KG per Axle |
| Air requirement | 100 PSI |
| Operating temperature range | 32-158F/0-70C |
| Timing accuracy | +/-1Ms |
| Drum speed accuracy | +/-1/100 th MPH |
| RPM accuracy | +/-1/10 th RPM |

Table 6: Shows specifications about the dynamometer

C. Blow off Valve

A blow-off valve (BOV) blows off boost pressure from the intake system once the throttle is released. This prevents a vacuum from pulling air through the intake system and creating a turbo "whistle" sound. The BOV also helps prevent a build-up of negative pressure in the intake tract, which could lead to harmful detonation. An aftermarket BOV is typically installed with the boost tube before the throttle plate. The purpose of a BOV is to open only above a certain pressure threshold so that under lower-pressure conditions, it remains closed (thus protecting against intake leaks). The valve works as follows when set up this way: The diaphragm is attached to a spring and one side of the valve. When the pressure inside the intake system drops below atmospheric, it pulls on the spring, causing it to push against that side of the valve. This opens up a hole that allows boost pressure to bypass the throttle plate and into the atmosphere.

Specifications

- A single Q BOV can handle up to 1,800 horsepower.
- Use if the ideal vacuum is between: -14in/hg to -17in/hg is the range of pressures.
- PSI (pounds per square inch): -9.00
- BV 44MM -2psi turbocharge spring for turbocharge applications
- The aluminum mounting clamp with the V-Band design has a spotless and unusual appearance. The clamp's hardware is stainless steel for a long-lasting, corrosion-free look.

A Viton O-ring is used to seal the valve, and it is held in place to prevent it from clinging to the seat and pulling out. The valve stem and guide are hard anodize-coated for wear resistance and lubricated with Teflon

The wastegate is a mechanism in turbocharged engines that limits the maximum boost pressure produced by the turbocharger. The wastegate consists of an inlet and outlet port, a valve, and a pressure actuator. When the engine's exhaust gases flow through the turbocharger, they boost pressure. The pressure within the turbocharger is regulated through a wastegate, which diverts some of the exhaust gas into the bypass duct whenever it senses that the boost level exceeds a certain set limit. When this happens, the pressure within the turbocharger drops until it reaches its target value [3].



Figure 49: The Wastegate mechanism consisting of an inlet and outlet port, valve and a pressure actuator.

Internal valve made of Nickel Chromium Alloy. 46mm is the assembly designation. For further boost level modification, there are five separate 17-7 hardened precipitation springs. Flange configuration mount in the standard clamp form. 6061 aluminum billet cap with a satin black anodized finish. For installation, all clamps are required. After being squeezed by a turbocharger, the air is cooled by the intercooler. It works by controlling how much fuel is consumed in each cylinder. A turbocharger increases the density of air by compressing it before it reaches the engine's cylinders. By compressing more air into each cylinder, the motor can burn more gasoline and produce more power with each explosion (2). The intercooler compensates for this by cooling compressed air, allowing more oxygen into the engine and increasing cylinder combustion. Controlling the air temperature also extends the life of the engine by ensuring that the air-to-fuel ratio in each cylinder is maintained at a safe level.

The manufacturer's team revealed in a first experiment that geometries, in addition to altering surge margin, can influence orifice noise, as reported by scientist Galindo [70]. A tapered duct seemed to increase orifice noise, yet the reservoir operated as a resonator, boosting surge margin while simultaneously decreasing orifice noise (2 dB) and radiative noise (3 dB). The elbow lengthening, on the other hand, maintained surge margins while having no influence on noise.

This is due to the fact that the noise levels were first lowered, but then rose to levels that were higher than before. We used an IGV to enhance flow swirl, however the device had the opposite effect of increasing the acoustic intensity of the orifice probe. The location of the downstream tapered section had a considerable impact on the surge margin of the system.

Using orifice nozzles in conjunction with convergent and divergent nozzles, researchers discovered that they could reduce orifice noise by 1 dB, 3 dB, and 20 percent, respectively, when placed intake geometries with convergent and divergent nozzles. A 20 percent decrease in the maximum permissible air mass flow was also achieved by using a convergent nozzle in the experiment.

In an experimental campaign with two different sound pressure levels, three different elbow inlet configurations were assessed and compared. The initial experiment found that the sharp-radius elbow (90°) provided the largest gain in sound intensity of 1 dB at the lowest allowable mass flow (0.1 kg/s) when the lowest permissible mass flow was used. This increase, however, was not fairly distributed over the compressor map, with the lowest permissible mass flow for each map configuration getting the most amount of attention overall. In all three elbows investigated, this pattern was seen, and it remained consistent throughout a range of sound pressure and mass flow rate values.

It has been shown that the temperature distribution in an input elbow may improve the circumferential skewness of a shaft. For its part, the relationship between the duration of flow and the formation of noise has been inverted. Another way of putting it is that larger radii increased noise in a diffuser, whereas smaller radii increased noise in an input duct. As a result of the increasingly smaller elbows, it is possible that these variations are generated by wind striking an uneven wall surface.

In order to better understand what impacts whoosh noise during unstable operating conditions rather than steady ones, it is preferable to examine what influences whoosh noise during unstable operating conditions rather than steady ones. It has been shown that, as a consequence, this method is more effective: it is possible to determine which components have an influence on whoosh noise under unstable operating conditions by comparing intake flow fields under unstable and stable operating conditions. It is necessary to explore the relationship between input jet noise and reverse flow in the lower mass flow areas of the compressor map in more depth. In general, if the inflow momentum is maintained, it is possible to reduce the inflow jet noise.

X. CONCLUSIONS AND FUTURE WORKS

We explained how to use certain numerical techniques that were verified as part of my study to future applications for research in this field in this thesis. This chapter summarizes the key discoveries from the previous chapters' research and includes significant contributions to the area of turbocharger compressors.

A. Conclusions

The findings of this doctoral thesis can be classified according to the processes that have been presented, validated, and debated. The outcomes of applying these processes to the compressor's acoustic output may then be summarized. This project achieves its goals and adds to our understanding of turbocharger compressors. In conclusion, the findings of this study contribute to a better knowledge of turbocharger compressor behavior as well as confirmation of particular measuring methodologies.

This knowledge is intended to help in the development of superior turbocharger designs and implementations, hence decreasing the noise emission issues raised by quieter and more fuel-efficient cars.

1) Methodology

Various experimental and computational methodologies for assessing the noise emission of turbochargers were detailed in this PhD thesis. The following are the key findings:

The use of beamforming wave decomposition in experimental studies of in-duct sound intensity in turbocharger compressor inlet and outlet pipes has shown to be a useful approach. The method for creating spectrograms and noise maps that characterize the compressor's acoustic performance along the region of interest of its operating conditions map using this information has been given.

When input orifice noise data are compared to in-duct sound intensity measurements in turbocharger applications, the two measures show a good correlation. The influence of the entire turbocharger system may be studied since exterior acoustic radiation measurements were taken and sequential insulation was employed.

To quantify turbocharger performance, this approach was further verified in a test cell equipped with an orifice intensity probe. The previously described Acoustic Particle Velocity probe was utilized to illustrate the technique's durability in a scenario where the compressor duct pressure spectrum content contains both pressure and pulsations from the engine. Other wave decomposition algorithms produced less coherent findings from all three sources.

Validation of the compressor's computational fluid dynamics simulations has been aided by beamforming with wave decomposition. Beamforming with wave decomposition has been used to evaluate simulated and experimental pressure spectra from compressors, notably at unstable operating circumstances, when combined with modal decomposition.

To describe the instability of a reversed flow, experimental measurements of local temperature, pressure, and velocity were taken. Particle Image Velocimetry (PIV) was used to image the reversed flow under various operating settings, and the results were linked to enhanced sound intensity propagation in the "whoosh" frequency region. An experimental installation enabling quick testing of custom 3D-printed inlet geometries up to 1/3 the diameter of the compressor wheel has been described, as well as a technique for assessing the effect of compressor intake geometries on surge margin and acoustic output.

2) Results

Data on the acoustic behavior of turbocharger compressors was discovered during the creation and implementation of the aforementioned methodological techniques, with the following being the most important.

Broadband whoosh noise appears at low frequencies, whereas tonal noise, induced by blade passage, exists at higher frequencies, according to an analysis of in-duct plane wave noise spectra. Both noises were present, although the latter was more prevalent over a wider frequency range. The first phenomena was linked to fluid effects, whereas the second was linked to transmission effects, according to non-dimensional analysis. The whoosh noise might also be heard across a wide frequency range and propagate at plane wave frequencies. This shows a clear distinction between these two broadband phenomena and gives a simple criterion for determining which is which.

Extreme low-frequency content may indicate the possibility for deep surge, and moderate surge is likely around the maximum efficiency condition, according to very-low frequency sound intensity levels in an anechoic chamber. The presence of whoosh noise in the spectra and spectrograms of a compressor map around maximum efficiency but before the beginning of surge shows that spinning stall or reversed flow vortices are not the cause of whoosh noise.

The presence of a whoosh noise band was verified via post-processing at various operating circumstances after CFD simulations effectively validated experimental data. Only after the maximum pressure ratio was attained did reverse flow appear. Vortex shedding was seen in the diffuser under all operating circumstances, and Fourier analysis indicated that the diffuser had the largest amplitude. In DMD analysis of outlet wall cells, modes linked to BPF and whoosh noise frequencies were determined as the most relevant in terms of coherence.

Stable flow over the compressor map nevertheless generated whoosh, as determined by both beamforming arrays and temperature and velocity probes, according to investigations using local variable characterization. Furthermore, upstream of the inducer and diffuser, where the backflow phenomena could not be identified by temperature or velocity measurements, distinctive noise was discovered.

Temperature and velocity data revealed that there was no backflow in this steady, high flow rate environment. Through study of temperature change, the experimental findings gave empirical data on backflow increase over the compressor map. The utilization of beamforming arrays and instruments set upstream and downstream of the diffuser and inducer blades revealed that no backflow was discovered. Even at this position, a typical hump in the sound spectrum was observed at the increased flow rate, indicating that the source of the noise is unrelated to reversed or stopped input flow. The acoustic performance of a compressor might be altered by adding other features, such as 90° elbows or reservoirs, according to the findings. The influence of elbow radius was studied in detail, demonstrating how noise intensity and circumferential temperature skewness varied as mass flow rate increased. According to preliminary findings, nozzles and IGVs that modify flow presentation have a considerable impact on noise in the whoosh band. These findings backed up prior findings, confirming that whoosh noise is caused by flow interaction in the diffuser under unstable conditions, particularly when convection transports its spectral content upstream to the diffuser's intake.

Advantages:

Basically, a super is shaped up of two segments that are associated by a shaft. On one side, warmed fumes exhaust drive a turbine that is coupled to one more turbine that brings air into the motor and packs it prior to delivering it into the air. This pressure gives the motor the more power and proficiency, as more air can be brought into the ignition chamber, considering more fuel to be provided, bringing about expanded power.

Alongside the extra power, turbochargers are often alluded to as "free power" gadgets in light of the fact that, not at all like superchargers, they needn't bother with the motor's ability to be utilized to work them. Since the turbocharger is fueled by the hot and extending gases that emerge from the motor, there is no decrease in the motor's general result power. Also, while going at higher elevations, turbocharged motors are not antagonistically affected in similar way as ordinarily suctioned motors are. The higher a motor controlled by normally suctioned fuel ascends in elevation, the more troublesome it gets for it to acquire oxygen inferable from the more slender climate. Turbocharging tackles this issue by driving oxygen into the motor's ignition chamber at pressures that are in many cases twice higher than those found in the general climate.

The utilization of turbochargers may likewise improve the mileage of a vehicle; in any case, there is a typical misconception about the connection between turbocharged vehicles and eco-friendliness. A motor that has normally suctioned fuel won't have its mileage improved by introducing a turbocharger on it. Makers might improve efficiency by scaling down a motor and afterward turbocharging it, as found in the video beneath.

Take, for instance, a 2.5L inline-4 chamber ordinarily suctioned motor and decrease its uprooting to 1.4L prior to turbocharging it to increment execution. The more modest, turbocharged motor would in any case give something similar (or somewhat better) execution appraisals, but since of its diminished dislodging, it would involve less gas because of its more modest uprooting.

3) Disadvantages

There are two major drawbacks of using a turbocharger as compared to a normally aspirated or supercharged engine. Primarily, there is heat. Because a turbo is fueled by hot exhaust fumes, it becomes hot during operation. Under some engine circumstances, the turbocharger itself may begin to glow red; however, this is not something that occurs in normal driving situations; rather, it occurs when the engine is pushed to its limits for an extended period, as is the case with some racing engines. Therefore you may see certain turbocharged sports vehicles have vents in the hood or down the side; this is done in an attempt to move air through the engine area and keep everything as cool as possible.

One of the most significant drawbacks of using a turbocharger is something known as turbo lag. The engine's response time is delayed when you press your foot down on the accelerator pedal under certain circumstances, causing you to feel the power you desire before you really begin to experience it. That is referred to as turbo lag. The turbocharger requires time to start spinning at an ideal speed when the engine is running at a low speed since there aren't many exhaust gases travelling through it. When the engine is running at a low speed, the turbocharger requires time to start spinning at an optimal speed. Although downshifting to a lower gear might mitigate the impacts of this, attentive drivers may still detect a split delay in reaction time from time to time.

So, the next time you're at a General Motors dealership, don't forget to look at the turbocharged automobiles on display. As a result of their lower displacement and less weight, they often have the same or more power than their V6 or even V8 counterparts. They also typically have superior fuel efficiency owing to the smaller displacement engine and lighter weight.

B. Future Works

Based on the information obtained from this doctorate thesis, future numerical simulations should be able to validate the predictions and learn more about the impact of geometry and flow presentation on the various acoustic phenomena of importance in turbocharger compressors. A study of the many basic geometries might be carried out, with the results being applied to a challenge in boat hull design. When waves are met in the moderate surge region—areas where waves are volatile—the bow and stern design would be beneficial. These places may be more susceptible to whoosh noise and other disturbing acoustic emissions, thus devising a novel approach for passing waves to avoid trapping air in this region or going through with less power is critical. Acoustic Particle Velocity measurements were used to study the noise emitted by each component of the turbocharger assembly, assisting in the identification of the most relevant sources for each acoustic phenomena discovered in the spectrum content. It would be possible to measure the acoustic properties of the compressor assembly, including the full scattering matrix, and create more realistic ways to analyze the compressor at different operating settings, if the inlet and outlet ducts of a turbocharger were modified by adding compression drivers. The correlation between the spectral content of the turbocharger compressor and experimental temperature data was better than that generated by previous heat transfer models when a more realistic CFD model was created using these modifications, improved boundary conditions, and heat transfer models, making it possible to better identify components in a Turbo compressor sound output. This new model should help us better understand the impact of various intake geometries and how they alter the flow pattern. This research would be most useful if it was conducted in combination with experimental observations using the setup described in this paper. The need for large amounts of data storage and processing can be avoided by combining advanced post-processing routines, such as the Dynamic Mode Decomposition technique described in Chapter 6, with existing solvers that can use streaming DMD algorithms to facilitate the matching of flow structures and their frequency contribution. These techniques make it easier to access critical flow patterns while also making it easier to comprehend frequency contributions.

Including noise and vibration caused by the turbulent boundary layer on the compressor blades in turbomachinery numerical models of internal flow. Experiments using a test apparatus—as detailed in this thesis—can be used to evaluate such advancements in modeling in order to construct a full model of turbocharger compressor acoustics. This concept might then be used to design cycles that are shorter.

1) Numerical Simulations

Numerical models of turbomachinery flow fields might help researchers better understand how flow fields interact inside a compressor and how they change over time.

Improved computational fluid dynamics models with more realistic inlet and outlet ducts and heat transfer models might help researchers better understand the spectral content created by turbocharger compressors and how it relates to experimental data. As a result, changes to the CFD model reported in this paper might be used to investigate the influence of alternative intake geometries on the flow exiting the compressor, as well as other relevant properties evaluated using an experimental setup similar to the one described in this paper.

Advanced post-processing procedures, such as Dynamic Mode Decomposition, might enhance acoustic models of turbocharger compressors. This method would make it easier to link important flow structures with their frequency contributions. The expanded setup may be confirmed by experimental data using one-way or completely coupled fluid/solid interaction modeling, resulting in a comprehensive model of turbocharger compressor acoustics that might be used for simulation-based design cycles.

2) Experimental Research

The experimental findings given in this paper shed fresh light on the mechanics of compression system surges. However, more research is needed to see if the phenomena found in this study extends to all types of compressors. CFD techniques might be used to model the phenomena using the same experimental approach.

The twin-scroll turbine's 3-port tests were not conducted under actual operating circumstances. This is not a concern because the data is supposed to be used to evaluate computer models. Nonetheless, the data received from the rig may be scaled to fit a real-world application. Additionally, passive data collected during a test may be utilized to detect the source sound data, regardless of the duct system in which it is created.

A complete study of the influence of geometry on intake flow patterns might be conducted, with an emphasis on how the presence of mild surge affects inlet flow and how changing this flow affects the transmission of whoosh noise and other unwanted acoustic emissions.

Furthermore, even if the "precise" Cremer method is applied, the radial wave-number cannot be solved below a certain frequency limit. This means that "precise" Cremer solutions can only be utilized for large-scale simulations in practice. It's also worth noting that the solutions for the upstream and downstream instances are considerably different, with the downstream case's limiting radial wave-number ($0 + 0i$) assuming no damping. Further investigation of this conclusion, as well as negative real portions, would be a fascinating extension of the current project. Although the underlying theory includes assumptions such as plug flow, Ingard-Myer boundary conditions, and a limiting pipe length, the optimal impedance for a specific circumstance may be calculated without them. Scientists might alter current facilities with the addition of compression drivers to give external excitations that could be used to evaluate acoustic features of the compressor assembly in order to construct a realistic acoustic model of the turbocharger. A turbocharger may also be deployed to enhance fuel efficiency without boosting power. [32] This is achieved by channeling waste heat from the combustion process into the turbo's "hot" intake side, which spins the turbine. The cold intake turbine (the opposite side of the turbo) compresses fresh intake air and pushes it into the engine's intake while the hot turbine side is fueled by exhaust energy. It is easier to ensure that all fuel is burned before being vented at the start of the exhaust stage by reusing this otherwise spent energy to increase the mass of air. A larger Carnot efficiency is gained as a consequence of the increased temperature induced by the higher pressure.

The reduction in atmospheric density that happens at higher altitudes leads in a reduced density of intake air. Aircraft engines are a logical usage for the turbocharger. The pressure of the surrounding air reduces fast when an aircraft travels to higher altitudes. The air pressure is half that at sea level at 18,000 feet (5,500 meters), so the engine generates less than half-power. Turbocharging is a technology used in aircraft engines to maintain manifold pressure constant as the altitude climbs (i.e. to compensate for lower-density air at higher altitudes) (i.e. to compensate for lower-density air at higher altitudes). Power lowers as a function of altitude in normally aspirated engines as atmospheric pressure decreases as the aircraft rises. Turbo-normalized systems are engines that utilize a turbocharger to maintain their power output at sea level. A turbo-normalized system seeks to maintain the manifold pressure at 29.5 inHg in most instances (100 kPa) (100 kPa).

BIBLIOGRAPHY

- [1] A. Broatch, J. Galindo, R. Navarro, and J. García-Tíscar. "Methodology for experimental validation of a CFD model for predicting noise generation in centrifugal compressors". *International Journal of Heat and Fluid Flow* 50, 2014, pp. 134–144 (pp. 52, 97, 101).
- [2] A. Broatch, J. Galindo, R. Navarro, J. García-Tíscar, A. Daglish, and R. K. Sharma. "Simulations and measurements of automotive turbocharger compressor whoosh noise". *Engineering Applications of Computational Fluid Mechanics* 9 (1), 2015, pp. 12–20 (pp. 55, 97).
- [3] A. Torregrosa, A. Broatch, R. Navarro, and J. García-Tíscar. "Acoustic characterization of automotive Turbocompressor". *International Journal of Engine Research* 16 (1), 2015, pp. 31–37 (p. 83).
- [4] A. Broatch, J. Galindo, R. Navarro, and J. García-Tíscar. "Numerical and experimental analysis of automotive turbocharger compressor aeroacoustics at different operating conditions". *International Journal of Heat and Fluid Flow* 61, Part B, 2016, pp. 245–255 (p. 97).
- [5] A. J. Torregrosa, A. Broatch, X. Margot, and J. García-Tíscar. "Experimental methodology for Turbocompressor in-duct noise evaluation based on beamforming wave decomposition". *Journal of Sound and Vibration* 376, 2016, pp. 60–71 (pp. 27, 153).
- [6] A. J. Torregrosa, A. Broatch, X. Margot, J. García-Tíscar, Y. Narvekar, and R. Cheung. "Local flow measurements in a turbocharger compressor inlet". Submitted to *Experimental Thermal and Fluid Science*, 2016.
- [7] A. J. Torregrosa, A. Broatch, J. V. Pastor, J. García-Tíscar, R. K. Sharma, and R. Cheung. "Measuring turbocharger compressor inlet backflow through laser particle image velocimetry". Submitted to *Experimental Thermal and Fluid Science*, 2016.
- [8] G. Daimler. "Gas- bzw. Petroleum-Kraftmaschine". N°34926 (Kaiserliche Patentamt). 1885 (p. 2).
- [9] L. Renault. "Perfectionnements aux moteurs à quatre temps". N°327452 (Office National de la Propriété Industrielle). 1902 (p. 2).
- [10] J. O. de Beeck, J. Thompson, and N. Booth. "Upcoming Emission Regulations for Passenger Cars: Impact on SCR System Requirements and Developments". *SAE Technical Paper* 2013-01-1072, 2013 (p. 4).
- [11] F. Schumann, F. Sarikoc, S. Buri, H. Kubach, and U. Spicher. "Potential of spray-guided gasoline direct injection for reduction of fuel consumption and simultaneous compliance with stricter emissions regulations". *International Journal of Engine Research* 14 (1), 2013, pp. 80–91 (p. 4).
- [12] K. S. Peat, A. J. Torregrosa, A. Broatch, and T. Fernández. "An investigation into the passive acoustic effect of the turbine in an automotive turbocharger". *Journal of Sound and Vibration* 295 (1-2), 2006, pp. 60–75 (p. 4).
- [13] B. Lecointe and G. Monnier. "Downsizing a Gasoline Engine Using Turbocharging with Direct Injection". *SAE Technical Paper* 2003-01-0542, 2003 (p. 4).
- [14] H. Stoffels and M. Schroeder. "NVH Aspects of a Downsized Turbocharged Gasoline Powertrain with Direct Injection". *SAE Technical Paper* 2003-01-1664, 2003 (p. 4).
- [15] C. Teng and S. Homco. "Investigation of Compressor Whoosh Noise in Automotive Turbochargers". *SAE Int. J. of Passeng. Cars-Mech. Syst.* 2 (1), 2009, pp. 1345–1351 (pp. 4, 11, 13, 16, 50, 84).
- [16] A. Stodola and L. Loewenstein. *Steam and gas turbines: with a supplement on the prospects of the thermal prime mover*. McGraw-Hill, 1927 (p. 4).
- [17] C. J. da Silveira Brizon and E. B. Medeiros. "Combining subjective and objective assessments to improve acoustic comfort evaluation of motor cars". *Applied Acoustics* 73 (9), 2012, pp. 913–920 (p. 5).
- [18] M. Nor, M. Fouladi, H. Nahvi, and A. Ariffin. "Index for vehicle acoustical comfort inside a passenger car". *Applied Acoustics* 69 (4), 2008, pp. 343–353 (p. 5).
- [19] J. Némec. "Noise of axial fans and compressors: Study of its radiation and reduction". *Journal of Sound and Vibration* 6 (2), 1967, pp. 230–236 (p. 9).
- [20] J. Griffiths. "The spectrum of compressor noise of a jet engine". *Journal of Sound and Vibration* 1 (2), 1964, pp. 127–140 (p. 9).
- [21] L. Mongeau, D. Thompson, and D. McLaughlin. "Sound Generation by Rotating Stall in Centrifugal Turbomachines". *Journal of Sound and Vibration* 163 (1), 1993, pp. 1–30 (pp. 10, 34, 66).
- [22] L. Mongeau, D. Thompson, and D. McLaughlin. "A method for characterizing aerodynamic sound sources in turbomachines". *Journal of Sound and Vibration* 181 (3), 1995, pp. 369–389 (pp. 10, 34, 66).
- [23] J.-S. Choi. "Aerodynamic noise generation in centrifugal turbomachinery". *KSME Journal* 8 (2), 1994, pp. 161–174 (pp. 10, 66).
- [24] J.-S. Choi, D. K. McLaughlin, and D. E. Thompson. "Experiments on the unsteady flow field and noise generation in a centrifugal pump impeller". *Journal of Sound and Vibration* 263 (3), 2003, pp. 493–514 (pp. 10, 66).
- [25] D. Wolfram and T. H. Carolus. "Experimental and numerical investigation of the unsteady flow field and tone generation in an isolated centrifugal fan impeller". *Journal of Sound and Vibration* 329 (21), 2010, pp. 4380–4397 (pp. 10, 66).
- [26] D. Wolfram and T. Carolus. "Detection and Analysis of Blade Tone Sources at Centrifugal Impellers Without Casing". In: *Aeroacoustics Conferences*. American Institute of Aeronautics and Astronautics, 2009 (pp. 10, 66).
- [27] T. H. Carolus, D. McLaughlin, and R. Basile. "Experimental investigation of the unsteady discharge flow field and the noise of a centrifugal fan impeller". In: *The Seventh International Congress on Sound and Vibration Garmisch-Partenkirchen, Germany*. 2000 (cited in pp. 10, 66).
- [28] E. P. Trochon. "A new type of silencers for turbocharger noise control". *SAE Technical Paper* 110 (6), 2001, pp. 1587–1592 (pp. 11–13, 15, 154).
- [29] D. Evans and A. Ward. "Minimizing Turbocharger Whoosh Noise for Diesel Powertrains". *SAE Technical Paper* 2005-01-2485, 2005 (cited in pp. 11, 13, 15, 84, 154).
- [30] D. Evans and A. Ward. "The reduction of turbocharger whoosh noise". In: *Proceedings of the 8th International Conference on Turbochargers and Turbocharging*, London, UK. 2006, pp. 29–42 (pp. 11, 84).
- [31] R. Kabral, H. Rammal, and M. Åbom. "Acoustical methods for investigating turbocharger flow instabilities". *SAE Technical Paper* 2013-01-1879 (p. 11).
- [32] R. Kabral and M. Åbom. "Investigation of flow-acoustic interaction in automotive turbocharger". In: *26th International Conference on Noise and Vibration Engineering, ISMA 2014*. KU Leuven. 2014, pp. 1327–1331 (p. 11).

- [33] Y. Lee, D. Lee, Y. So, and D. Chung. "Control of Airflow Noise from Diesel Engine Turbocharger". SAE Technical Paper (2011-01-0933), 2011 (pp. 11, 13, 17, 19, 20).
- [34] E. Guillou, R. DiMicco, E. Gutmark, A. Mohamed, and M. Gancedo. Characterization of a Ported Shroud Compressor using PIV Measurements. Tech. rep. 2010-01-1225. SAE Technical Paper, 2010 (pp. 12, 13, 17, 22, 24).
- [35] N. Figurella, R. Dehner, A. Selamet, K. Tallio, K. Miazgowicz, and R. Wade. "Noise at the mid to high flow range of a turbocharger compressor". Noise Control Engineering Journal 62 (5), 2014, pp. 306–312 (pp. 12, 13, 18, 21, 34, 134).
- [36] N. Figurella, R. Dehmer, A. Selamet, K. Tallio, et al. "Effect of inlet vanes on centrifugal compressor acoustics and performance". Noise Control Engineering Journal 62 (4), 2014, pp. 232–237 (pp. 12, 13, 18).
- [37] G. Gaudé, T. Lefèvre, R. Tanna, K. Jin, T. J. B. McKitterick, and S. Armenio. "Experimental and computational challenges in the quantification of turbocharger vibro-acoustic sources". In: Proceedings of the 37th International Congress and Exposition on Noise Control Engineering (INTERNOISE 2008). Vol. 2008. 3. Institute of Noise Control Engineering. 2008, pp. 5754–5767 (pp. 12–14, 34, 58).
- [38] T. Raitor and W. Neise. "Sound generation in centrifugal compressors". Journal of Sound and Vibration 314, 2008, pp. 738–756 (pp. 12, 13, 15).
- [39] A. V. Pai, S. J. Walsh, D. J. O'Boy, and R. Chen. "Air intake system noise in a turbocharged petrol engine during transient operation". In: INTER-NOISE and NOISE-CON Congress and Conference Proceedings. 2013, pp. 3656–3663 (pp. 13, 84).
- [40] A. V. Pai, S. J. Walsh, D. J. O'Boy, and R. Chen. "Turbocharger surge noise measurement and solution using experimental techniques". In: Proceedings of the 22nd International Congress on Sound and Vibration. 2015, pp. 2433–2441 (pp. 13, 18, 84).
- [41] H. Tiikola, H. Rämäl, M. Abom, and H. Boden. "Investigations of Automotive Turbocharger Acoustics". SAE International Journal of Engines 4 (2), 2011, pp. 2531–2542 (cited in pp. 13, 17, 34).
- [42] F. Kameier and W. Neise. "Rotating blade flow instability as a source of noise in axial turbomachines". Journal of Sound and Vibration 203 (5), 1997, pp. 833–853 (cited in p. 15).
- [43] A. Karim, K. Miazgowicz, B. Lizotte, and A. Zouani. "Computational Aero-Acoustics Simulation of Compressor Whoosh Noise in Automotive Turbochargers". SAE Technical Paper (2013-01-1880), 2013 (pp. 19, 24).
- [44] F. Mendonça, O. Baris, and G. Capon. "Simulation of Radial Compressor Aeroacoustics using CFD". In: Proceedings of ASME Turbo Expo 2012. GT2012-70028. ASME. 2012, pp. 1823–1832 (pp. 19, 100).
- [45] F. Hellström, E. Guillou, M. Gancedo, R. DiMicco, et al. Stall Development in a Ported Shroud Compressor using PIV Measurements and Large Eddy Simulation. Tech. rep. SAE Technical Paper 2010-01-0184, 2010 (pp. 20, 22).
- [46] E. Guillou. "Flow characterization and dynamic analysis of a radial compressor with passive method of surge control". PhD thesis. University of Cincinnati, 2011 (p. 20).
- [47] X. Margot, A. Gil, A. Tiseira, and R. Lang. "Combination of CFD and Experimental Techniques to Investigate the Flow in Centrifugal Compressors Near the Surge Line". SAE Technical Paper Series 2008-01-0300, 2008 (p. 20).
- [48] R. Lang. "Contribución a la Mejora del Margen de Bombeo en Compresores Centrífugos de Sobrealimentación". PhD thesis. Universitat Politècnica de València, 2011 (pp. 21, 23, 134, 157, 171).
- [49] J. Galindo, A. Tiseira, R. Navarro, and M. López. "Influence of tip clearance on flow behavior and noise generation of centrifugal compressors in near-surge conditions". International Journal of Heat and Fluid Flow 52, 2015, pp. 129–139 (p. 21).
- [50] J. Andersen, F. Lindström, and F. Westin. "Surge definitions for radial compressors in automotive turbochargers". SAE International Journal of Engines 1 (1), 2009, pp. 218–231 (pp. 21, 134, 142).
- [51] A. Liu and X. Zheng. "Methods of surge point judgment for compressor experiments". Experimental Thermal and Fluid Science 51, 2013, pp. 204–213 (pp. 21, 133, 169).
- [52] N. Pedersen, P. S. Larsen, and C. B. Jacobsen. "Flow in a centrifugal pump impeller at design and off-design conditions-part I: particle image velocimetry (PIV) and laser Doppler velocimetry (LDV) measurements". Journal of Fluids Engineering 125 (1), 2003, pp. 61–72 (p. 21).
- [53] J. M. F. Oro, E. B. Marigorta, K. M. A. Díaz, and R. BallesterosTajadura. "Forced and unforced unsteadiness in an axial turbomachine". Experimental Thermal and Fluid Science 33 (3), 2009, pp. 449–459 (p. 21).
- [54] A. K. Vester, S. S. Sattarzadeh, and R. Örlü. "Combined hot-wire and PIV measurements of a swirling turbulent flow at the exit of a 90° pipe bend". Journal of Visualization, 2015, pp. 1–13 (p. 21).
- [55] M. Wernet. "Development of digital particle imaging velocimetry for use in turbomachinery". Experiments in Fluids 28 (2), 2000, pp. 97–115 (pp. 21, 22, 171).
- [56] B. Liu, X. Yu, H. Liu, H. Jiang, H. Yuan, and Y. Xu. "Application of SPIV in turbomachinery". Experiments in fluids 40 (4), 2006, pp. 621–642 (pp. 21, 22).
- [57] A. Dazin, G. Cavazzini, G. Pavesi, P. Dupont, et al. "High-speed stereoscopic PIV study of rotating instabilities in a radial vaneless diffuser". Experiments in fluids 51 (1), 2011, pp. 83–93 (p. 21).
- [58] Y. Wu, S. Liu, H. Yuan, and J. Shao. "PIV measurement on internal instantaneous flows of a centrifugal pump". Science China Technological Sciences 54 (2), 2011, pp. 270–276 (pp. 21, 171).
- [59] M. Fike, G. Bombek, M. Hriberšek, and A. Hribernik. "Visualisation of rotating stall in an axial flow fan". Experimental Thermal and Fluid Science 53, 2014, pp. 269–276 (pp. 21, 157).
- [60] M. P. Wernet. "Application of DPIV to study both steady state and transient turbomachinery flows". Optics & Laser Technology 32 (7), 2000, pp. 497–525 (pp. 21, 22).
- [61] M. P. Wernet, M. M. Bright, and G. J. Skoch. "An investigation of surge in a high-speed centrifugal compressor using digital PIV". Journal of turbomachinery 123 (2), 2001, pp. 418–428 (p. 21).
- [62] M. Voges, M. Beversdorff, C. Willert, and H. Krain. "Application of particle image velocimetry to a transonic centrifugal compressor". Experiments in Fluids 43 (2-3), 2007, pp. 371–384 (p. 22).
- [63] S. Ohuchida, H. Tamaki, K. Tomoki, K. Yamada, and M. Maruyama. "Internal Flow Measurements of Turbomachinery using PIV". IHI Engineering Review 46 (1), 2013, pp. 22–28 (p. 22).

- [64] B. Cukurel, P. B. Lawless, and S. Fleeter. "Particle image velocity investigation of a high-speed centrifugal compressor diffuser: spanwise and loading variations". *Journal of Turbomachinery* 132 (2), 2010, p. 021010 (p. 22).
- [65] E. Guillou, M. Gancedo, R. DiMicco, E. Gutmark, et al. "Surge characteristics in a ported shroud compressor using PIV measurements and large eddy simulation". In: 9th International Conference on Turbochargers and Turbocharging. 2010 (p. 22).
- [66] E. Guillou, M. Gancedo, E. Gutmark, and A. Mohamed. "PIV investigation of the flow induced by a passive surge control method in a radial compressor". *Experiments in fluids* 53 (3), 2012, pp. 619–635 (p. 22).
- [67] M. Gancedo, E. Gutmark, and E. Guillou. "PIV measurements of the flow at the inlet of a turbocharger centrifugal compressor with recirculation casing treatment near the inducer". *Experiments in Fluids* 57 (2), 2016, pp. 1–19 (pp. 22, 171).
- [68] J. Galindo, A. Tiseira, F. J. Arnau, and R. Lang. "On-Engine Measurement of Turbocharger Surge Limit". *Experimental Techniques* 37 (1), 2013, pp. 47–54 (pp. 22, 32, 44, 84, 86, 140).
- [69] J. Galindo, J. R. Serrano, X. Margot, A. Tiseira, N. Schorn, and H. Kindl. "Potential of flow pre-whirl at the compressor inlet of automotive engine turbochargers to enlarge surge margin and overcome packaging limitations". *International journal of heat and fluid flow* 28 (3), 2007, pp. 374–387 (pp. 23, 24, 200).
- [70] J. R. Serrano, X. Margot, A. Tiseira, and L. M. García-Cuevas. "Optimization of the inlet air line of an automotive turbocharger". *International Journal of Engine Research* 14 (1), 2013, pp. 92–104 (p. 23).
- [71] L. Wang, C. Yang, B. Zhao, D. Lao, C. Ma, and D. Li. "The change of the inlet geometry of a centrifugal compressor stage and its influence on the compressor performance". *Journal of Thermal Science* 22 (3), 2013, pp. 197–208 (p. 23).
- [72] E. M. Greitzer. "Surge and rotating stall in axial flow compressors—Part I: Theoretical compression system model". *Journal of Engineering for Power* 98 (2), 1976, pp. 190–198 (p. 23).
- [73] K. Hansen, P. Jorgensen, and P. Larsen. "Experimental and theoretical study of surge in a small centrifugal compressor". *Journal of Fluids Engineering* 103 (3), 1981, pp. 391–395 (p. 23).
- [74] A. Engeda, Y. Kim, R. Aungier, and G. Direnzi. "The inlet flow structure of a centrifugal compressor stage and its influence on the compressor performance". *Journal of fluids engineering* 125 (5), 2003, pp. 779–785 (p. 23).
- [75] D. Li, C. Yang, M. Zhou, Z. Zhu, and H. Wang. "Numerical and experimental research on different inlet configurations of high-speed centrifugal compressor". *Science China Technological Sciences* 55 (1), 2012, pp. 174–181 (p. 23).
- [76] J. Galindo, F. Arnau, A. Tiseira, R. Lang, H. Lahjailly, and T. Gimenes. "Measurement and Modeling of Compressor Surge on Engine Test Bench for Different Intake Line Configurations". *SAE Technical Paper* 2011-01-0370, 2011 (pp. 23, 84, 86).
- [77] J. M. Desantes, J. M. Luján, B. Plá, and J. A. Soler. "Potential of using a nozzle at the compressor inlet of a high-speed direct-injection diesel engine". *Proceedings of the Institution of Mechanical Engineers, Part D: Journal of Automobile Engineering* 225 (2), 2011, pp. 178–189 (p. 23).
- [78] N. Kyrtatos and N. Watson. "Application of aerodynamically induced prewhirl to a small turbocharger compressor". *Journal of Engineering for Gas Turbines and Power* 102 (4), 1980, pp. 943–950 (p. 24).
- [79] M. Copping and E. Swain. "Performance prediction of an industrial centrifugal compressor inlet guide vane system". *Proceedings of the Institution of Mechanical Engineers, Part A: Journal of Power and Energy* 214 (2), 2000, pp. 153–164 (p. 24).
- [80] B. Semlitsch, V. JyothishKumar, M. Mihaescu, L. Fuchs, E. Gutmark, and M. Gancedo. "Numerical Flow Analysis of a Centrifugal Compressor with Ported and without Ported Shroud". *SAE Technical Paper* 2014-01-1655, 2014 (cited in p. 24).
- [81] H. Chen and J. Yin. "Turbocharger compressor development for diesel passenger car applications". In: 8th International Conference on Turbochargers and Turbocharging. Ed. by C. E. F. G. Institution of Mechanical Engineers. Woodhead Publishing, 2006, pp. 15–27 (p. 24).
- [82] J. Luján, V. Bermúdez, J. R. Serrano, and C. Cervelló. "Test bench for turbocharger groups characterization". *SAE Technical Paper* (2002-01-0163), 2002 (p. 29).
- [83] G. Piñero, L. Vergara, J. M. Desantes, and A. Broatch. "Estimation of velocity fluctuation in internal combustion engine exhaust systems through beamforming techniques". *Measurement Science & Technology* 11 (11), 2000, pp. 1585–1595 (pp. 35, 36).
- [84] C. L. Morfey. "Sound transmission and generation in ducts with flow". *Journal of Sound and Vibration* 14 (1), 1971, pp. 37–55 (p. 35).
- [85] E. Dokumaci. "On the calculation of acoustic power". *Journal of Sound and Vibration* 238 (5), 2000, pp. 869–876 (p. 35).
- [86] B. Van Veen and K. Buckley. "Beamforming: A versatile approach to spatial filtering". *ASSP Magazine, IEEE* 5 (2), 1988, pp. 4–24 (p. 35).
- [87] J. E. Piper. *Beamforming narrowband and broadband signals*. Ed. by N. Kolev. INTECH Open Access Publisher, 2011 (p. 35).
- [88] K. Holland and P. Davies. "The measurement of sound power flux in flow ducts". *Journal of Sound and Vibration* 230 (4), 2000, pp. 915–932 (p. 38).
- [89] A. Torregrosa, A. Broatch, V. Bermudez, and I. Andres. "Experimental assessment of emission models used for IC engine exhaust noise prediction". *Experimental Thermal and Fluid Science* 30 (2), 2005, pp. 97–107 (p. 38).
- [90] A. P. Dowling and J. E. F. Williams. *Sound and Sources of Sound*. Ellis Horwood publishers, 1983 (p. 39).
- [91] M. Åbom and H. Bodén. "Error analysis of two-microphone measurements in ducts with flow". *Journal of the Acoustical Society of America* 83 (6), 1988, pp. 2429–2438 (p. 39).
- [92] A. F. Seybert. "Two-sensor methods for the measurement of sound intensity and acoustic properties in ducts". *Journal of the Acoustical Society of America* 83 (6), 1988, pp. 2233–2239 (pp. 39, 78, 84, 87).
- [93] L. J. Eriksson. "Higher order mode effects in circular ducts and expansion chambers". *Journal of the Acoustical Society of America* 68, 1980, p. 545 (pp. 40, 86, 128, 152).
- [94] F. Payri, J. M. Desantes, and A. Broatch. "Modified impulse method for the measurement of the frequency response of acoustic filters to weakly nonlinear transient excitations". *Journal of the Acoustical Society of America* 107 (2), 2000, pp. 731–738 (p. 41).
- [95] J. Galindo, J. R. Serrano, C. Guardiola, and C. Cervelló. "Surge limit definition in a specific test bench for the characterization of automotive turbochargers". *Experimental Thermal and Fluid Science* 30 (5), 2006, pp. 449–462 (pp. 42, 44).
- [96] J. Galindo, H. Climent, C. Guardiola, and A. Tiseira. "On the effect of pulsating flow on surge margin of small centrifugal compressors for automotive engines". *Experimental Thermal and Fluid Science* 33 (8), 2009, pp. 1163–1171 (p. 48).

- [97] F. Jacobsen. "Active and reactive, coherent and incoherent sound fields". *Journal of Sound and Vibration* 130 (3), 1989, pp. 493–507 (p. 51).
- [98] S. Elliott. "Errors in acoustic intensity measurements". *Journal of Sound and Vibration* 78 (3), 1981, pp. 439–443 (p. 51).
- [99] H.-E. de Bree, P. Leussink, T. Korthorst, H. Jansen, T. S. Lammerink, and M. Elwenspoek. "The μ -flown: a novel device for measuring acoustic flows". *Sensors and Actuators A: Physical* 54 (1), 1996, pp. 552–557 (p. 51).
- [100] F. Jacobsen and H.-E. de Bree. "A comparison of two different sound intensity measurement principles". *The Journal of the Acoustical Society of America* 118 (3), 2005, pp. 1510–1517 (pp. 51, 92).
- [101] D. F. Comesaña, S. Steltenpool, G. Carrillo Pousa, H.-E. de Bree, and K. R. Holland. "Scan and Paint: Theory and Practice of a Sound Field Visualization Method". *ISRN Mechanical Engineering* 2013, 2013 (pp. 51, 92).
- [102] O. Wolff, E. Tijs, and H.-E. de Bree. "A PU Probe Array-Based Panel Noise Contribution Analysis Whilst Driving". In: *SAE Technical Paper*. SAE International, 2009 (p. 51).
- [103] I. Andrés. "Contribución al estudio y caracterización de la generación de ruido de flujo en el sistema de escape (in Spanish)". PhD thesis. Universidad Politécnica de Valencia, 2003 (p. 53).
- [104] W. Neise and B. Barsikow. "Acoustic similarity laws for fans". *Journal of Engineering for Industry* 104 (2), 1982, pp. 162–168 (p. 66).
- [105] J. Galindo, J. Serrano, H. Climent, and A. Tiseira. "Experiments and modelling of surge in small centrifugal compressor for automotive engines". *Experimental Thermal and Fluid Science* 32 (3), 2008, pp. 818–826 (pp. 84, 132).
- [106] R. Navarro García. "A numerical approach for predicting flow-induced acoustics at near-stall conditions in an automotive turbocharger compressor". PhD thesis. 2014 (pp. 98, 101).
- [107] STAR-CCM+. Version Release 8.04. CD-Adapco. 2013 (p. 100).
- [108] M. L. Shur, P. R. Spalart, M. K. Strelets, and A. K. Travin. "A hybrid RANS-LES approach with delayed-DES and wall-modelled LES capabilities". *International Journal of Heat and Fluid Flow* 29 (6), 2008, pp. 1638–1649 (p. 100).
- [109] A. Travin, M. Shur, M. Strelets, and P. Spalart. "Detached-eddy simulations past a circular cylinder". *Flow, Turbulence and Combustion* 63 (1-4), 2000, pp. 293–313 (p. 100).
- [110] O. Baris and F. Mendonça. "Automotive Turbocharger Compressor CFD and Extension Towards Incorporating Installation Effects". In: *Proceedings of ASME Turbo Expo 2011: Power for Land, Sea and Air*. ASME, 2011, pp. 2197–2206 (p. 100).
- [111] J. Serrano, P. Olmeda, F. Arnau, M. Reyes-Belmonte, and A. Lefebvre. "Importance of Heat Transfer Phenomena in Small Turbochargers for Passenger Car Applications". *SAE International Journal of Engines* 6 (2), 2013, pp. 716–728 (p. 100).
- [112] J. R. Serrano, F. J. Arnau, R. Novella, and M. Á. Reyes-Belmonte. "A Procedure to Achieve 1D Predictive Modeling of Turbochargers under Hot and Pulsating Flow Conditions at the Turbine Inlet". *SAE Technical Paper* (2014-01-1080), 2014, 13pp (p. 100).
- [113] J. Serrano, P. Olmeda, F. Arnau, A. Dombrovsky, and L. Smith. "Methodology to characterize heat transfer phenomena in small automotive turbochargers: Experiments and modelling based analysis". In: *ASME Turbo Expo 2014: Turbine Technical Conference and Exposition*. American Society of Mechanical Engineers. 2014, pp. 1–13 (p. 100).
- [114] F. Payri, J. M. Desantes, and A. J. Torregrosa. "Acoustic boundary condition for unsteady one-dimensional flow calculations". *Journal of Sound and Vibration* 188 (1), 1995, pp. 85–110 (p. 106).
- [115] A. Torregrosa, P. Fajardo, A. Gil, and R. Navarro. "Development of a non-reflecting boundary condition for its application in 3D computational fluid dynamic codes". *Engineering Applications of Computational Fluid Mechanics* 6 (3), 2012, pp. 447–460 (p. 106).
- [116] J. Galindo, A. Tiseira, P. Fajardo, and R. Navarro. "Coupling methodology of 1D finite difference and 3D finite volume CFD codes based on the Method of Characteristics". *Mathematical and Computer Modelling* 54 (7-8), 2011. Mathematical models of addictive behaviour, medicine & engineering, pp. 1738–1746 (p. 106).
- [117] E. Sundström, B. Semlitsch, and M. Mihaescu. "Centrifugal compressor: The sound of surge". In: *21st AIAA/CEAS Aeroacoustics Conference*. 2015 (p. 116).
- [118] E. Sundström, B. Semlitsch, and M. Mihaescu. "Assessment of the 3D Flow in a Centrifugal compressor using Steady-State and Unsteady Flow Solvers". In: *SAE Technical Paper*. SAE International, 2014 (p. 116).
- [119] J. L. Lumley. "The structure of inhomogeneous turbulent flows". In: *Atmospheric Turbulence and Radio Wave Propagation – Proceedings of the International Colloquium*. Nauka, Moscow, 1967, pp. 166–178 (p. 122).
- [120] N. Aubry. "On the hidden beauty of the proper orthogonal decomposition". *Theoretical and Computational Fluid Dynamics* 2 (5-6), 1991, pp. 339–352 (pp. 122, 123).
- [121] P. J. Schmid. "Dynamic mode decomposition of numerical and experimental data". *Journal of Fluid Mechanics* 656, 2010, pp. 5–28 (pp. 122–126).
- [122] S. Bagheri. "Koopman-mode decomposition of the cylinder wake". *Journal of Fluid Mechanics* 726, 2013, pp. 596–623 (pp. 122, 125).
- [123] P. J. Schmid, L. Li, M. P. Juniper, and O. Pust. "Applications of the dynamic mode decomposition". *Theoretical and Computational Fluid Dynamics* 25 (1-4), 2011, pp. 249–259 (pp. 123–125).
- [124] M. R. Jovanović, P. J. Schmid, and J. W. Nichols. "Sparsity-promoting dynamic mode decomposition". *Physics of Fluids* (1994-present) 26 (2), 2014, p. 024103 (pp. 123, 125, 126).
- [125] A. Sakowitz, M. Mihaescu, and L. Fuchs. "Flow decomposition methods applied to the flow in an IC engine manifold". *Applied Thermal Engineering* 65 (1), 2014, pp. 57–65 (cited in pp. 123, 125).
- [126] C. W. Rowley, I. Mezić, S. Bagheri, P. Schlatter, and D. S. Henningson. "Spectral analysis of nonlinear flows". *Journal of fluid mechanics* 641, 2009, pp. 115–127 (pp. 123, 125).
- [127] K. K. Chen, J. H. Tu, and C. W. Rowley. "Variants of dynamic mode decomposition: boundary condition, Koopman, and Fourier analyses". *Journal of nonlinear science* 22 (6), 2012, pp. 887–915 (pp. 123, 125).
- [128] J. Dahan, R. Futrzynski, C. O'Reilly, and G. Efraimsson. "Aero-acoustic source analysis of landing gear noise via dynamic mode decomposition". In: *21st International Congress on Sound and Vibration*. 2014 (pp. 123, 126).
- [129] R. Futrzynski and G. Efraimsson. *Dymode: A parallel dynamic mode decomposition software*. KTH Royal Institute of Technology. 2015 (pp. 125, 126).

- [130]Y. T. Delorme, A.-E. M. Kerlo, K. Anupindi, M. D. Rodefeld, and S. H. Frankel. "Dynamic mode decomposition of Fontan hemodynamics in an idealized total cavopulmonary connection". Fluid Dynamics Research 46 (4), 2014, p. 041425 (p. 126).
- [131]J. F. Williams and D. L. Hawkins. "Sound generation by turbulence and surfaces in arbitrary motion". Philosophical Transactions of the Royal Society of London A: Mathematical, Physical and Engineering Sciences 264 (1151), 1969, pp. 321–342 (p. 126).
- [132]S. Koff and E. Greitzer. "Axisymmetrically stalled flow performance for multistage axial compressors". Journal of Turbomachinery 108 (2), 1986, pp. 216–223 (p. 132).
- [133]G. Liśkiewicz, L. Horodko, M. Stickland, and W. Kryłowicz. "Identification of phenomena preceding blower surge by means of pressure spectral maps". Experimental Thermal and Fluid Science 54, 2014, pp. 267–278 (p. 151).
- [134]H. Chen and V. Lei. "Casing treatment and inlet swirl of centrifugal compressors". In: Proceedings of ASME Turbo Expo 2012. GT2012-69340. ASME. 2012 (p. 169).
- [135]L. Ding, T. Wang, B. Yang, W. Xu, and C. Gu. "Experimental investigation of the casing treatment effects on steady and transient characteristics in an industrial centrifugal compressor". Experimental Thermal and Fluid Science 45, 2013, pp. 136–145 (p. 169).
- [136]A. Kalpakli, R. Örlü, and P. Alfredsson. "Vortical patterns in turbulent flow downstream a 90° curved pipe at high Womersley numbers". International Journal of Heat and Fluid Flow 44, 2013, pp. 692–699 (p. 201).
- [137]A. K. Vester and R. Örlü. "Turbulent pipe flow downstream a 90° pipe bend with and without superimposed swirl". International Journal of Heat and Fluid Flow 41, 2013, pp. 103–111 (p. 201).
- [138]Tiikoja, Heiki & Rämmal, Hans & Abom, Mats & Bodén, Hans. (2011). Investigations of Automotive Turbocharger Acoustics. SAE International Journal of Engines. 4. 2531-2542. 10.4271/2011-24-0221.
- [139]Engineering Explained: 6 Different Types Of Turbocharger And The Advantages Of Each Setup. (n.d.). Car Throttle; www.carthrottle.com. Retrieved April 20, 2022, from <https://www.carthrottle.com/post/engineering-explained-6-different-types-of-turbocharger-and-the-advantages-of-each-setup/>

LIST OF FIGURES

Figure 1:Google Books indexed the normalized significance of chosen English phrases in literature. The data is released under the Creative Commons Attribution 3.0 License

Figure 2: Turbocharger inner view

Figure 3: The most acoustic events in a turbocharger compressor outlet are depicted in this idealized picture of a typical SIL spectrum in a turbocharger compressor outlet

Figure 4:Unbalanced whistle Noise and Pulsation Noise due to added mass

Figure 5: This diagram of the flow rig shows the engine core, asynchronous dynamometer, screw compressor, and air distribution system including control valves and reservoirs

Figure 6: The interior of the anechoic chamber reveals the turbocharger setup and pipes required to operate it

Figure 7: A dimensional design was employed for the majority of the experiment's development and some key dimensions

Figure 8: Three elements tuned to a specific angle (θ) can be combined to form a narrowband beamformer

Figure 9: At the inlet, the pressure wave amplitude traveling forward (towards the compressor) is smaller than the one coming from the compressor. The pressure waves reverse at the outlet

Figure 10: The inlet and outlet pressure power spectral densities at 160 krpm and 60 g/s are shown in Figure 3 with the frequency limitations described in equations 3.3.6 and 3.3.7. The blade passing frequency can also be identified by observing the spectra

Figure 11: This figure illustrates the proposed turbocharger instrumentation setup. Color indicates the location of each three-sensor beamforming array. This figure also shows clearance requirements for beamforming arrays using a cylindrical waveguide

Figure 12: According to the graphs shown here, the calibration of the outlet sensors in an impulse test rig showed excellent pressure-speed match across the spectrum

Figure 13: These images of the two free-field microphones, Mic 1 and Mic 2, placed 10 mm and 20 mm from the inlet duct's orifice, show the drop in acoustic pressure when the compressor is turned on (both are placed at 10mm from the duct's orifice; Mic 2 is moved

Figure 14: The microphone being used here is a radiated noise microphone. It's being installed around the turbocharger, featuring a commercial set of compressor inlet and outlet pipes that will be sequentially insulated for evaluating the contribution of each par

Figure 15: Turbocharger internal components

Figure 3.13:Assembly of Engine (SOLIDWORKS)

Figure 17: turbocharger assembly

Figure 18: The spectra of total pressure (solid line) and decomposed pressure (dotted line) are plotted for both 80 krpm and the highest mass flow and 160 krpm and the lower mass flow

Figure 19: Averaged RMS Sound Pressure Level recorded during consecutive damping measurements on the 160 krpm speed line for various air mass flow rates

Figure 20: Correlation of the sound intensity in the inlet duct and sound intensity in the orifice, using both LCMV beamforming and the Two Microphone Method

Figure 21: The turbine, which contains a moving set of airfoils (or blades), compresses the air as it passes between them. This causes the pressure and mass rate of the airflow to increase, which in turn provides more air to the cylinders

Figure 22: Images of the acoustic measures experiment, which includes the intensity probe and transducer array installed on the expanded intake pipe

Figure 23: In the CFD model, a polyhedral mesh of the rotor walls (grey) and surrounding fluid (blue) was employed

Figure 24: The drawings show the location of the compressor inlet and outlet pipes as well as the piezoelectric sensor arrays. The compressor inlet and outlet pipes are simulated with both the experimental wave decomposition and highlighting of the CFD simulation

Figure 25: Here's an image that shows the CFD domain, highlighting a compressor wheel and including three different kinds of pressure monitors selected during the setup. They are positioned in sections of the outlet and inlet ducts

Figure 26: A comparison of the total spectral content of each monitor type will show that piezoelectric sensors provide superior performance

Figure 27: Two acoustic modes in a CFD monitor can be represented schematically by the solid lines, and the different types of monitors can be identified by the different line styles

Figure 28: Comparison of experimental and model-simulated total pressure in the outlet case, using the wall monitor, shows that mode onset occurs at approximately 0.5% higher total pressure than simulated decomposed pressure

Figure 29: The experimental results were compared with those from a simulation of the outlet case, where pressure was decomposed into modes. In both simulations, pressure reached the same mode-onset value

Figure 30: The specified geometries are drawn. Except for the tapered duct, which employed a broader pipe, the straight pipe at the top was used as a reference and attached upstream of each geometry to monitor the instantaneous pressure

Figure 31: With pressure being gradually reduced and the air mass flow gradually dropping to a deep surge condition, the different geometries each recorded non-dimensional pressure

Figure 32: The presented approach yielded the lowest permitted air mass flow for the various basic geometries examined

Figure 33: For each intake geometry at the stable operating point closer to surge, noise is radiated to the anechoic chamber in the form of sound waves

Figure 34: A comparison of sound spectra for each of the simple inlet geometries is given for the configuration with the highest amplitude at the stable operating point.

Figure 35: The cross-sectional view of the inlet geometries considered for the on-engine campaign.

Figure 36: The image below shows a 3D-printed IGV device is fitted to the inlet duct of a compressor, revealing the inlet and impeller

Figure 37: The straight intake utilized as a reference in the on-engine inlet geometric variation test has a loudness level map between 1 and 3 kHz

Figure 38: The figure shows the sound intensity level maps for the several geometries utilized in the on-engine test between 1 and 3 kHz

Figure 39: Performance fluctuation for various intake geometry over the engine's usual operating range.

Figure 40: Comparison of mean sound intensity levels for various intake geometries across the engine's usual operating range

Figure 41: The 0.75D elbow inlet is meant to fit into the compressor intake adapter and contain the linear thermocouple array, as shown in this mechanical drawing

Figure 42: The 3D-printed prototypes were created using CAD models of compressor elbow inlets of various radius (decreasing in radius from left to right)

Figure 43: CAD model of the compressor assembly, such as the temperature and pressure instruments, as well as the mounting system, with the 0.75D elbow intake attached to the common adapter

Figure 44: In-duct sound intensity levels at the inlet (left) and exit (right) for each of the specified inlet elbows compared to the reference straight duct. 1.5D, 1D, and 0.75D, from top to bottom

Figure 45: The results of the sound intensity level differences for both inlet and outlet sound pressure levels were compiled into histograms that illustrate the percentage of the compressor map at which each different level occurred for each tested elbow configuration

Figure 46: In the 45 g/s plane wave range spectra at both inlet and exit, variations between the straight reference duct and each of the elbow arrangements may be seen, pointing to the efficacy of a specific elbow

Figure 47: Use this map to show the differences in the temperature of circumferential segments for each of your selected elbows vs. the reference straight section

Figure 48: Temperature standard deviation discrepancies between each of the tested elbow variations and the reference straight inlet pipe are represented by histograms. The proportion of the interpolated compressor map where each distinct level occurred is indicated

Figure 49: The Wastegate mechanism consisting of an inlet and outlet port, valve and a pressure actuator

ABBREVIATIONS AND SYMBOLS

BPF: Blade Pass Frequency

TCN: Turbo Charge Network

CFD: Computational Fluid Dynamics

TC: Turbochargers

AEC: Adiabatic Productivity

NACA: National Advisory Committee for Aeronautics

SPL: Sound Pressure Level

LDA: Lobe Displacement Angle

TL: Transmission Losses

OP: Operating Point

PR: Pressure Ratio

PVL: Particle Velocity Level

CHRA: Center Housing Assembly

LCMV: Linear Constrained Minimum Variance

EC: Engine Control Unit

HIL: Hardware in Loop

MVM: Mean Value Model

EUUP: Electronic Unit Pump

AS: Air System

IS: Injection System

TGS: Torque generation System

PS: Protection System

RPA: Research and Production Association

LGDTM: Laboratory of Gas Dynamics Turbo Machines

DES: Detached Eddy Simulations

PWD: Pressure Wave Decomposition

FFT: Fast Fourier Transform

SLS: Selective Laser Sintering

PIV: Particle Image Velocimetry

BOV: Blow off valve

DMD: Dynamic Mode Decomposition

1:D One Dimensional

NVH: Noise Vibration and Harness

GDI: Gasoline Direct Injection

VGT: Variable Geometry Turbocharger

RPM: Revolutions per minute



10.22214/IJRASET



45.98



IMPACT FACTOR:
7.129



IMPACT FACTOR:
7.429



INTERNATIONAL JOURNAL FOR RESEARCH

IN APPLIED SCIENCE & ENGINEERING TECHNOLOGY

Call : 08813907089  (24*7 Support on Whatsapp)